

**Active three-way catalysis of rhodium particles
on lanthanoid-containing zirconium oxide**

(ランタノイド添加ジルコニウム酸化物に担持した
ロジウムの高活性な三元触媒作用)

Hisaya Kawabata

Department of Applied Chemistry
Graduate School of Engineering
Hiroshima University

2015

Contents

Chapter 1: General Introduction	7
1.1 Environmental impacts of auto-emissions	7
1.2 Three-way catalysis.....	8
1.3 New aspects of the three-way catalysis.....	10
1.4 Advantages of rhodium under the new catalytic conditions	11
1.4.1 Characteristics of precious metals used in catalysis	11
1.4.2 Factors affecting rhodium activity.....	12
1.4.3 Advantages and disadvantages of rhodium.....	13
1.5 Deactivation of rhodium	13
1.5.1 Deactivation caused by the oxidation and the solid solution formation	13
1.5.2 Sintering of rhodium particles	15
1.6 Measures to inhibit Rh-deactivation	16
1.7 A new strategy for designing effective three-way catalysts	18
References.....	20
Chapter 2: Active three-way catalysis of rhodium particles under an oxidative atmosphere on a La-containing ZrO₂ support	25
2.1 Introduction.....	25
2.2 Experimental	26
2.2.1 Catalyst preparation.....	26
2.2.2 Three-way catalytic studies	26
2.2.3 Characterization.....	27
2.2.3.1 Transmission electron microscopy (TEM)	27
2.2.3.2 X-ray photoelectron spectroscopy (XPS)	27
2.2.3.3 Temperature-programmed reduction using CO (CO-TPR).....	27

2.2.3.4 Other characterization.....	28
2.3 Results and Discussion.....	29
2.3.1 Three-way catalytic activity under fluctuaing atmosphere	29
2.3.2 Particles size and rhodium dispersion.....	30
2.3.3 Rhodium oxidation state	32
2.3.4 Rhodium property	34
2.4 Conclusion	36
References.....	37
Chapter 3: Self-regeneration of three-way catalyst rhodium particles on a La-containing ZrO₂ support under an oxidative atmosphere.....	39
3.1 Introduction.....	39
3.2 Experimental	41
3.2.1 Catalyst preparation.....	41
3.2.2 Three-way catalytic studies	41
3.2.3 Aging procedure.....	42
3.2.4 Steam-reforming reaction	42
3.2.5 Characterization.....	42
3.2.5.1 X-ray diffraction (XRD)	42
3.2.5.2 Transmission electron microscopy (TEM)	42
3.2.5.3 X-ray photoelectron spectroscopy (XPS)	43
3.2.5.4 Temperature-programmed reduction using CO (CO-TPR).....	43
3.2.5.5 Other characterization.....	43
3.3 Results.....	44
3.3.1 Effect of oxygen on the performance of the three-way rhodium-based catalysts.....	44
3.3.2 Rhodium particle size and dispersion property.....	48
3.3.3 Oxidation state of rhodium	55
3.3.4 Temperature-programmed reduction using CO (CO-TPR).....	59
3.3.5 Effect of La addition in the Rh-based catalysts on the performance of the steam reforming reaction	63
3.3.6 Effect of the steam reforming reaction on the oxidation state of rhodium	65

3.3.7 Effect of the steam reforming reaction on the three-way catalytic activity	68
3.3.8 Influence of La concentration on the catalytic activity	69
3.3.9 Influence of La concentration on the crystal structure.....	70
3.3.10 Influence of La concentration on the reducibility of rhodium	75
3.3.11 Influence of aging time on the sintering of rhodium particles	78
3.4 Discussion	80
3.5 Conclusions.....	83
References.....	84
Chapter 4: Highly active three-way catalysis of rhodium particles on a Y-stabilized La-containing ZrO₂ support.....	87
4.1 Introduction.....	87
4.2 Experimental	89
4.2.1 Catalyst preparation.....	89
4.2.2 Three-way catalytic reaction.....	90
4.2.3 Aging procedure.....	90
4.2.4 Steam-reforming reaction	90
4.2.5 Characterization.....	91
4.2.5.1 X-ray diffraction (XRD)	91
4.2.5.2 Transmission electron microscopy (TEM)	91
4.2.5.3 Temperature-programmed reduction using CO (CO-TPR).....	91
4.2.5.4 <i>In situ</i> Fourier transform infrared (FT-IR) spectra.....	92
4.2.5.5 Other characterization techniques.....	92
4.3 Results.....	93
4.3.1 Crystal phases of supports	93
4.3.2 Effects of oxidation treatment on the performance of the three-way rhodium-based catalysts	96
4.3.3 Rhodium particle sizes and dispersion on different supports	105
4.3.4 Temperature-programmed reduction by CO (CO-TPR)	111
4.3.5 Infrared spectra	115
4.3.6 Steam reforming reaction activity and its effect on three-way catalysis	116

4.4 Discussion	120
4.5 Conclusions.....	123
References.....	124
Chapter 5: Summary and General Conclusions.....	127
5.1 Summary of each Chapter.....	127
5.1.1 Summary of Chapter 2.....	127
5.1.2 Summary of Chapter 3.....	127
5.1.3 Summary of Chapter 4.....	128
5.2 General Conclusions	130
List of Publications	131
Acknowledgements	133

Chapter 1

General Introduction

Chapter 1: General Introduction

1.1 Environmental impacts of auto-emissions

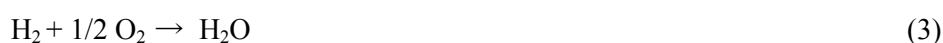
Emissions from the transport sector, from cars, airplanes, and ships, are predominant sources of air pollution.¹ These emissions cause a decrease in the ozone layer, occurrence of acid rain, and contribute to CO₂-induced global warming. In particular, the emissions from cars affect urban air quality and human health. Unlike combustion in power plants, combustion in vehicle engines is incomplete; hence, their emissions contain volatile fuel constituents, carbonaceous deposits, nitrogen oxides, and carbon monoxide. Carbon monoxide (CO) directly affects human health. Nitrogen oxide (NO) and nitrogen dioxide (NO₂) form through oxidation of nitrogen from air in the engine cylinders at high temperature. In particular, NO participates in photochemical reactions with hydrocarbons to form photochemical smog in the presence of sunlight.²⁻⁴ Despite these impacts, cars are indispensable to human society as a means of transport, and their future use is inevitable. Therefore, converting the harmful emissions from cars is very important for environmental protection.

Regulation of vehicle emissions has inspired development of emission control technologies. The first emission regulation was established in the 1970s in the United States, and was subsequently implemented in Europe and the Japan.⁵⁻⁷ The level of regulation is becoming more stringent worldwide. Catalytic removal of vehicle emissions, using a three-way catalyst, has been in practical use since 1975 because of its long lifetime, high performance, and durability. Until now, alongside diesel particulate filters and oxidation catalysts for converting diesel emissions, the three-way catalyst has been an effective measure for reducing the impacts of gasoline engine emissions for more than thirty years.

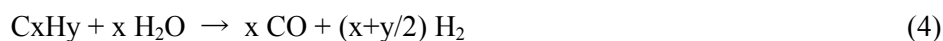
1.2 Three-way catalysis

Three-way catalysis for automotive exhaust purification is one of the most important and interesting processes in vehicle operation. It includes the multiple processes listed below.⁵

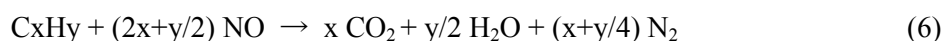
(Oxidation)



(Steam reforming)



(NO reduction)



(Water-gas shift)



These reactions, known as “three-way catalysis”, promote CO oxidation, hydrocarbon oxidation, and NO reduction, simultaneously. The highest conversion of the three components of the exhaust gas (Hydrocarbons, CO and NO) occurs at stoichiometric ratio. The stoichiometric ratio is given by an air to fuel ratio (A/F) of 14.7. However, when the exhaust atmosphere has excess oxygen (a lean atmosphere, A/F > 14.7) or excess reductant (a rich atmosphere, A/F < 14.7), there is a decrease in the conversion of hydrocarbons, CO and NO. Under lean conditions, NO_x conversion decreases because of a shortage of the reductant; while under rich condition, the conversion of CO and hydrocarbons decrease because of a shortage of oxygen. An engine control unit (ECU) controls the stoichiometry of the exhaust atmosphere by monitoring the oxygen concentration, using O₂ sensors in the front and at the bottom of the catalyst bed. The concentration of oxygen in the exhaust strongly affects the three-way catalytic activity. Composition of hydrocarbons, reaction temperature, and the space velocity of the exhaust gas also influence three-way catalytic activity. In practice, the reaction temperature occasionally

rises to 1200 K. Space velocity also varies from 60,000 h⁻¹ under average engine operating conditions, up to 200,000 h⁻¹ during acceleration of the vehicle. In addition, poisoning can affect catalytic activity. Combustion of lubricant oil causes P- and Ca-containing deposits to form on the catalyst surface. Given these factors, maintaining efficient three-way catalytic activity is critical. Moreover, three-way catalysis needs to be active for more than 10 years to ensure their protective role, even under severe reaction conditions.

1.3 New aspects of the three-way catalysis

Reaction conditions for three-way catalysis have changed with new engine developments. The “idling-stop” engine control recently applied to minimize fuel consumption causes a large A/F fluctuation, and exposes catalysts to more oxidizing conditions. The idling-stop control works as follows: engine operation automatically switches off when the car stops for a short period, while releasing the break or engaging other power demands re-starts the engine. Such engine mode changes affect the reaction atmosphere. Typically, auto-exhaust flows to the catalyst converter continuously while cruising or accelerating. When the car stops, the exhaust flow returns to zero. While stopped, the oxygen sensor sometimes indicates that there is excess oxygen in the catalyst bed from an intake. When the engine re-starts, the exhaust again begins to flow over the catalyst. During this whole period, the three-way catalysts continue to convert exhaust gases. Since excess oxygen can deactivate the three-way catalysts through oxidation of the precious metals and their support materials, a precise A/F control or precise camshaft timing to prevent air entering the exhaust is required to suppress A/F fluctuations. However, management of air intake during an idling-stop remains difficult. Adding excess fuel to the combustion re-start after the idling-stop can reduce the oxidized precious metals, but leads to a decrease in fuel economy. Moreover, carbonaceous deposits associated with this measure can deactivate the catalyst by covering their active sites. Thus, there are considerable risks involved to the catalysts in the practical implementation of such measures. To attain a higher fuel economy, increased exposure of the catalysts to excess oxygen appears unavoidable. Hence, we should assume lean exhaust conditions for designing future three-way catalysts.

To minimize A/F fluctuations, oxygen storage components (OSC) comprising cerium-containing oxides have been employed to store and release oxygen. Cerium oxides store oxygen by changing valence state from Ce^{3+} to Ce^{4+} in an oxygen-excess atmosphere. While in an oxygen-deficient atmosphere, they release oxygen from the matrix through reduction of Ce^{4+} to Ce^{3+} . Such processes work well for controlling auto-exhaust fluctuations, contributing to a stable A/F ratio. However, in practice, oxygen storage components can maintain the A/F ratio for only 5 to 10 s. Transient conditions induced by an idling-stop last as long as 10 to 30 s, i.e., they are longer than present oxygen storage components can compensate. Therefore, a new strategy that can cope with these longer transient excess oxygen conditions is required to protect the three-way catalysts.

1.4 Advantages of rhodium under the new catalytic conditions

Precious metals (Pt, Pd and Rh) are the active elements of three-way catalysis. Characteristics of these metals determine the properties of the three-way catalysts. Here, we summarize these properties, and discuss their possibilities under the new three-way catalytic conditions.

1.4.1 Characteristics of precious metals used in catalysis

Rhodium shows excellent catalytic activity compared with the other precious metals (Pt, Pd, Ir and Ag), especially in NO_x conversion. However, its activity decreases with exposure to excess oxygen.⁸ In contrast, platinum is used as an active metal for diesel oxidation catalysts because of its high activity for oxidation of hydrocarbons, CO, and carbon under an excess oxygen atmosphere. However, the activity of platinum under the stoichiometric A/F ratio at which present engines are operating is inferior to that of rhodium, especially for NO_x conversion. Although platinum is effective in the oxidation of CO and hydrocarbons under lean conditions, platinum catalysts must be used with rhodium catalysts to achieve high NO_x conversion at the given stoichiometric A/F ratio.

Palladium also is highly active for CO and hydrocarbon oxidation, but its NO_x conversion also is inferior to that of rhodium. Several reports show that palladium oxide is more active in these oxidation reactions than Pd metal.⁹⁻¹¹ Although palladium may act as an active metal under oxidative conditions, its low NO_x conversion is an important drawback to consider. Therefore, we chose to develop active rhodium catalysts in this study to cope with the oxidative atmosphere of the new three-way catalytic reaction conditions.

1.4.2 Factors affecting rhodium activity

For many reactions, including those in three-way catalysis, particle size, morphology and the oxidation state of metals are crucial factors affecting catalytic activity.¹² In particular, oxidative reaction conditions affect the oxidation state of rhodium, since the valence state of rhodium changes between 0 and 3 under different conditions. It is known that oxidation of rhodium results in a decrease in its three-way catalytic activity, as observed for Rh/Al₂O₃ aged under an oxidizing atmosphere at high temperature.^{13, 14} For CO oxidation, however, the active state of rhodium is the surface oxide.¹⁵⁻¹⁷ Thus, further investigation is needed to clarify the relationship between rhodium oxidation states and its catalytic activity. The maximum temperature of the catalyst bed also influences the particle size of the active metal during engine operations. The higher the temperature of the catalyst bed, the more agglomeration occurs for both the active metal and its support. This increase in particle size leads to a decrease in active surface. The new oxidative reaction conditions may indirectly influence particle size through release of exothermic heat into the catalyst bed. As excess oxygen flows to the catalyst under high temperature, CO oxidation may cause a rapid increase in the catalyst bed temperature on re-start of the engine. In such cases, the catalyst bed temperature could rise over 1173 K. Unexpected increases in the temperature of the catalyst bed can be avoided by adopting an engine control system, which stops the idling-stop, if the temperature reaches a certain value. However, this measure limits the operation of the idling-stop engine control and leads to a decrease in fuel economy. Thus, both starting material and reaction atmosphere influence the size and morphology of rhodium particles, while the oxidative reaction conditions affect particle growth. Hence, suppression of the deactivation of the rhodium catalyst is an important target for research in three-way catalysis.

1.4.3 Advantages and disadvantages of rhodium

Prices of precious metals influence the development of a new three-way catalyst. Rhodium is known to have price risks because it is produced as a by-product of mining platinum and palladium in limited regions (e.g., South Africa). The amount of rhodium production is very small compared to these other precious metals. The automotive industry uses almost 100 % of the rhodium production as exhaust catalysts. Therefore, the unit price of rhodium fluctuates with speculative investments. Although rhodium is a key catalytic element for designing three-way catalyst systems with high NO_x conversion, minimizing rhodium amount is desirable for a stable production cost. In other words, we need to enhance the catalytic activity of rhodium particles using a minimum amount of rhodium.

1.5 Deactivation of rhodium

Oxidation, formation of solid solution and sintering products are major factors in rhodium deactivation. Here, we summarize the drawbacks of using rhodium, and investigate which factor is most affected by the new three-way catalytic atmosphere.

1.5.1 Deactivation caused by the oxidation and the solid solution formation

Oxidative gas conditions accelerate the formation of a solid solution between rhodium and the support. Rhodium aluminate formation was widely studied by H. S. Gandhi and co-workers at the Ford Research Laboratory during early three-way catalyst developments. They found that rhodium undergoes a phase change caused by thermal aging over α -Al₂O₃, γ -Al₂O₃, and zirconia supports, based on measurements of CO adsorption, thermal stability and H₂-NO reactivity.¹⁸ Increasing the aging temperature sharply decreased NO conversion of Rh/ γ -Al₂O₃, while NO conversion for Rh/ α -Al₂O₃ moderately decreased under the increased aging temperature. The rhodium surface concentration for Rh/ γ -Al₂O₃ determined by CO adsorption was far below the saturation value after aging, indicating that there were strong Rh and γ -Al₂O₃ interactions during high temperature aging. In contrast, although Rh/ZrO₂ had lower NO conversion compared to

Rh/ γ -Al₂O₃, little decrease in the activity of the NO-H₂ reaction occurred during aging. H. C. Yao and co-workers also studied the effect of aging temperature on Rh/ γ -Al₂O₃ interactions, using CO and NO chemisorptions.¹⁹ They pointed out that rhodium oxide diffuses into γ -Al₂O₃ during aging above 873 K, leading to the formation of rhodium aluminates. A. T. Bell and co-workers investigated rhodium oxidation states with XPS (X-ray photoelectron spectroscopy).²⁰ They concluded that rhodium in the support oxide matrix was detected as a Rh⁴⁺ signal, with a high binding energy for Rh/ γ -Al₂O₃ aged at 1273 K in air. Many other researchers also reported a strong interaction between rhodium and Al₂O₃.²¹⁻²⁷ A similarity in crystal structure between rhodium oxide and the support oxide enhances rhodate formation. A. T. Bell and co-workers also investigated the phase stability of rhodium oxides in α -Al₂O₃ supported rhodium catalysts aged in air, using high resolution transmission electron microscopy.²⁸ RhO₂ formed at 773 K oxidation, while Rh₂O₃ formed after an oxidation at 1273 K. These oxide phases on the alumina support did not always fit with predicted phases from bulk thermodynamics. These findings demonstrate that epitaxial stabilization of phases plays an important role in solid solution formation. Epitaxy is most pronounced when a facet of the metal oxide particle fits into that of the support. Many researchers have described the formation of cerium-rhodates from rhodium supported on cerium-containing oxides.²⁹⁻³² Given that rhodium oxide is the starting material for rhodate formation, the new oxidative conditions in the three-way catalytic atmosphere may also enhance such rhodate formation. Thus, a zirconia-based oxide appears to be a good candidate for rhodium particle support in the design of a new active three-way catalyst.

1.5.2 Sintering of rhodium particles

Sintering is a process involving the increase in particle size of both precious metals and the support materials at a high temperature, leading to a loss of active surface area. Sintering is one of the main factors causing deterioration of the three-way catalysts, and has been extensively studied over the last decades. Three-way catalysts are often exposed to high temperature exhaust gas during acceleration of vehicles, with temperatures often rising above 1173 K. Sintering processes depend on atmospheric conditions; sintering rates under oxidative conditions are slower than under reductive conditions. A layer of chemisorbed oxygen atoms plays an important role in stabilizing small particles. Relative to other precious metals, rhodium is oxophilic¹², reflecting its lower cohesive energy (or the melting point) compared with platinum and palladium.³³ Under a new three-way catalytic atmosphere that incorporates oxidative exhaust gas, formation of surface oxides could occur through sintering. However, sintering of the rhodium particles during three-way catalysis is not fully understood.

1.6 Measures to inhibit Rh-deactivation

Various measures were studied to ameliorate the disadvantages of using rhodium. We summarize these measures below, and discuss their applicability as measures for a new three-way catalytic condition.

One measure to prevent rhodium deactivation is alteration of the support structure. R. K. Usmen and co-workers investigated the influence of La^{3+} ions on the rhodium-support interaction.³⁴ La incorporated into alumina prevents diffusion of rhodium due to formation of a two-dimensional La-Al structure under high-temperature oxidizing conditions. Both NO conversion and CO conversion were improved by La addition. Combination of oxides, such as CeO_2 and ZrO_2 , with Al_2O_3 is also effective for preventing the interaction of rhodium and Al_2O_3 .³⁵⁻³⁷

Moderate metal-support interaction possibly inhibits sintering of metals. Tanabe and co-workers reported that Rh-O-Nd bonds formed on Nd_2O_3 -enriched zirconia, effectively inhibiting rhodium sintering because these bonds acted as an anchor.³⁸ The bond between rhodium oxide and Nd_2O_3 forms under oxidizing conditions. Such interaction could be due to the similarity of the structure between rhodium oxides and Nd_2O_3 . This type of sintering inhibition has also been reported for platinum catalysts supported on Ce-containing oxides by the same group.³⁹⁻⁴⁵ They have pointed out that both creation of metallic Pt and management of adsorbed carbonaceous species on metallic Pt, are important for achieving high activity under low temperature. Their research has revealed that chemically induced Pt sintering and re-dispersion occur within a few seconds and are reversible. The re-dispersion process progresses under a cyclic atmosphere, with formation of Pt-O-Ce bonds under an oxidative atmosphere, and breaking of these bonds to liberate metallic Pt under a reductive atmosphere. The driving force for this process can be attributed to the formation of PtOx on the support oxide surface. Similar support effects are reported for palladium catalysts.^{9, 10, 46}

Another measure for sintering extent is based on LaFeO_3 perovskite structure. Using X-ray absorption fine-structure (XAFS) analyses, Tanaka and co-workers revealed that the perovskite $\text{LaFe}_{0.95}\text{Pd}_{0.05}\text{O}_3$ has a cyclic exchange of Pd in its crystal structure.⁴⁷⁻⁵³ In-situ XAFS measurements showed that this cycle functions under conditions of real automotive exhaust gases, namely with a self-regenerative function. Rh-containing perovskite has a similar self-regenerative property, exchanging between the perovskite matrices, $\text{A}^{3+}\text{B}^{3+}\text{O}_3$ and



These measures depend on a cyclic condition, involving alternation in rich and lean atmospheres of the automotive exhaust gas. The new three-way catalytic conditions, involve an oxidative atmosphere that could affect these cyclic conditions, especially the re-dispersion processes because of their limited reductive atmospheres. Therefore, sintering inhibition, using metal-support interactions to achieve high conversions after exposure to oxidative conditions, is essential to the design of effective future three-way catalysts.

Machida and co-workers demonstrated that aluminium phosphate ($AlPO_4$) is another promising support for rhodium that inhibits rhodium sintering by interaction between rhodium and the support.^{54, 55} The thermal stability of highly dispersed rhodium particles was maintained by a non-reactive but strong anchoring effect, unlike with a Al_2O_3 support.

Using other oxides, rather than alumina or Ce-containing oxides appears to be a good alternative for rhodium support. Burch and co-workers investigated ZrO_2 as a rhodium support.⁵⁶ They found that Rh/ZrO_2 was more active than Rh/Al_2O_3 during methane oxidation. Temperature-programmed reduction (TPR) results show that zirconia has a weak interaction with rhodium particles. Rhodium supported ZrO_2 -containing alumina also has a high methane oxidation activity after aging at 773 K.⁵⁶ TPR profiles show that the reducibility of rhodium oxide was improved by ZrO_2 addition. Such interactions between rhodium particles and zirconia are worth investigating further, because of the structural flexibility of zirconia as a support material. The non-oxygen storage capacity of zirconia mixed oxides is also a promising factor for designing an active catalyst that can work under the new three-way catalytic conditions, involving an oxidative atmosphere.

1.7 A new strategy for designing effective three-way catalysts

In this thesis, we introduce a new design for active three-way catalysis. To support rhodium, we selected zirconia mixed oxides. A zirconium oxide matrix has a weak interaction with rhodium particles, and can be easily chemically and structurally modified by adding other elements such as alkali earth or lanthanoids.⁵⁷⁻⁵⁹ Moreover, we assume that using a non-oxygen storage material is desirable for a fluctuating exhaust atmosphere, since oxygen storage and release may interfere with rhodium's properties, leading to oxidation of rhodium particles.

Our motives for designing an effective three-way catalyst are listed below:

- 1) To lower the activation temperature (i.e., low light-off temperature)
- 2) To maintain high conversion at high temperature
- 3) To retain high catalytic activity after exposure to oxidative atmospheres

The first objective of this thesis is to develop a highly active three-way catalyst for the new idling-stop engine condition. The second objective is to design an active three-way catalyst based on knowledge of its support interactions. As such, this thesis focuses on the three-way catalysis of rhodium particles supported by La-containing zirconium oxides.

The first chapter (Chapter 2) shows that lanthanoid greatly affects rhodium properties. We show that using rhodium with a La-containing ZrO_2 support effectively eliminates hydrocarbons and NO_x from synthetic auto exhaust. Rhodium particles were able to be maintained at low oxidation state on ZrO_2 - La_2O_3 mixed oxide support, even after treatment with 5% O_2 at 773 K.

Chapter 3 shows that this new catalyst retains its high activity in three-way catalysis after an aging treatment at 1273 K, which simulates 80 000 km of mileage in real vehicles. We introduce a new strategy to keep rhodium active, using the steam reforming reaction that occurs during three-way catalysis as a "self-regenerative" function. We highlight the role of that such a catalyst support plays in designing effective three-way catalysts with a high tolerance to oxidative conditions.

In Chapter 4, we investigate the effect of Y addition to the ZrO_2 -based support, especially on rhodium properties. Our novel highly active three-way catalyst, involving rhodium supported on

Y- and La- containing zirconia is proposed as a new measure for vehicles and engines with idling-stop engine control. Chapter 5 presents a summary and our general conclusions.

References

1. R. N. Colvile, E. J. Hutchinson, J. S. Mindell and R. F. Warren, *Atmos. Environ.*, 2001, **35**, 1537-1565.
2. V. I. Parvulescu, P. Grange and B. Delmon, *Catal. Today*, 1998, **46**, 233-316.
3. M. Iwamoto and H. Hamada, *Catal. Today*, 1991, **10**, 57-71.
4. A. Fritz and V. Pitchon, *Appl. Catal. B*, 1997, **13**, 1-25.
5. G. C. Koltsakis and A. M. Stamatelos, *Prog. Ener. Combust. Sci.*, 1997, **23**, 1-39.
6. M. V. Twigg, *Appl. Catal. B*, 2007, **70**, 2-15.
7. M. V. Twigg, *Catal. Today*, 2011, **163**, 33-41.
8. H. S. Gandhi, G. W. Graham and R. W. McCabe, *J. Catal.*, 2003, **216**, 433-442.
9. Y. Yazawa, H. Yoshida, N. Takagi, S. Komai, A. Satsuma and T. Hattori, *J. Catal.*, 1999, **187**, 15-23.
10. H. Yoshida, T. Nakajima, Y. Yazawa and T. Hattori, *Appl. Catal. B*, 2007, **71**, 70-79.
11. A. K. Datye, J. Bravo, T. R. Nelson, P. Atanasova, M. Lyubovsky and L. Pfefferle, *Appl. Catal. A*, 2000, **198**, 179-196.
12. M. A. Newton, *Chem. Soc. Rev.*, 2008, **37**, 2644-2657.
13. K. Dohmae, T. Nonaka and Y. Seno, *Surf. Inter. Anal.*, 2005, **37**, 115-119.
14. K. Dohmae, Y. Nagai, T. Tanabe, A. Suzuki, Y. Inada and M. Nomura, *Surf. Inter. Anal.*, 2008, **40**, 1751-1754.
15. M. E. Grass, Y. W. Zhang, D. R. Butcher, J. Y. Park, Y. M. Li, H. Bluhm, K. M. Bratlie, T. F. Zhang and G. A. Somorjai, *Angew. Chem. Int. Ed.*, 2008, **47**, 8893-8896.
16. J. Gustafson, R. Westerstrom, O. Balmes, A. Resta, R. van Rijn, X. Torrelles, C. T. Herbschleb, J. W. M. Frenken and E. Lundgren, *J. Phys. Chem. C*, 2010, **114**, 4580-4583.
17. J. Gustafson, R. Westerstrom, A. Resta, A. Mikkelsen, J. N. Andersen, O. Balmes, X. Torrelles, M. Schmid, P. Varga, B. Hammer, G. Kresse, C. J. Baddeley and E. Lundgren, *Catal. Today*, 2009, **145**, 227-235.
18. H. C. Yao, H. K. Stepien and H. S. Gandhi, *J. Catal.*, 1980, **61**, 547-550.
19. H. C. Yao, S. Japar and M. Shelef, *J. Catal.*, 1977, **50**, 407-418.
20. Z. WengSieh, R. Gronsky and A. T. Bell, *J. Catal.*, 1997, **170**, 62-74.

21. M. Zimowska, J. B. Wagner, J. Dzedzic, J. Camra, B. Borzeczka-Prokop and M. Najbar, *Chem. Phys. Lett.*, 2006, **417**, 137-142.
22. C. A. Rice, S. D. Worley, C. W. Curtis, J. A. Guin and A. R. Tarrer, *J. Chem. Phys.*, 1981, **74**, 6487-6497.
23. C. Wong and R. W. McCabe, *J. Catal.*, 1989, **119**, 47-64.
24. J. G. G. Chen, M. L. Colaianni, P. J. J. Chen, J. T. Yates and G. B. Fisher, *J. Phys. Chem.*, 1990, **94**, 5059-5062.
25. D. D. Beck, T. W. Capehart, C. Wong and D. N. Belton, *J. Catal.*, 1993, **144**, 311-324.
26. D. D. Beck and C. J. Carr, *J. Catal.*, 1993, **144**, 296-310.
27. R. Burch, P. K. Loader and N. A. Cruise, *Appl. Catal. A*, 1996, **147**, 375-394.
28. Z. Weng-Sieh, R. Gronsky and A. T. Bell, *J. Catal.*, 1998, **174**, 22-33.
29. S. Bernal, J. J. Calvino, M. A. Cauqui, J. M. Gatica, C. Larese, J. A. P. Omil and J. M. Pintado, *Catal. Today*, 1999, **50**, 175-206.
30. S. Bernal, G. Blanco, J. J. Calvino, G. A. Cifredo, J. A. P. Omil, J. M. Pintado and A. Varo, *New Developments in Selective Oxidation Ii*, 1994, **82**, 507-514.
31. S. Bernal, F. J. Botana, J. J. Calvino, G. A. Cifredo and J. A. Perezomil, *Catal. Today*, 1995, **23**, 219-250.
32. J. M. Gatica, R. T. Baker, P. Fornasiero, S. Bernal, G. Blanco and J. Kaspar, *J. Phys. Chem. B*, 2000, **104**, 4667-4672.
33. D. Bazin, *Top. Catal.*, 2002, **18**, 79-84.
34. R. K. Usmen, R. W. McCabe, L. P. Haack, G. W. Graham, J. Hepburn and W. L. H. Watkins, *J. Catal.*, 1992, **134**, 702-712.
35. S. Suhonen, M. Valden, M. Hietikko, R. Laitinen, A. Savimaki and M. Harkonen, *Appl. Catal. A*, 2001, **218**, 151-160.
36. T. Montini, L. De Rogatis, V. Gombac, P. Fornasiero and M. Graziani, *Appl. Catal. B*, 2007, **71**, 125-134.
37. M. Sugiura, M. Ozawa, A. Suda, T. Suzuki and T. Kanazawa, *Bull. Chem. Soc. J.*, 2005, **78**, 752-767.
38. T. Tanabe, A. Morikawa, M. Hatanaka, N. Takahashi, Y. Nagai, A. Sato, O. Kuno, H. Suzuki and H. Shinjoh, *Catal. Today*, 2012, **184**, 219-226.
39. Y. Nagai, T. Hirabayashi, K. Dohmae, N. Takagi, T. Minami, H. Shinjoh and S. Matsumoto, *J. Catal.*, 2006, **242**, 103-109.
40. Y. Nagai, K. Dohmae, Y. Ikeda, N. Takagi, T. Tanabe, N. Hara, G. Guilera, S.

- Pascarelli, M. A. Newton, O. Kuno, H. Y. Jiang, H. Shinjoh and S. Matsumoto, *Angew. Chem. Inter. Ed.*, 2008, **47**, 9303-9306.
41. H. Shinjoh, M. Hatanaka, Y. Nagai, T. Tanabe, N. Takahashi, T. Yoshida and Y. Miyake, *Top. Catal.*, 2009, **52**, 1967-1971.
42. M. Hatanaka, N. Takahashi, T. Tanabe, Y. Nagai, K. Dohmae, Y. Aoki, T. Yoshida and H. Shinjoh, *Appl. Catal. B.*, 2010, **99**, 336-342.
43. H. Hirata, K. Kishita, Y. Nagai, K. Dohmae, H. Shinjoh and S. Matsumoto, *Catal. Today*, 2011, **164**, 467-473.
44. Y. Nagai, K. Dohmae, Y. Ikeda, N. Takagi, N. Hara, T. Tanabe, G. Guilera, S. Pascarelli, M. A. Newton, N. Takahashi, H. Shinjoh and S. Matsumoto, *Catal. Today*, 2011, **175**, 133-140.
45. T. Tanabe, Y. Nagai, K. Dohmae, N. Takagi, N. Takahashi, S. Matsumoto and H. Shinjoh, *Appl. Catal. B.*, 2011, **105**, 41-49.
46. Y. Yazawa, H. Yoshida and T. Hattori, *Appl. Catal. A.*, 2002, **237**, 139-148.
47. Y. Nishihata, J. Mizuki, H. Tanaka, M. Uenishi and M. Kimura, *J. Phys. Chem. Sol.*, 2005, **66**, 274-282.
48. H. Tanaka, *Catal. Surv. from Asia*, 2005, **9**, 63-74.
49. M. Uenishi, H. Tanaka, M. Taniguchi, I. Tan, Y. Sakamoto, S. Matsunaga, K. Yokota and T. Kobayashi, *Appl. Catal. A.*, 2005, **296**, 114-119.
50. M. Uenishi, M. Taniguchi, H. Tanaka, M. Kimura, Y. Nishihata, J. Mizuki and T. Kobayashi, *Appl. Catal. B.*, 2005, **57**, 267-273.
51. H. Tanaka, I. Tan, M. Uenishi, M. Taniguchi, M. Kimura, Y. Nishihata and J. Mizuki, *J. Alloy. Comp.*, 2006, **408**, 1071-1077.
52. H. Tanaka, I. Tan, M. Uenishi, M. Taniguchi, Y. Nishihata and J. Mizuki, in *Science of Engineering Ceramics Iii*, eds. T. Ohji, T. Sekino and K. Niihara, Editon edn., 2006, vol. 317-318, pp. 827-832.
53. H. Tanaka, M. Uenishi, M. Taniguchi, I. Tan, K. Narita, M. Kimura, K. Kaneko, Y. Nishihata and J. Mizuki, *Catal. Today*, 2006, **117**, 321-328.
54. M. Machida, K. Murakami, S. Hinokuma, K. Uemura, K. Ikeue, M. Matsuda, M. R. Chai, Y. Nakahara and T. Sato, *Chem. Mater.*, 2009, **21**, 1796-1798.
55. K. Ikeue, K. Murakami, S. Hinokuma, K. Uemura, D. J. Zhang and M. Machida, *Bull. Chem. Soc. J.*, 2010, **83**, 291-297.
56. R. Burch and P. K. Loader, *Appl. Catal. A.*, 1996, **143**, 317-335.

57. C. K. Loong, J. W. Richardson, M. Ozawa and M. Kimura, *J. Alloy. Comp.*, 1994, **207**, 174-177.
58. T. Hirata, E. Asari and M. Kitajima, *J. Soli. Stat. Chem.*, 1994, **110**, 201-207.
59. C. K. Loong, P. Thiyagarajan, J. W. Richardson, M. Ozawa and S. Suzuki, *J. Catal.*, 1997, **171**, 498-505.

Chapter 2

Active three-way catalysis of rhodium particles under an oxidative atmosphere on a La-containing ZrO₂ support

Chapter 2: Active three-way catalysis of rhodium particles under an oxidative atmosphere on a La-containing ZrO₂ support

2.1 Introduction

Controlling the oxidation state of an active metal is crucial in the design of effective three-way catalysts used in practical applications, because oxidant and reductant concentrations in a real automotive exhaust change constantly. Rhodium is a key catalyst component as an active metal to convert both hydrocarbons and NO_x effectively.^{1,2} Under oxidative gaseous conditions, rhodium readily forms oxides and tends to react with the alumina support to form other phases at high temperature. These phase changes cause deactivation of the catalyst.³⁻⁷ To minimise the influence of fluctuations in the exhaust gas, oxygen storage components such as CeO₂-ZrO₂ mixed oxides are often used as the support or as an additive element in catalyst layers. Oxygen vacancies associated with Ce³⁺ also provide active sites for the NO-CO reaction⁸, and additives promote the water-gas shift reaction.^{9,10} The oxygen storage capacity, however, can be saturated with large fluctuations of oxygen concentration. Furthermore, the ability of oxygen storage components to control the rhodium oxidation state by minimising the influence of these fluctuations is limited. Thus, it is desirable to develop another strategy to control the state of rhodium in the exhaust gas through the interaction between the support surface and the rhodium particles.

In this chapter, we report that rhodium on lanthanum-containing zirconium oxide is highly active for the elimination of NO_x, carbon monoxide and hydrocarbons (i.e. three-way catalysis) from a synthetic auto exhaust gas under fluctuating air-fuel ratio conditions, even though the support has no oxygen storage capacity. X-ray photoelectron spectroscopy (XPS), CO-temperature programmed reduction (TPR) and transmission electron microscopy (TEM) reveal that rhodium in the reduced form is stabilised on the ZrO₂-La₂O₃ mixed oxide. This phenomenon leads to an improved performance in that the catalyst can immediately start converting auto exhaust gas after treatment with 5% oxygen for 5 min at 773 K, where this mimics typical exhaust gas conditions during “idling-stop” conditions as applied to engine

operation that save fuel by switching off the engine when the car stops.

2.2 Experimental

2.2.1 Catalyst preparation

ZrO₂-La₂O₃ mixed oxide was prepared by an ammonium co-precipitation method. ZrO(NO₃)₂·6H₂O (60.8 g) and La(NO₃)₃·6H₂O (5.2 g) or Pr(NO₃)₃·6H₂O (5.2 g) were dissolved in 200 g of water, followed by addition of an aqueous NH₄OH solution (1.0%) to raise the pH to 12 or more. The precipitate was dried at 423 K for 2h in air, and calcined at 773 K for 2 h in air. The additive content of the lanthanoid was 5.0 wt% as oxide (La₂O₃ or Pr₆O₁₁). The lanthanoid oxide/ZrO₂ mixed oxides are referred to as Zr-La-O and Zr-Pr-O, respectively. Pure ZrO₂ support (BET surface area: 52.3 m² g⁻¹) was purchased from Kishida Chemical Co., Ltd (Osaka, Japan). Rhodium (0.33 wt% as rhodium metal) was loaded on these oxide supports by impregnation using an aqueous solution of Rh(NO₃)₃·H₂O, followed by calcination in air at 773 K. For evaluating the three-way catalytic reaction, the Rh-loaded ZrO₂ mixed oxide catalysts were deposited on a cordierite honeycomb. To do this, the Rh-loaded powder catalysts were mixed with distilled water and colloidal zirconia (ZSL-10D, Dai-ichi Kigenso Kogyo, Osaka, Japan) was used for binding the catalyst powder to the cordierite honeycomb. The slurry-coated cordierite honeycomb was dried at 473 K for 2 h in air, then calcined at 773 K for 2 h in air. The amount of catalyst coated on the cordierite honeycomb was 100 g dm⁻³. The resulting products were termed “fresh” catalysts.

2.2.2 Three-way catalytic studies

The catalytic activity was evaluated using a fixed-bed continuous flow reactor. The Rh/ZrO₂, Rh/Zr-La-O, or Rh/Zr-Pr-O catalysts were dispersed on a Cordierite honeycomb (loading amount: 100 g L⁻¹). The reaction gas was a mixture of 500 ppm C₃H₆, 1000 ppm NO, 0.7% CO, 0.2% H₂, 0.6% O₂, 10% H₂O and the balance of nitrogen. Oxygen, carbon monoxide and hydrogen were added periodically under fluctuating conditions. One cycle of 1.0 Hz frequency consisted of four periods. The first period involved oxygen insertion into the static gas for 0.25 s; the second, no insertion of added gas; the third, insertion of carbon monoxide and hydrogen for 0.25 s; and the last, no insertion resulting in oxygen, carbon monoxide and hydrogen

concentrations changing periodically between 0.43 and 1.86%, 0.7 and 2.9% and 0.20 and 0.74% for the three gases, respectively. The flow rate of the reaction gas was $26 \text{ dm}^3 \text{ min}^{-1}$ corresponding to a GSHV of $60,000 \text{ h}^{-1}$. Before measurement of the catalytic performance, the catalysts were pre-treated under a flow of gas mixture at 773 K for 10 min and then cooled to 373 K under flowing nitrogen. Products were analysed continuously using a flame ionization detector for hydrocarbon, infrared for carbon monoxide, and chemical luminescence for NO contents with a Horiba MEXA-9100 evaluation system (Kyoto, Japan).

2.2.3 Characterization

For each of the characterization techniques described in sections 2.2.3.1–2.2.3.4, catalysts were used in powder form without the cordierite honeycomb.

2.2.3.1 Transmission electron microscopy (TEM)

TEM images were taken with a JEM-3000F microscope (JEOL Ltd., Japan). To image the catalyst following the catalytic reaction, the samples were treated under the reaction gas at 773 K for 10 min followed by cooling to room temperature under a nitrogen flow prior to specimen preparation.

2.2.3.2 X-ray photoelectron spectroscopy (XPS)

XPS spectra were obtained with a PerkinElmer ESCA5600 by using Mg K α radiation (400 W). Binding energies were referred to as C1s (284.5 eV). Before measurement of the XPS spectra, two types of pre-treatment were carried out. The first pre-treatment method was used to obtain information on rhodium during the reaction using TEM measurements, where samples were treated under the reaction gas at 773 K for 10 min and then cooled to room temperature under nitrogen flow. The other was to obtain information on rhodium under oxidative gas conditions, where samples were pre-treated under a flow of 5.0% O₂ at 773 K for 10 min, and then cooled to room temperature under nitrogen flow.

2.2.3.3 Temperature-programmed reduction using CO (CO-TPR)

CO-TPR was carried out using CO (0.6%)/He as reducing gas ($100 \text{ cm}^3 \text{ min}^{-1}$) at a heating rate of 30 K min^{-1} . Prior to TPR measurements, samples were pre-treated under a flow of 5.0% O₂ at 773 K for 10 min, and then cooled to 323 K under a flow of helium.

2.2.3.4 Other characterization

Rhodium dispersions were measured by using a CO pulse chemisorption method at 300 K. The catalysts were pre-treated as follows: the catalysts were first heated in a flow of O₂ at 573 K (heating rate: 30 K min⁻¹) for 10 min; the catalyst temperature was then raised to 673 K, in a H₂ flow, and maintained at this temperature for 10 min prior to cooling to 300 K in a He flow. A thermal conductivity detector was used for measuring the concentration of CO. The dispersion was calculated from the CO uptake, assuming that CO adsorbed on the surface of the Rh particles at a stoichiometry ratio of CO:Rh = 1:1.¹³ The specific surface area of the catalysts was measured, using the BET one-point method, on a Shimadzu Micromeritics Flowsorb 2300.

2.3 Results and Discussion

2.3.1 Three-way catalytic activity under fluctuating atmosphere

Table 2.1 compares the conversions of hydrocarbons, carbon monoxide and NO_x at 673 K under static conditions and fluctuating oxygen conditions. NO_x conversion for Rh/ZrO₂ under static conditions was 95.6%, but under fluctuating oxygen conditions, the conversion decreased to 53.2%. The decrease in NO_x conversion under the fluctuating oxygen conditions are due to the large amount of oxygen content that mimics exhaust gas during “idling stop” engine operation. Similar results were obtained for Rh/Zr–Pr–O; NO_x conversion decreased to 58.6% under fluctuating oxygen conditions, while the catalyst showed 92.3% NO_x conversion under static conditions. Rh/Zr–La–O exhibited a 95.4% NO_x conversion under static conditions, and showed as high as 73.2% NO_x conversion under fluctuating conditions. The selectivity to N₂ and CO₂ for each catalyst was almost equal to 100% at 673K indicating neither production of N₂O nor coke formation on the catalysts. These results demonstrate that Rh/Zr–La–O converts NO_x under fluctuating conditions much more efficiently than Rh/ZrO₂ and Rh/Zr–Pr–O, even though the catalyst has no oxygen storage capacity unlike the cerium-containing oxides. This performance is notable because most of three-way catalysts show low activity for NO_x conversion under the fluctuating oxygen.

Table 2.1 Effect of oxygen fluctuation on conversion at 673 K

Catalyst	Conversion (%) under static conditions			Conversion (%) under fluctuating oxygen		
	HC	CO	NO _x	HC	CO	NO _x
Rh/ZrO ₂	98.2	97.2	95.6	96.5	99.2	53.2
Rh/Zr–La–O	98.7	97.8	95.4	98.7	98.9	73.2
Rh/Zr–Pr–O	96.4	96.6	92.3	96.2	94.4	58.6

2.3.2 Particles size and rhodium dispersion

TEM micrographs (Fig. 2.1) reveal that the size of the rhodium particles on Zr–La–O was similar to that on ZrO₂. In Rh/ZrO₂, rhodium particles (2–5 nm in size) were seen clearly at the surface of the ZrO₂ primary particles (Fig. 2.1 a). In the case of Rh/Zr–La–O, rhodium particles (~2 nm in size) were detected (Fig. 2.1 b). BET surface areas of Rh/ZrO₂, Rh/Zr–La–O and Rh/Zr–Pr–O were 53.2, 85.8, and 99.1 m² g⁻¹, respectively. Rh dispersions determined by CO adsorption at 300 K of Rh/ZrO₂, Rh/Zr–La–O and Rh/Zr–Pr–O were 54.9 %, 87.4 % and 83.3 %, respectively. Though Rh/Zr–La–O showed much higher activity compared to Rh/Zr–Pr–O under oxygen fluctuation, the two catalysts have almost the same rhodium dispersion. Thus, the Rh dispersion cannot explain the high performance of Rh/Zr–La–O. The order of the particle size, Rh dispersion and the surface areas does not coincide with that of the catalytic performance.

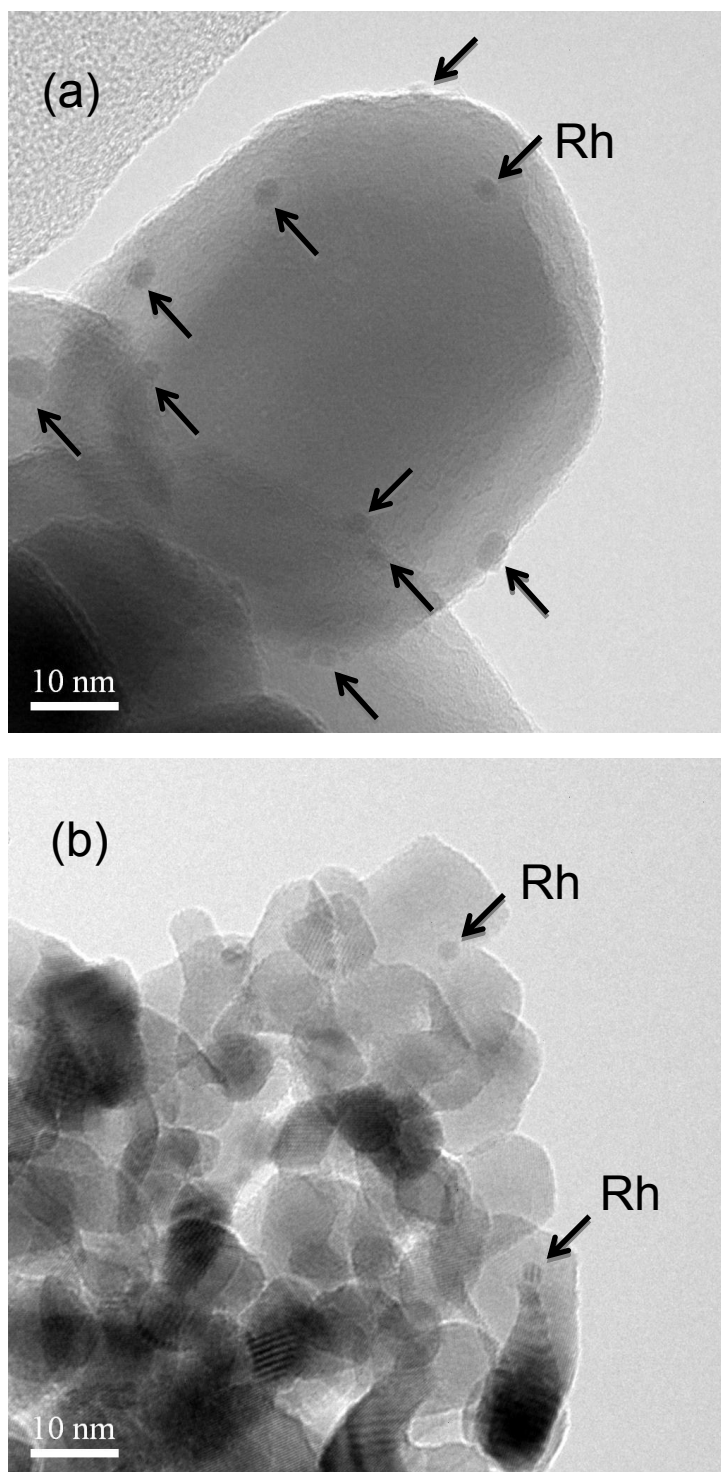


Fig. 2.1 TEM micrographs of fresh (a) Rh/ZrO₂, (b) Rh/Zr-La-O after three-way catalytic reaction at 773 K for 10 min.

2.3.3 Rhodium oxidation state

To identify the rhodium particle state, catalysts were investigated after two types of pre-treatment by XPS. Rhodium 3d XPS spectra of the catalysts after treatment with the reaction gas at 773 K are shown in Fig. 2.2(A). The rhodium 3d_{5/2} peak appeared at 307.2 eV for Rh/ZrO₂ (Fig. 2.2(A) a), and that for Rh/Zr-La-O (Fig. 2.2(A) c) is assigned to metallic rhodium. The rhodium 3d_{5/2} peak of Rh/Zr-Pr-O (Fig. 2.2(A) b) appeared at a binding energy of 307.8 eV, which is slightly higher than those of Rh/Zr-La-O and Rh/ZrO₂ and indicates that the rhodium on Zr-Pr-O is partially oxidised during a three-way catalytic reaction. Rhodium is known to exhibit catalytic performance in reduced form for three-way catalytic reactions.¹¹ Furthermore, XPS spectra after treatment with 5% O₂ at 773 K demonstrate a clear difference in rhodium oxidation state depending on the supports. For Rh/ZrO₂ and Rh/Zr-Pr-O, peaks at 308.7 eV assignable to Rh₂O₃ were observed. Rhodium atoms are not incorporated into the lattice of oxide supports, because no Rh 3d signal typical for such state was observed at around 310 eV.⁷ In contrast, the rhodium 3d peak of Rh/Zr-La-O was observed at 307.9 eV. This indicates that part of the rhodium remained in reduced form, or that the rhodium adopted an oxidation state lower than 3 (i.e. $x < 3$ in Rh₂O_x). In other words, rhodium is oxidised to Rh₂O₃ for Rh/ZrO₂ and Rh/Zr-Pr-O after oxygen treatment, but rhodium particles dispersed on Zr-La-O were not readily oxidised even under a flow of 5% O₂ at 773 K.

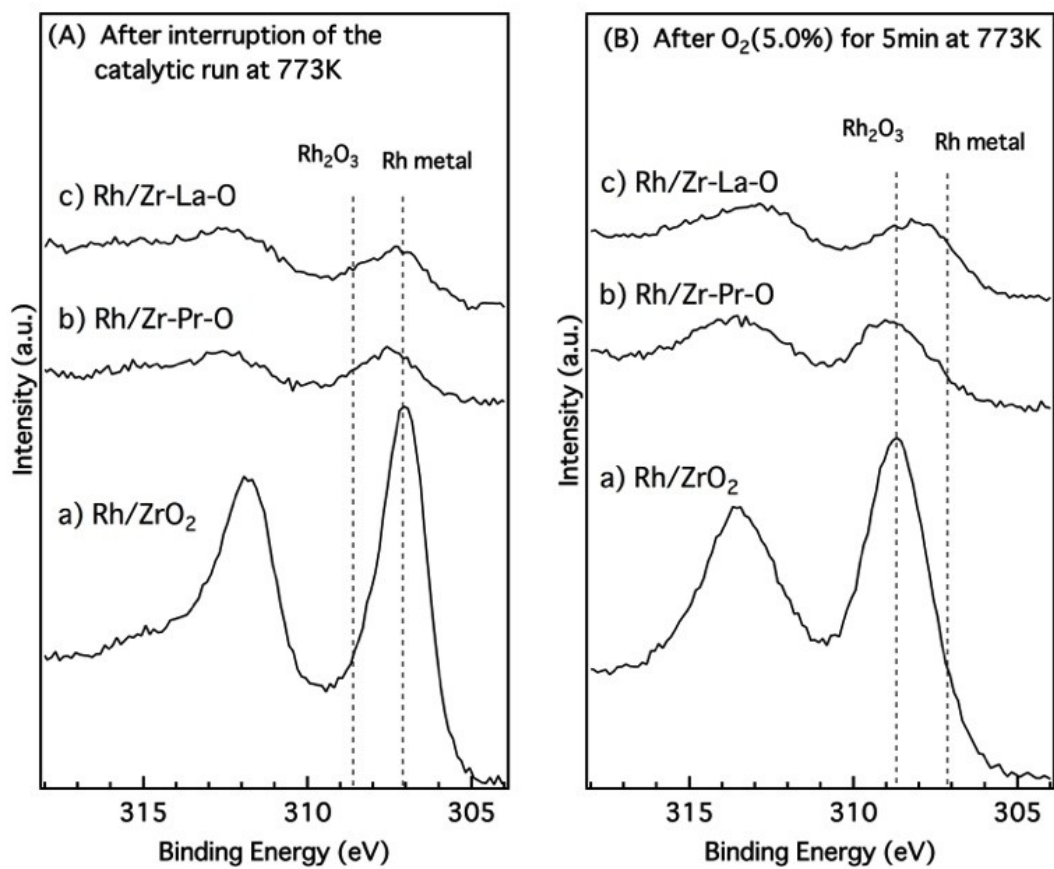


Fig. 2.2 Rhodium 3d XPS spectra of catalysts after pre-treatment with three-way catalytic reaction gas at 773 K (A) and after pre-treatment with 5% O₂ at 773 K (B).

2.3.4 Rhodium property

CO-TPR measurements were carried out to confirm quantitatively the oxidation state of the rhodium on the catalysts (Fig. 2.3). After oxidation pre-treatment, the amount of CO₂ formed during TPR was evaluated using a mass spectrometer. The supports without rhodium were also measured and the amount of evolved carbon dioxide subtracted from the data of the rhodium-containing catalysts to estimate the rhodium oxidation states. The O/Rh ratio calculated from the TPR data was 0.14 for Rh/ZrO₂. The rhodium state of Rh/ZrO₂ as analysed by XPS after exposure to 5% O₂ was trivalent (Rh₂O₃). Since the XPS technique analyzes only the metal surface with a depth of sub-nano order, the experimental results indicate that the rhodium particles on Rh/ZrO₂ are oxidised to Rh₂O₃ only at the particle surface, and these surface Rh₂O₃ were easily reduced by carbon monoxide (Fig. 2.3b). Similar results have also been reported by Burch and Loader.¹² They pointed out that rhodium supported on zirconium was easily reduced by carbon monoxide at around 473 K.

The O/Rh ratio calculated from the CO-TPR data for Rh/Zr-Pr-O is 1.57, which is almost equal to the stoichiometric value. XPS results for Rh/Zr-Pr-O after exposure to 5% O₂ show the presence of Rh₂O₃. These results indicate that almost all of the rhodium particles on the Zr-Pr-O are oxidised to Rh₂O₃ after the oxidation pre-treatment. In contrast, the O/Rh ratio for Rh/Zr-La-O was 0.79. This value is in agreement with the XPS results for Rh/Zr-La-O where the rhodium oxidation state remained between Rh⁰ and Rh³⁺ even after oxidation pre-treatment.

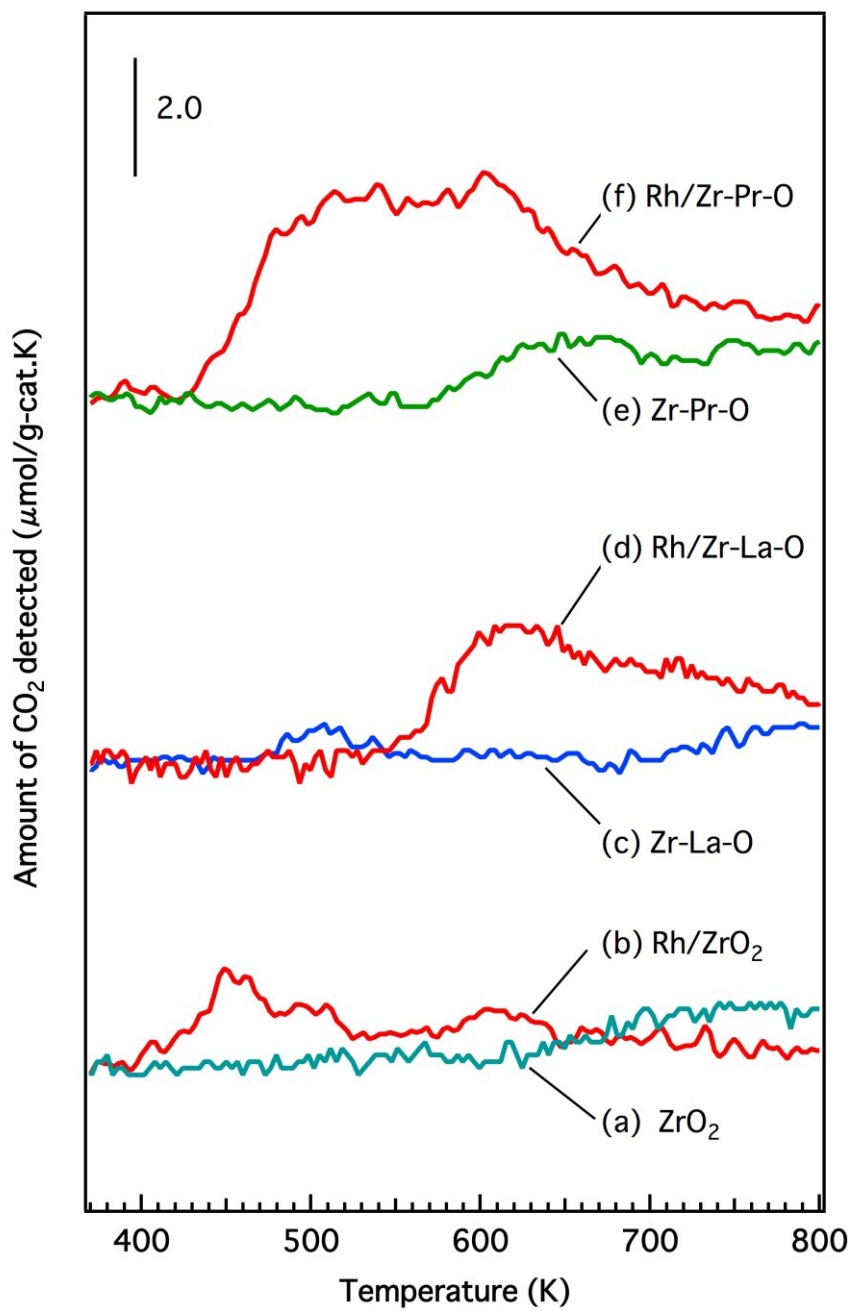


Fig. 2.3 CO-TPR of fresh (a)ZrO₂, (b)Rh/ZrO₂, (c) Zr-La-O, (d) Rh/Zr-La-O, (e) Zr-Pr-O and (f) Rh/Zr-Pr-O after 5% O₂/He treatment for 10 min at 773 K.

2.4 Conclusion

All results obtained in this study demonstrate that rhodium on the Zr–La–O support can be stabilised at a relatively lower valence state. This phenomenon brought about the high catalytic performance of Rh/Zr–La–O under fluctuating oxygen conditions even though the catalyst has no oxygen storage function. This outstanding property of rhodium on Zr–La–O is most likely a result of the interaction between the metal particles and the La-containing support. These results highlight a probable new strategy for highly active three-way catalysts by controlling the oxidation state of the nano-sized metal particles while taking advantage of the metal-support interaction. We confirmed that Rh/Zr–La–O maintained remarkable performance under oxygen fluctuated condition after aging in a stream of 2% O₂, 10% H₂O/N₂ at 1273 K for 24 h. More detailed analysis of aged catalysts is represented in Chapter 3.

References

1. H. S. Gandhi, G. W. Graham and R. W. McCabe, *J. Catal.*, 2003, 216, 433-442.
2. K. C. Taylor, *Catalysis Reviews-Science and Engineering*, 1993, 35, 457-481.
3. C. Wong and R. W. McCabe, *J. Catal.*, 1989, 119, 47-64.
4. J. G. G. Chen, M. L. Colaianni, P. J. J. Chen, J. T. Yates and G. B. Fisher, *J. Phys. Chem.*, 1990, 94, 5059-5062.
5. R. W. McCabe, R. K. Usmen, K. Ober and H. S. Gandhi, *J. Catal.*, 1995, 151, 385-393.
6. Z. Weng-Sieh, R. Gronsky and A. T. Bell, *J. Catal.*, 1998, 174, 22-33.
7. K. Dohmae, T. Nonaka and Y. Seno, *Surface and Interface Analysis*, 2005, 37, 115-119.
8. J. G. Nunan, H. J. Robota, M. J. Cohn and S. A. Bradley, *J. Catal.*, 1992, 133, 309-324.
9. A. Trovarelli, *Catalysis Reviews-Science and Engineering*, 1996, 38, 439-520.
10. T. Bunluesin, R. J. Gorte and G. W. Graham, *Appl. Catal. B*, 1998, 15, 107-114.
11. R. K. Usmen, R. W. McCabe, L. P. Haack, G. W. Graham, J. Hepburn and W. L. H. Watkins, *J. Catal.*, 1992, 134, 702-712.
12. R. Burch and P. K. Loader, *Appl. Catal. A*, 1996, 143, 317-335.
13. J. A. Anderson, M. Fernandez Garcia (Eds.), *Supported Metals in Catalysis*, ICP, London, 2005, p.140.

Chapter 3

Self-regeneration of three-way catalyst rhodium supported on La-containing ZrO_2 in an oxidative atmosphere

Chapter 3: Self-regeneration of three-way catalyst rhodium particles on a La-containing ZrO₂ support under an oxidative atmosphere

3.1 Introduction

Three-way catalysis for automotive exhaust purification is one of the most important and interesting processes that has been extensively applied for numerous years.¹⁻⁵ Although catalysts for three-way catalytic reactions have been studied to improve catalytic activity and durability, the development of efficient catalysts to comply with the stringent emission regulations, adopted worldwide, remains a challenge.

The conditions to which the catalyst is subjected in an automotive exhaust are severe because of rapid temperature rises, accumulation of deposits on the catalyst layer, and fluctuation of the gas phase composition that depends on the state of engine operation. The most influential condition that impedes on the catalytic activity is atmospheric change, as instigated by changes in the oxidant and reductant concentrations. Recently, a new engine operation was commercialized to minimize fuel consumption—the engine automatically switches off when the car stops for a short while. This new operation creates increased transient and fluctuating conditions, including a high oxygen concentration that impedes on the efficiency of the three-way catalytic process.

Rhodium is a catalytically active key component of a three-way catalyst for the effective conversion of CO, hydrocarbons, and NO_x to H₂O, CO₂, and N₂.^{6,7} However, under oxidative gaseous conditions, rhodium readily forms oxides and tends to react with the alumina support to form other phases at high temperatures. These phase changes cause deactivation of the catalyst.⁸⁻¹² Therefore, controlling the oxidation state of the active rhodium is crucial for the design of highly efficient, rhodium-based, three-way catalysts for practical applications.

To minimize the influence of fluctuations in the exhaust gas, oxygen storage components, such as CeO₂–ZrO₂ mixed oxides, are often used as the support or as additive elements as catalyst layers. The oxygen vacancies associated with Ce³⁺ provide active sites for the NO–CO reaction¹³ and the additives promote the water–gas shift reaction.^{14,15}

In Chapter 2, we have demonstrated the high catalytic activity of rhodium-supported La-containing ZrO₂ for the elimination of NO_x, CO, and hydrocarbons, *via* a three-way catalytic process, from a synthetic auto exhaust gas under fluctuating air–fuel ratio conditions in the absence of an oxygen storage capacity.¹⁶ The use of the La-containing ZrO₂ support stabilized

the reduced form of rhodium, obtained after treatment with 5% of oxygen for 5 min at 773 K. In contrast, rhodium-supported ZrO_2 showed a much lower activity when subjected to fluctuating oxygen conditions.

This chapter examines the structure and performance of catalysts, aged under oxidative conditions. The oxidation state of the aged catalyst was affected by the steam reforming reaction. The produced hydrogen effectively promoted the self-regeneration of the oxidized catalyst. The findings highlight the potential of the herein developed materials as an effective support in three-way catalysts suited for recently developed vehicles and new engine operations.

3.2 Experimental

3.2.1 Catalyst preparation

The lanthanoid- (La, Ce, Pr, or Nd) containing ZrO_2 mixed oxides were prepared by an ammonia-assisted co-precipitation method. The content of the lanthanoid oxide was 5 wt%. $\text{La}(\text{NO}_3)_3 \cdot 6\text{H}_2\text{O}$ (99.9%), $\text{Ce}(\text{NO}_3)_3 \cdot 6\text{H}_2\text{O}$ (99.9%), $\text{Pr}(\text{NO}_3)_3 \cdot 6\text{H}_2\text{O}$ (99.9%), and $\text{Nd}(\text{NO}_3)_3 \cdot 6\text{H}_2\text{O}$ (99.9%) were purchased from RARE METALLIC Co., Ltd. (Japan). In a typical synthesis, $\text{ZrO}(\text{NO}_3)_2 \cdot 6\text{H}_2\text{O}$ (60.8 g, >98%, nacalai tesque) and $\text{La}(\text{NO}_3)_3 \cdot 6\text{H}_2\text{O}$ (5.2 g) were first dissolved in 200 g of water, to which an aqueous NH_4OH solution (1%, Wako Pure Chemical Industries, Ltd., Osaka, Japan) was added to raise the solution pH (≥ 12). The obtained precipitate was separated from the reaction solution, dried at 423 K for 2 h in air, and then calcined at 773 K for 2 h in air to produce the ZrO_2 - La_2O_3 mixed oxide. The lanthanoid oxide/ ZrO_2 mixed oxides are referred to as Zr-La-O, Zr-Ce-O, Zr-Pr-O, and Zr-Nd-O, respectively. The ZrO_2 support (Brunauer-Emmett-Teller (BET) surface area: $52.3 \text{ m}^2 \text{ g}^{-1}$) was purchased from Kishida Chemical Co., Ltd (Osaka, Japan). Rhodium (0.33 wt% as rhodium metal) was loaded on the oxide support by impregnation, using an aqueous solution of $\text{Rh}(\text{NO}_3)_3 \cdot \text{H}_2\text{O}$ (Dai-ichi Kigenso Kogyo, Osaka, Japan). The obtained Rh-loaded oxide supports were dried at 393 K for 12 h in air and subsequently calcined in air at 773 K. The resulting catalysts are termed as fresh catalysts.

3.2.2 Three-way catalytic studies

The activity of the prepared Rh-based catalysts was evaluated using a fixed-bed continuous flow reactor. For evaluation of the three-way catalytic reaction, the Rh-loaded lanthanoid-containing ZrO_2 mixed oxides catalysts were coated on a cordierite honeycomb using the following process. The Rh-loaded powder catalysts were mixed with distilled water and colloidal zirconia (ZSL-10D, Dai-ichi Kigenso Kogyo, Osaka, Japan) that was used for binding the catalyst powder to the cordierite honeycomb. The mixed slurry-coated cordierite honeycomb was dried at 473 K for 2 h in air, then calcined at 773 K for 2 h in air. The amount of catalyst coated on the cordierite honeycomb was 100 g dm^{-3} . The reaction gas was a mixture of 500 ppm C_3H_6 ,

1000 ppm NO, 0.7% CO, 0.2% H₂, 0.6% O₂, 10% H₂O. Nitrogen was used as a diluent. The gas composition mimics the actual exhaust gas emitted at ~3000 rpm of engine operation. The flow rate of the reaction gas was 26 dm³ min⁻¹ that corresponds to a gas hourly space velocity of 60 000 h⁻¹. Prior to catalytic performance measurements, the catalysts were pre-treated under a flow of the gas mixture at 773 K for 10 min and then cooled to 373 K under a flow of nitrogen. The three-way catalytic activity was evaluated across a range of temperatures from 373 to 773 K (heating rate: 30 K min⁻¹). The products were monitored using a flame ionization detector for hydrocarbon, infrared absorption for CO, and chemical luminescence for NO on a Horiba MEXA-9100 evaluation system (Kyoto, Japan).

3.2.3 Aging procedure

Accelerated durability tests, or aging treatments, were conducted by treating the fresh catalysts at 1273 K for 24 h in a 2 % O₂ and 10 % H₂O atmosphere (diluent: N₂). This aging treatment simulated empirically a 80 000 km of mileage for real vehicles.

3.2.4 Steam-reforming reaction

The reaction gas was a mixture of 660 ppm C₃H₆ and 2 % H₂O (molar ratio of H₂O/C=10). Nitrogen was used as a diluent. The flow rate of the steam-reforming reaction gas was 26 dm³ min⁻¹ that corresponds to an hourly gas space velocity of 60000 h⁻¹. The activity of the steam-reforming reaction was measured using a fixed-bed continuous flow reactor the same as three-way catalytic activity measurements. Prior to the activity evaluations, the catalyst was pre-treated under three-way catalytic reaction gas at 773 K for 10 min and then cooled to 373 K under a flow of nitrogen.

3.2.5 Characterization

3.2.5.1 X-ray diffraction (XRD)

Powder XRD patterns were measured on a RINT-2000 (Rigaku) using monochromated Cu K α ($\lambda = 1.54056 \text{ \AA}$). Crystalline phases were identified using PDF files. The mean crystal size of the powders was determined using the Scherer's equation.

3.2.5.2 Transmission electron microscopy (TEM)

TEM images were taken on a JEM-3000F microscope (JEOL Ltd., Japan). To image the catalyst

following the catalytic reaction, the samples were treated under the reaction gas at 773 K for 10 min followed by cooling to room temperature under a nitrogen flow prior to specimen preparation.

3.2.5.3 X-ray photoelectron spectroscopy (XPS)

XPS spectra were recorded on a PerkinElmer ESCA5600, using Mg K α (400 W, 1253.6 eV). Binding energies are referred as C1s (284.5 eV). Prior to XPS measurements, the samples underwent two types of treatments. One process involved treatment with the reaction gas at 773 K for 10 min followed by cooling to room temperature under a nitrogen flow. The other treatment was conducted under a flow of 5% O₂ at 773 K for 10 min followed by cooling to room temperature under a nitrogen flow.

3.2.5.4 Temperature-programmed reduction using CO (CO-TPR)

CO-TPR was carried out using CO (0.6%)/He as the reductant gas (100 cm³ min⁻¹) at a heating rate of 30 K min⁻¹. Prior to the TPR measurements, samples were pre-treated under a flow of 5% O₂ at 773 K for 10 min, and then cooled to 323 K under a flow of helium.

3.2.5.5 Other characterization

Rhodium dispersions were measured by using a CO pulse chemisorption method at 300 K. The catalysts were pre-treated as follows: the catalysts were first heated in a flow of O₂ at 573 K (heating rate: 30 K min⁻¹) for 10 min; the catalyst temperature was then raised to 673 K, in a H₂ flow, and maintained at this temperature for 10 min prior to cooling to 300 K in a He flow. A thermal conductivity detector was used for measuring the concentration of CO. The dispersion was calculated from the CO uptake, assuming that CO adsorbed on the surface of the Rh particles at a stoichiometry ratio of CO:Rh = 1:1. The specific surface area of the catalysts was measured, using the BET one-point method, on a Shimadzu Micromeritics Flowsorb 2300.

3.3 Results

3.3.1 Effect of oxygen on the performance of the three-way rhodium-based catalysts

As mentioned earlier, tolerance against oxidative conditions is a very important criterion for three-way catalysts in view of the recent developments in engine operations. The effect of oxidation treatments on the performance of the fresh (Figs. 3.1 and 3.2) and aged (Figs. 3.3 and 3.4) catalysts is discussed. The oxidation treatment was conducted in 5% oxygen at 773 K for 10 min. Both fresh and aged Rh/Zr–La–O catalysts were highly tolerant to the oxidation treatment when compared with the other Rh-supported catalysts. All fresh catalysts, except for Rh/Zr–Pr–O, showed comparable hydrocarbon conversions prior to the oxidation treatment, as shown in Fig. 3.1a. Contrarily, after the oxidation treatment, Rh/Zr–La–O showed the best activity among the catalysts tested (Fig. 3.1b). The catalytic performance decreased in the order of Rh/Zr–La–O > Rh/ZrO₂ > Rh/Zr–Nd–O > Rh/Zr–Ce–O > Rh/Zr–Pr–O. Similar results were obtained for the NO_x conversion, as shown in Fig. 3.2. Rh/Zr–La–O also exhibited the best performance after the oxidation treatment.

In the case of the aged catalysts, the superior efficiency of Rh/Zr–La–O was more distinct: the catalyst showed a significantly high performance even after the oxidation treatment. Figure 3.3 shows the conversion of hydrocarbon by the aged catalysts. The hydrocarbon conversion efficiency was highly dependent on the support, as shown in Fig. 3.3a. After the oxidation treatment, the conversion curves of all the tested catalysts shifted to higher temperatures, but the Rh/Zr–La–O catalyst maintained a relatively high performance in contrast to the other catalysts (Fig. 3.3b).

As observed in Fig. 3.4a, in the absence of the oxidation treatment, aged Rh/Zr–Ce–O and Rh/Zr–Nd–O were more effective than aged Rh/Zr–La–O, towards NO_x conversion. The conversion curves of aged Rh/Zr–Ce–O and Rh/Zr–Nd–O catalysts, which underwent the oxidation pre-treatment, were shifted to a much higher temperature (Fig. 3.4b). As a result, aged Rh/Zr–La–O exhibited a superior performance over the other catalysts. It is worth noting that this performance was achieved after the aging treatment that simulates 80 000 km of mileage in real vehicles.

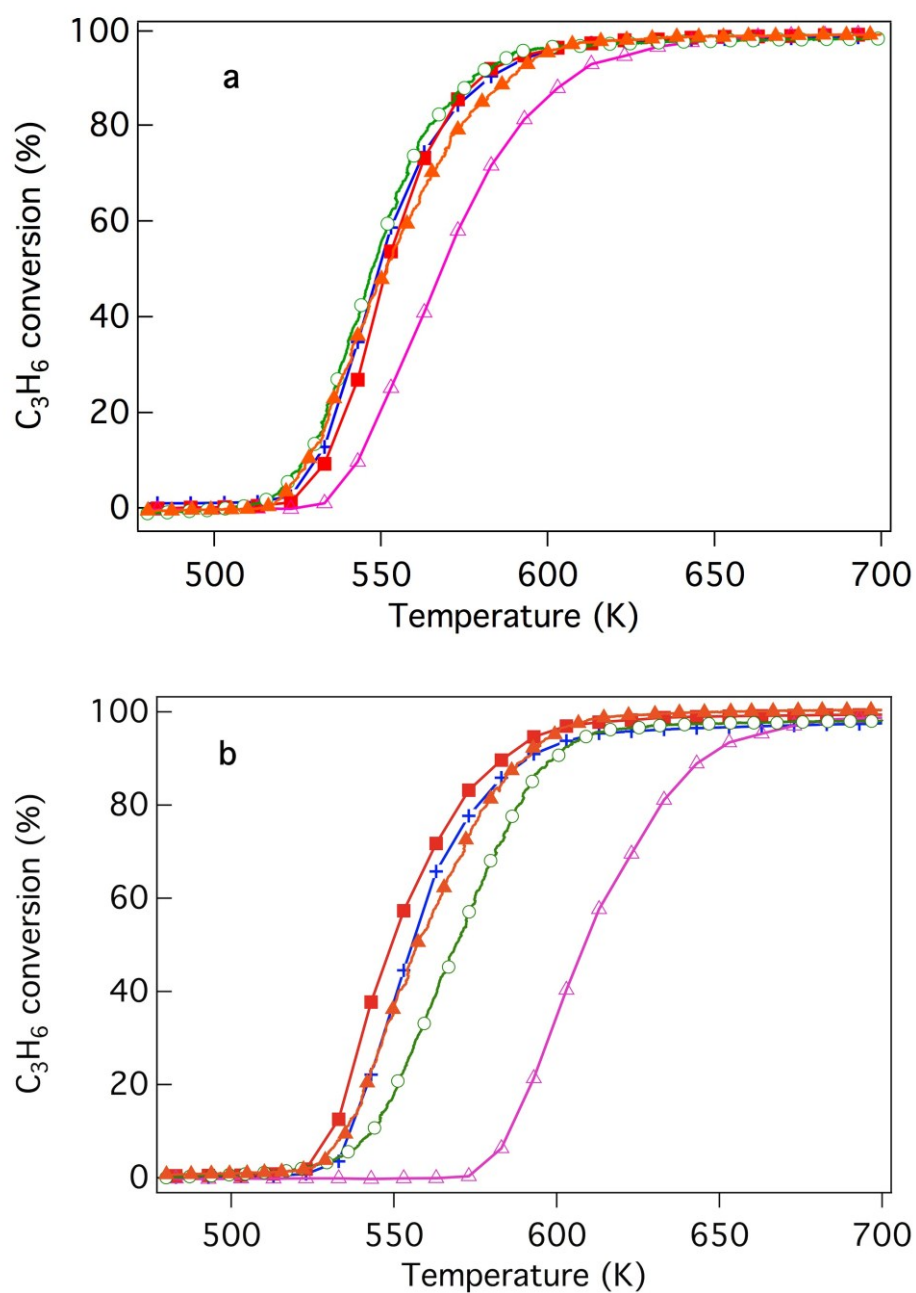


Fig. 3.1 C_3H_6 conversion by the fresh three-way catalysts that underwent (a) no oxidation treatment and (b) an oxidation treatment. The catalysts studied are (+) Rh/ZrO₂, (■) Rh/Zr-La-O, (○) Rh/Zr-Ce-O, (△) Rh/Zr-Pr-O, and (▲) Rh/Zr-Nd-O.

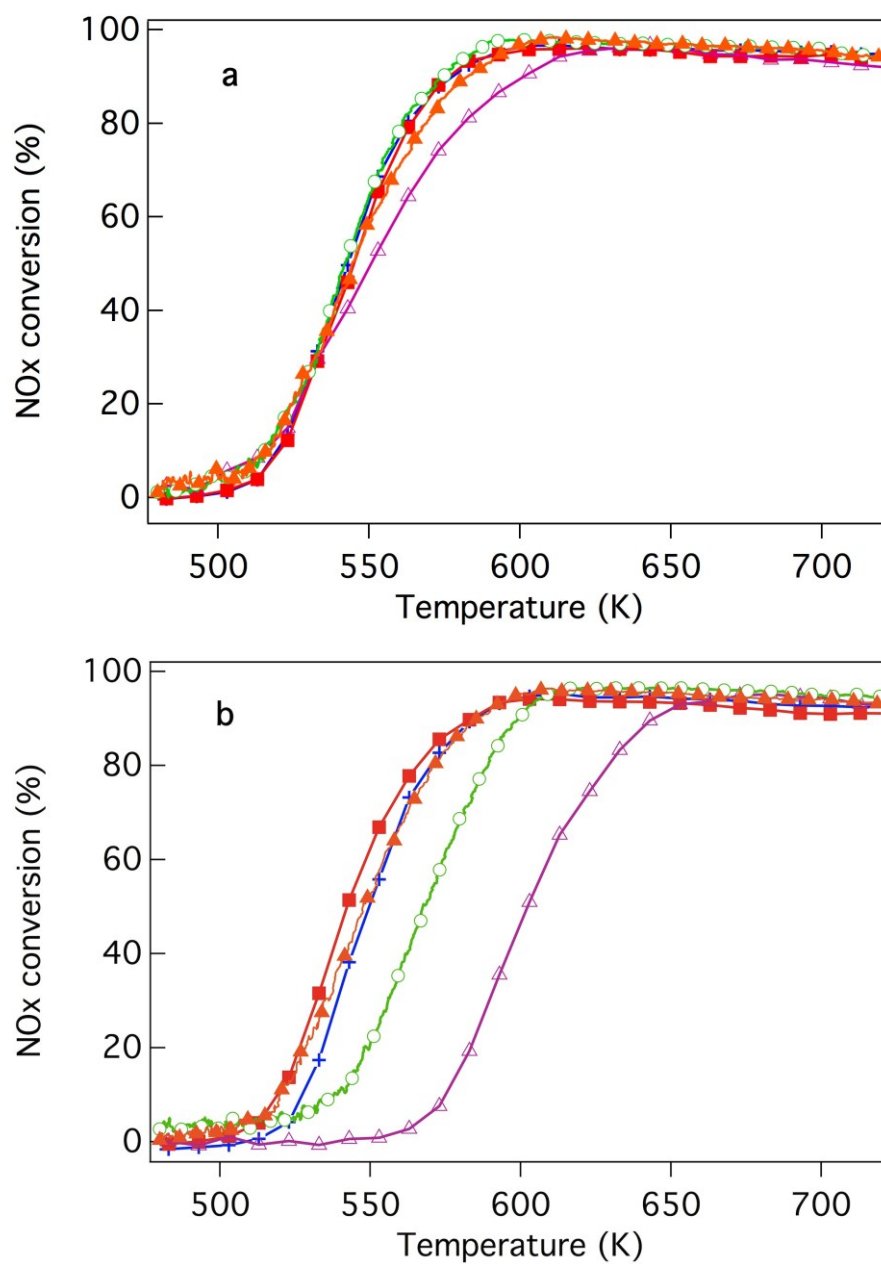


Fig. 3.2 NO_x conversion by the fresh three-way catalysts that underwent (a) no oxidation treatment and (b) an oxidation treatment. The catalysts studied are (+) Rh/ZrO₂, (■) Rh/Zr-La-O, (○) Rh/Zr-Ce-O, (△) Rh/Zr-Pr-O, and (▲) Rh/Zr-Nd-O.

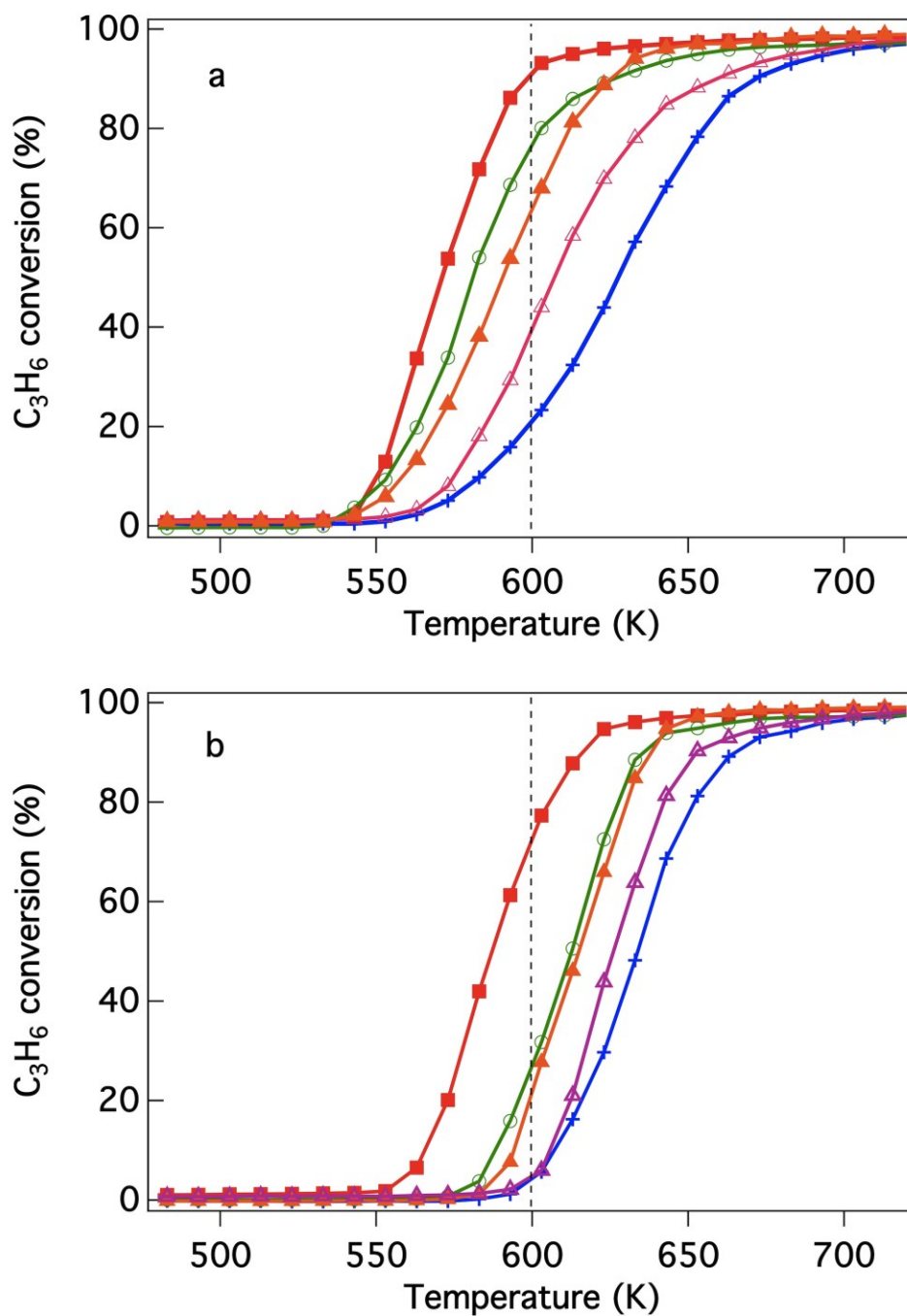


Fig. 3.3 C_3H_6 conversion by the aged three-way catalysts that underwent (a) no oxidation treatment and (b) an oxidation treatment. The catalysts studied are (+) Rh/ZrO₂, (■) Rh/Zr-La-O, (○) Rh/Zr-Ce-O, (△) Rh/Zr-Pr-O, and (▲) Rh/Zr-Nd-O.

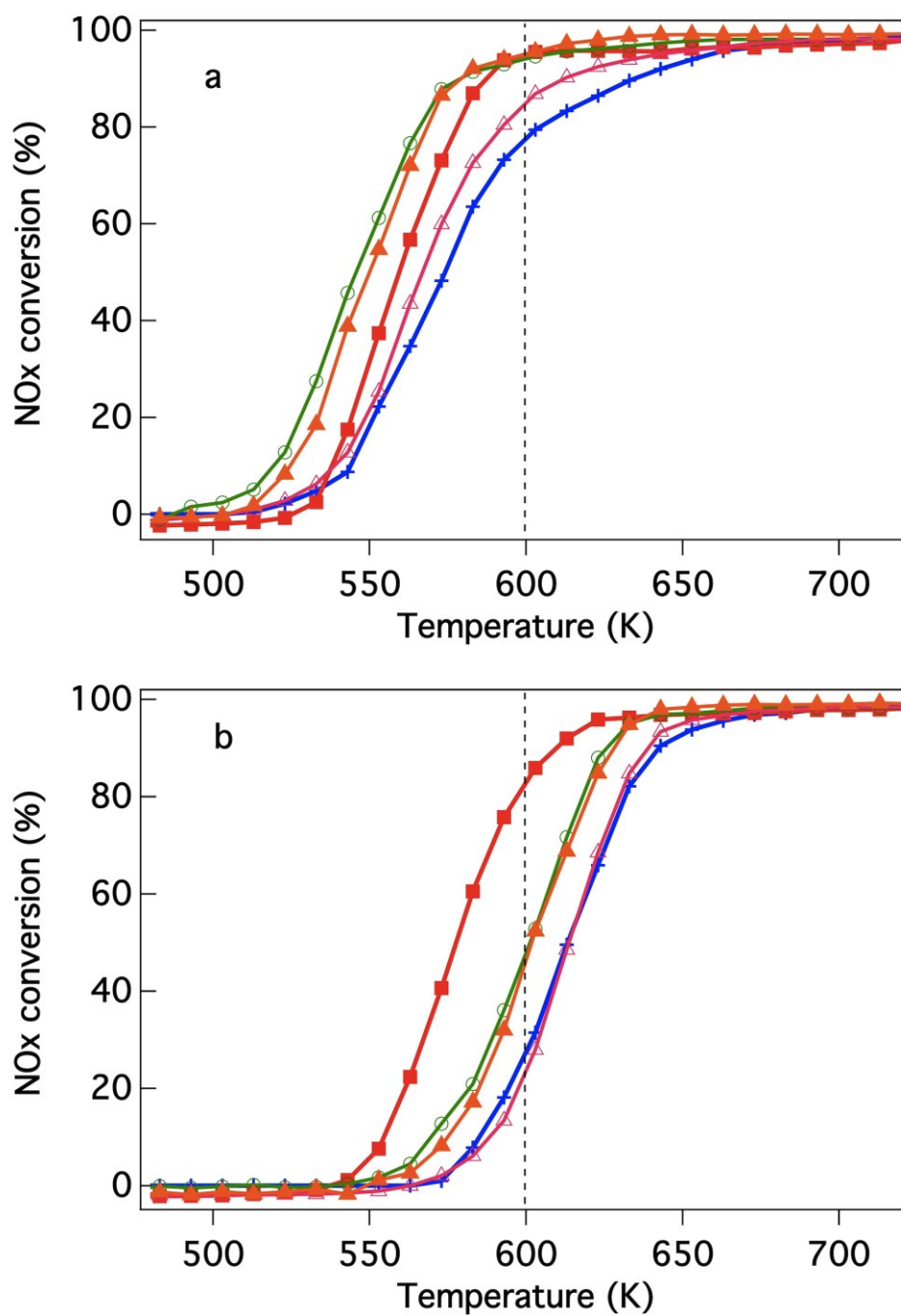


Fig. 3.4 NO_x conversion by the aged three-way catalysts that underwent (a) no oxidation treatment and (b) an oxidation treatment. The catalysts studied are (+) Rh/ZrO₂, (■) Rh/Zr-La-O, (○) Rh/Zr-Ce-O, (△) Rh/Zr-Pr-O, and (▲) Rh/Zr-Nd-O.

3.3.2 Rhodium particle size and dispersion property

Figures 3.5a, b, and c show TEM images of the fresh Rh/ZrO₂, Rh/Zr-La-O, and Rh/Zr-Pr-O, respectively, after the three-way catalytic run at 773 K. The particle size of both Zr-La-O and Zr-Pr-O supports was 10–15 nm whereas the particle size of the ZrO₂ support was 50–70 nm. BET surface areas of the fresh Rh/ZrO₂, Rh/Zr-La-O, and Rh/Zr-Pr-O were 53.2, 85.8, and 99.1 m² g⁻¹, respectively. These surface areas are in accordance with the particle sizes. Figure 3.5d, e, and f show TEM images of aged Rh/ZrO₂, Rh/Zr-La-O, and Rh/Zr-Pr-O, respectively. The growth of the oxide support particles was observed. In particular, the size of the ZrO₂ particles was 50–100 nm, which is larger than the particle size of the fresh catalyst support.

Rhodium particles on the ZrO₂ support were observed, as indicated by the arrows in Fig. 3.5. Both fresh Rh/Zr-La-O (Fig. 3.5b) and Rh/Zr-Pr-O (Fig. 3.5c) featured rhodium particles with a size of ~2 nm. Aged Rh/ZrO₂ comprised larger spherical rhodium particles (diameter: 10 nm), as shown in Fig. 3.5d. In contrast, the rhodium particles supported on Zr-Pr-O (Fig. 3.5f) were considerably bigger (diameter *ca.* 100 nm). The measured particle size agrees with that estimated by Scherrer's equation, using the Rh (111) diffraction peak. The strong contrast observed in the TEM image in Fig. 3.5f suggests the presence of thick rhodium particles in the aged Rh/Zr-Pr-O. The size of the rhodium particles, supported on Zr-La-O, was about 100 nm (Fig. 3.5e). Rhodium agglomerates were also noted because of the elevated aging temperature conditions. However, the low contrast between the rhodium particles and the oxide support particles suggests the presence of thin and plate-like rhodium particles.

The dispersion of Rh in the fresh and aged Rh/ZrO₂, Rh/Zr-La-O, and Rh/Zr-Pr-O samples was determined by CO adsorption at 300 K, and the results are presented in Table 3.1. The rhodium dispersion in the fresh catalysts is greater than 50%. In addition, the fresh catalysts exhibited higher rhodium dispersions as opposed to those featured by the aged catalysts. The results were consistent with the TEM analysis. The addition of La₂O₃ and Pr₆O₁₁ to ZrO₂ favored high rhodium dispersions and high catalyst surface areas.

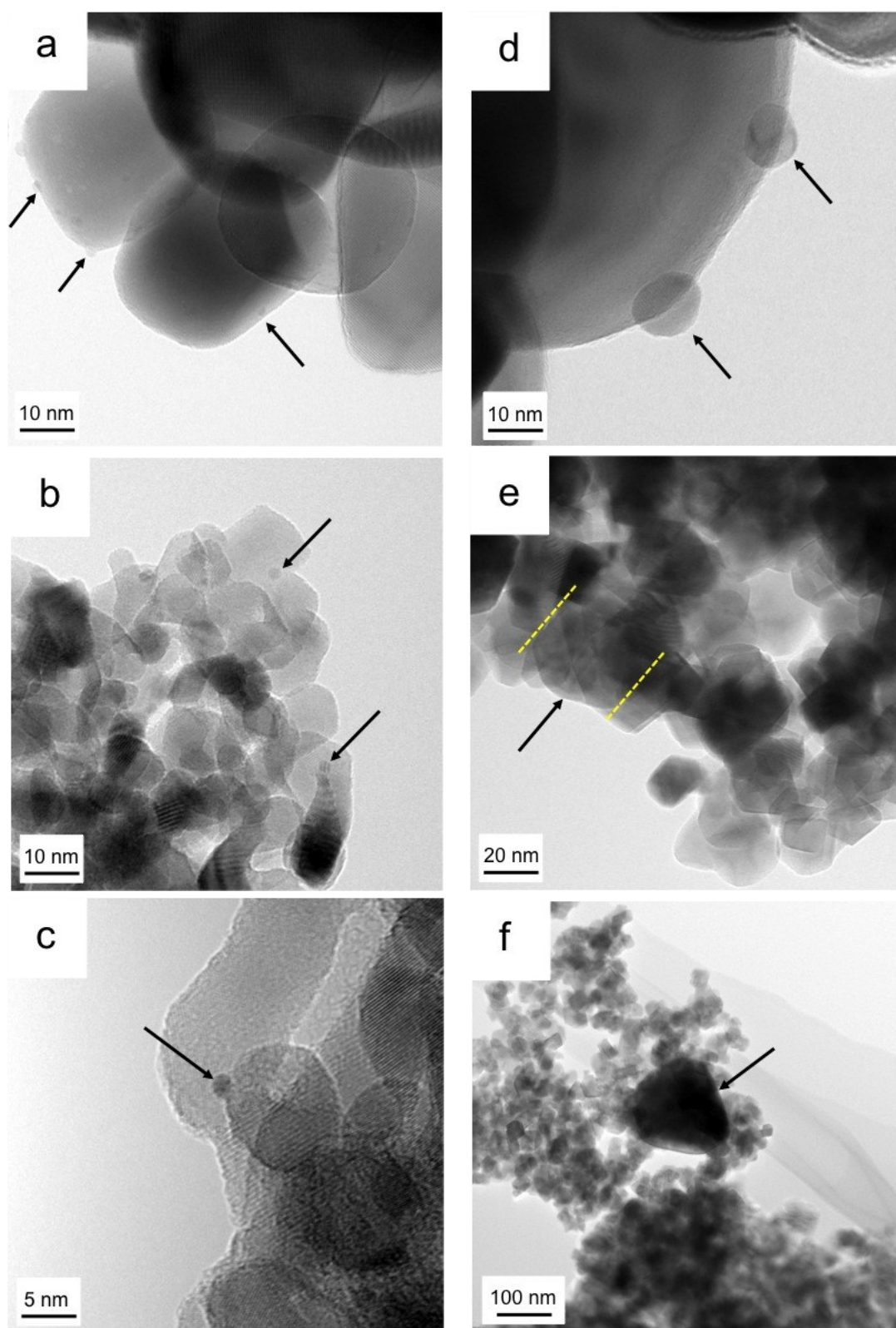


Fig. 3.5 TEM images of (a) fresh Rh/ZrO₂, (b) fresh Rh/Zr-La-O, (c) fresh Rh/Zr-Pr-O, (d) aged Rh/ZrO₂, (e) aged Rh/Zr-La-O, and aged (f) Rh/Zr-Pr-O. Aging was conducted at 1273 K and in 2% O₂ and 10% H₂O/N₂ for 24 h.

Table 3.1 Properties of catalysts

Catalysts	BET surface area/m ² g ⁻¹		Rh dispersion ^a /%	
	Fresh	Aged ^b	Fresh	Aged ^b
Rh/ZrO ₂	52.3	16.4	54.9	6.5
Rh/Zr-La-O	85.8	29.6	87.4	4.5
Rh/Zr-Ce-O	38.5	16.0	60.8	2.7
Rh/Zr-Pr-O	99.1	33.3	83.3	3.8
Rh/Zr-Nd-O	52.1	22.0	65.3	2.9

^a Determined by CO chemisorption.

^b Aged at 1273 K for 24 h in 2% of O₂ and 10% of H₂O/N₂ atmosphere.

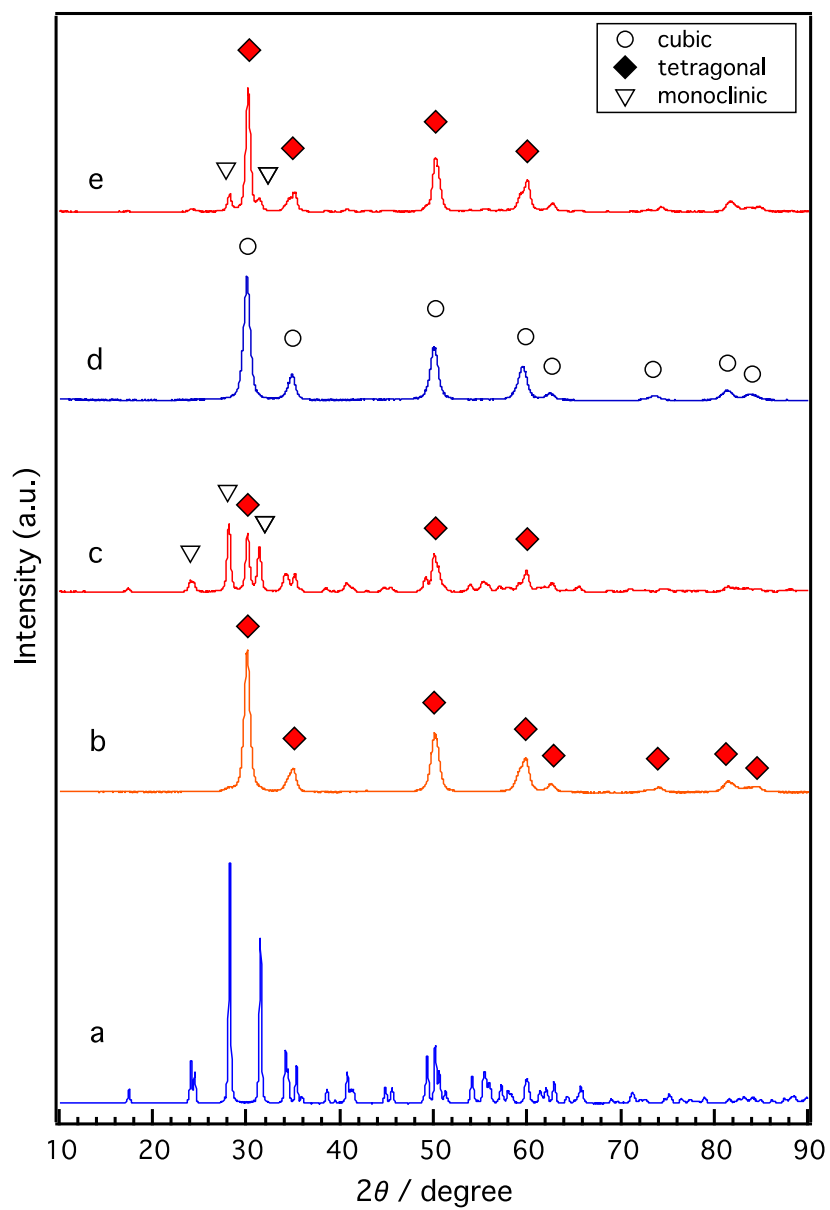


Fig. 3.6 XRD patterns of the fresh catalysts: (a) Rh/ ZrO_2 , (b) Rh/Zr-La-O, (c) Rh/Zr-Ce-O, (d) Rh/Zr-Pr-O and (e) Rh/Zr-Nd-O.

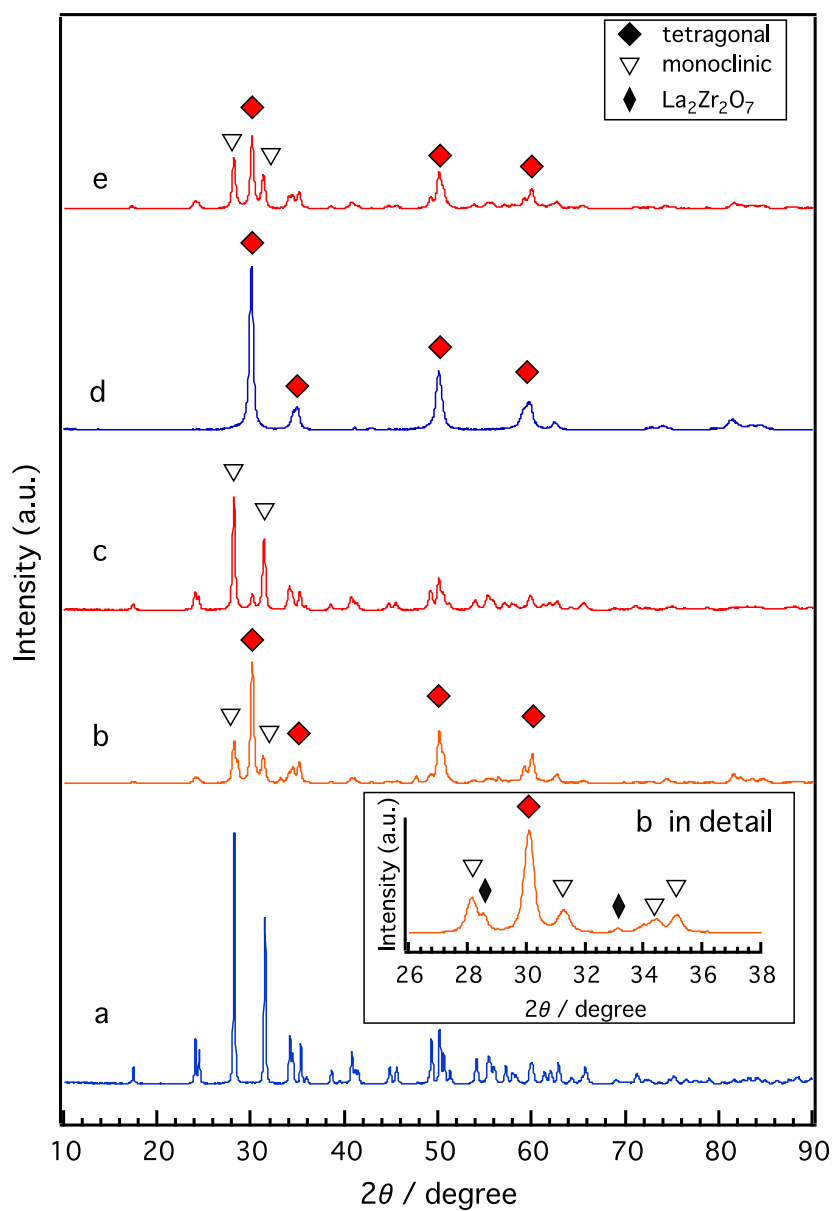


Fig. 3.7 XRD patterns of the aged catalysts: (a) Rh/ZrO₂, (b) Rh/Zr-La-O, (c) Rh/Zr-Ce-O, (d) Rh/Zr-Pr-O and (e) Rh/Zr-Nd-O. Aging was conducted at 1273 K and in 2% O₂ and 10% H₂O/N₂ for 24 h.

Table 3.2 ZrO₂ and other phases detected by XRD

	Fresh	Aged ^a
Rh/ZrO ₂	monoclinic	monoclinic
Rh/Zr–La–O	tetragonal	monoclinic, tetragonal and La ₂ Zr ₂ O ₇
Rh/Zr–Ce–O	monoclinic and tetragonal	monoclinic and tetragonal
Rh/Zr–Pr–O	cubic	tetragonal
Rh/Zr–Nd–O	monoclinic and tetragonal	monoclinic and tetragonal

^a Aged at 1273 K for 24 h in 2% of O₂ and 10% of H₂O/N₂ atmosphere.

3.3.3 Oxidation state of rhodium

XPS spectra of the fresh catalysts after treatment with the reaction gas at 773 K for 10 min are shown in Fig. 3.8A. Both Rh/ZrO₂ and Rh/Zr–La–O (Fig. 3.8A Curves a and b, respectively) featured a rhodium 3d_{5/2} peak at 307.2 eV that was assigned to metallic rhodium.¹⁷ In contrast, Rh/Zr–Ce–O and Rh/Zr–Pr–O (Fig. 3.8A Curves c and d, respectively) featured rhodium 3d_{5/2} peaks at higher binding energies of 308.2 eV and 307.8 eV, respectively. This indicated that the rhodium on Zr–Ce–O and Zr–Pr–O was partially oxidized during the three-way catalytic reaction. The rhodium 3d_{5/2} peak of Rh/Zr–Nd–O (Fig. 3.8A Curve e) appeared at 308.5 eV, indicating that rhodium was oxidized to Rh³⁺ during the reaction.

A distinct difference in the XPS spectra of Rh/Zr–La–O and the other catalysts was noted following treatment with 5% O₂ at 773 K, as shown in Fig. 3.8B. The spectra of Rh/ZrO₂ and Rh/Zr–Pr–O both featured a peak at 308.7 eV that was attributed to Rh³⁺ (Fig. 3.8B Curves a and d, respectively). The rhodium 3d_{5/2} peak of Rh/Zr–Ce–O appeared at 308.5 eV (Fig. 3.8B Curve c), which is comparable to the binding energy associated with the rhodium trivalent state. The rhodium 3d_{5/2} peak of Rh/Zr–Nd–O, after the oxidation treatment, was observed at 309.2 eV (Fig. 3.8B Curve e), which is a slightly higher binding energy than that associated with Rh³⁺. In contrast, the rhodium 3d_{5/2} peak of Rh/Zr–La–O was observed at an intermediate binding energy of 307.9 eV (Fig. 3.8B Curve b) between those associated with Rh⁰ and Rh³⁺. These results demonstrate that the rhodium particles, supported on Zr–La–O, were not readily oxidized under the current conditions (5% O₂ at 773 K). Conversely, the rhodium particles, supported on ZrO₂, Zr–Ce–O, Zr–Pr–O, and Zr–Nd–O, were oxidized to Rh³⁺ under the same oxidation treatment.

Figure 3.9 shows the Rh 3d XPS spectra of the aged catalysts, subjected to either the reaction gas at 773 K for 10 min or the oxidation process. Following treatment with the reaction gas, Rh/Zr–La–O featured a rhodium 3d_{5/2} peak at 307.2 eV, corresponding to metallic Rh (Fig. 3.9A Curve b). Contrarily, rhodium in Rh/ZrO₂ was completely oxidized to the trivalent state under the same conditions (Fig. 3.9A Curve a). This demonstrates that the addition of La stabilized the low oxidation state of rhodium during the three-way catalytic reaction. XPS spectra of both Rh/Zr–Ce–O and Rh/Zr–Pr–O also featured a 3d_{5/2} peak at a binding energy comparable to that associated with Rh⁰ (Fig. 3.9A Curves c and d, respectively). XPS spectrum of Rh/Zr–Nd–O

showed a peak at a binding energy (308.2 eV) comparable to that corresponding to Rh^{3+} (Fig. 3.9A Curve e). However, rhodium is not incorporated into the oxide lattice because the Rh 3d peak corresponding to the trivalent state that is typically observed at ~ 310 eV is not detected. The spectrum of Rh/Zr–La–O, following the oxidation treatment at 773 K, displayed a weak Rh $3d_{5/2}$ peak at ~ 307.5 eV (Fig. 3.9B Curve b). This observation agrees with the findings discussed earlier relating to the stabilization of the rhodium low oxidation state by the La-containing support. Both Rh/ZrO₂ and Rh/Zr–Nd–O XPS spectra showed a Rh 3d peak, corresponding to Rh^{3+} (Fig. 3.9B Curves a and e). A slight shift to the higher binding energies was observed for Rh/ZrO₂ and Rh/Zr–Ce–O following the oxidation treatment (Fig. 3.9B Curves a and c, respectively).

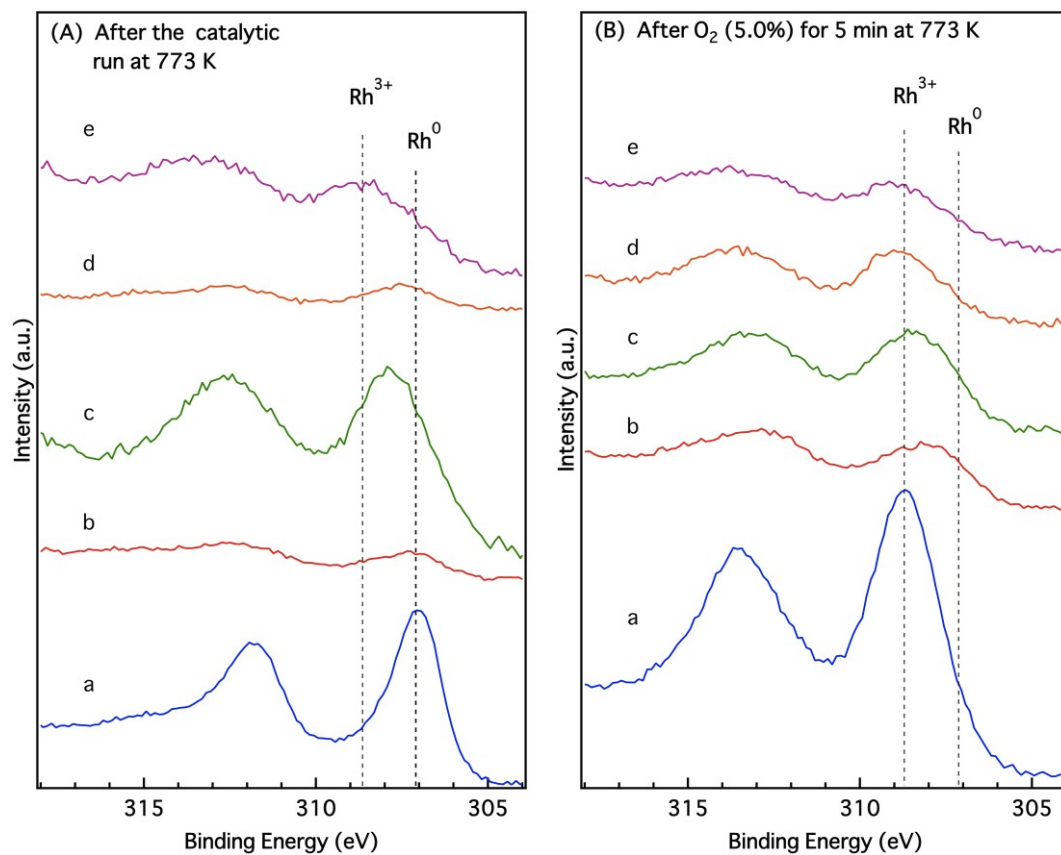


Fig. 3.8 Rh 3d spectra of the fresh catalysts, subjected to (A) the three-way catalytic reaction at 773 K for 10 min and (B) a 5% O₂ at 773 K for 5 min. The catalysts studied are (a) Rh/ZrO₂, (b) Rh/Zr–La–O, (c) Rh/Zr–Ce–O, (d) Rh/Zr–Pr–O, and (e) Rh/Zr–Nd–O.

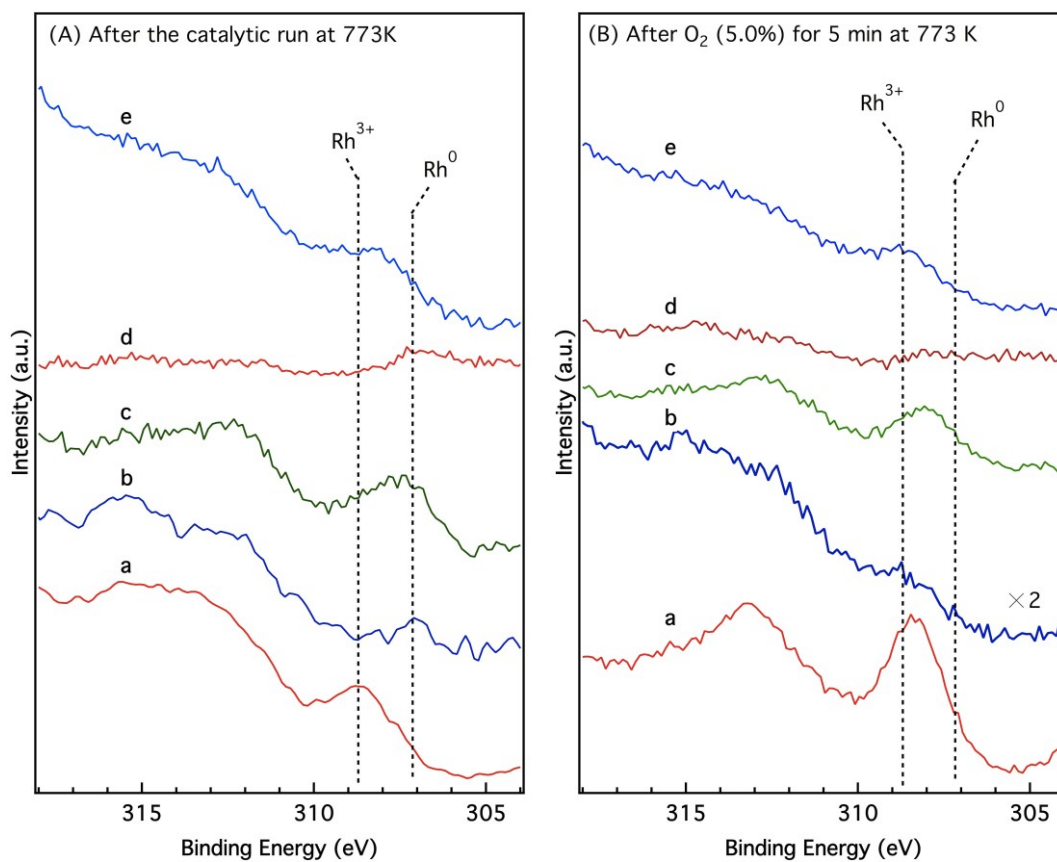


Fig. 3.9 Rh 3d spectra of the aged catalysts, subjected to (A) the three-way catalytic reaction at 773 K for 10 min and (B) a 5% O_2 at 773 K for 5 min. The catalysts studied are (a) Rh/ZrO_2 , (b) $\text{Rh}/\text{Zr-La-O}$, (c) $\text{Rh}/\text{Zr-Ce-O}$, (d) $\text{Rh}/\text{Zr-Pr-O}$, and (e) $\text{Rh}/\text{Zr-Nd-O}$.

3.3.4 Temperature-programmed reduction using CO (CO-TPR)

Temperature-programmed reduction profiles of the fresh catalysts are presented in Fig. 3.10. Rh/Zr–Ce–O, Rh/Zr–Pr–O, and Rh/Zr–Nd–O spectra displayed broad peaks in the region of 450–600 K (Fig. 3.10c, d, e, respectively). The O/Rh ratios of the different prepared catalysts, calculated from the TPR data, are shown in Table 3.3. High O/Rh atomic ratios (1.09–1.57) were observed for fresh Rh/Zr–Ce–O, Rh/Zr–Pr–O, and Rh/Zr–Nd–O. These results agree with the XPS findings in Fig. 3.8B that showed the occurrence of oxidation of the metallic rhodium in these three catalysts. The TPR profile of Rh/ZrO₂ (Fig. 3.10a) displayed two peaks at around 450 K and 600 K (broad peak). XPS analysis confirmed the oxidation of Rh⁰ to Rh³⁺ in Rh/ZrO₂ after exposure to a 5% O₂ atmosphere. However, the fresh Rh/ZrO₂ featured a low O/Rh ratio, as observed in Table 3.3. As XPS is a surface-sensitive technique, these findings indicate that, for Rh/ZrO₂, only the surface of the rhodium particles are oxidized to Rh³⁺. Similar results have been reported for Rh/ZrO₂ by Burch and Loader.¹⁸ Their results also showed that the rhodium, supported on ZrO₂, was easily reduced by CO at ~473 K. In contrast, Rh/Zr–La–O featured a slightly higher O/Rh ratio of 0.70. This value agrees with the XPS analysis of Rh/Zr–La–O that showed that the rhodium oxidation state remained between Rh⁰ and Rh³⁺ after the oxidation pre-treatment at 773 K. Moreover, Rh/Zr–La–O showed a significant different profile to the ones obtained for the other catalysts: the reduction peak of Rh/Zr–La–O was observed at a higher temperature.

Fig. 3.11 shows the CO-TPR profiles of the aged catalysts. The aged Rh/Zr–La–O (Fig. 3.11b) produced a broad reduction profile, similar to that of the fresh Rh/Zr–La–O (Fig. 3.10b). Conversely, relatively sharp peaks at ~500 K were observed for Rh/ZrO₂, Rh/Zr–Ce–O, Rh/Zr–Pr–O, and Rh/Zr–Nd–O (Fig. 3.11a, c, d, and e, respectively). This significant difference between Rh/Zr–La–O and the other catalysts is discussed in Section 3.4.

Table 3.3 Amount of CO₂ released during CO-TPR and O/Rh ratios

Catalysts	Amount of CO ₂ released/ $\mu\text{mol g}^{-1}$		O/Rh ratio ^a /%	
	Fresh	Aged ^b	Fresh	Aged ^b
Rh/ZrO ₂	45	59	0.14	0.20
Rh/Zr-La-O	224	121	0.70	0.42
Rh/Zr-Ce-O	349	229	1.09	0.79
Rh/Zr-Pr-O	502	148	1.57	0.51
Rh/Zr-Nd-O	381	165	1.19	0.57

^a Determined by CO-TPR.

^b Aged at 1273 K for 24 h in 2% of O₂ and 10% of H₂O/N₂ atmosphere.

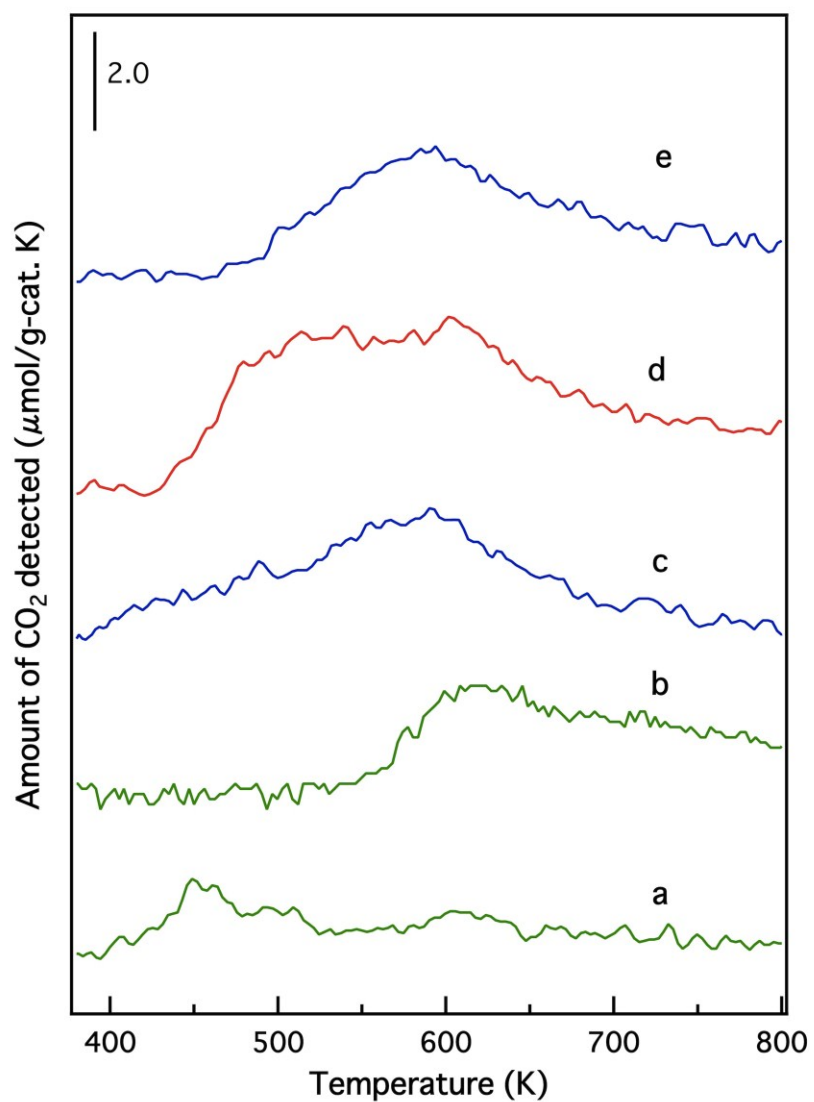


Fig. 3.10 CO-TPR profiles of the fresh catalysts: (a) Rh/ZrO₂, (b) Rh/Zr–La–O, (c) Rh/Zr–Ce–O, (d) Rh/Zr–Pr–O, and (e) Rh/Zr–Nd–O.

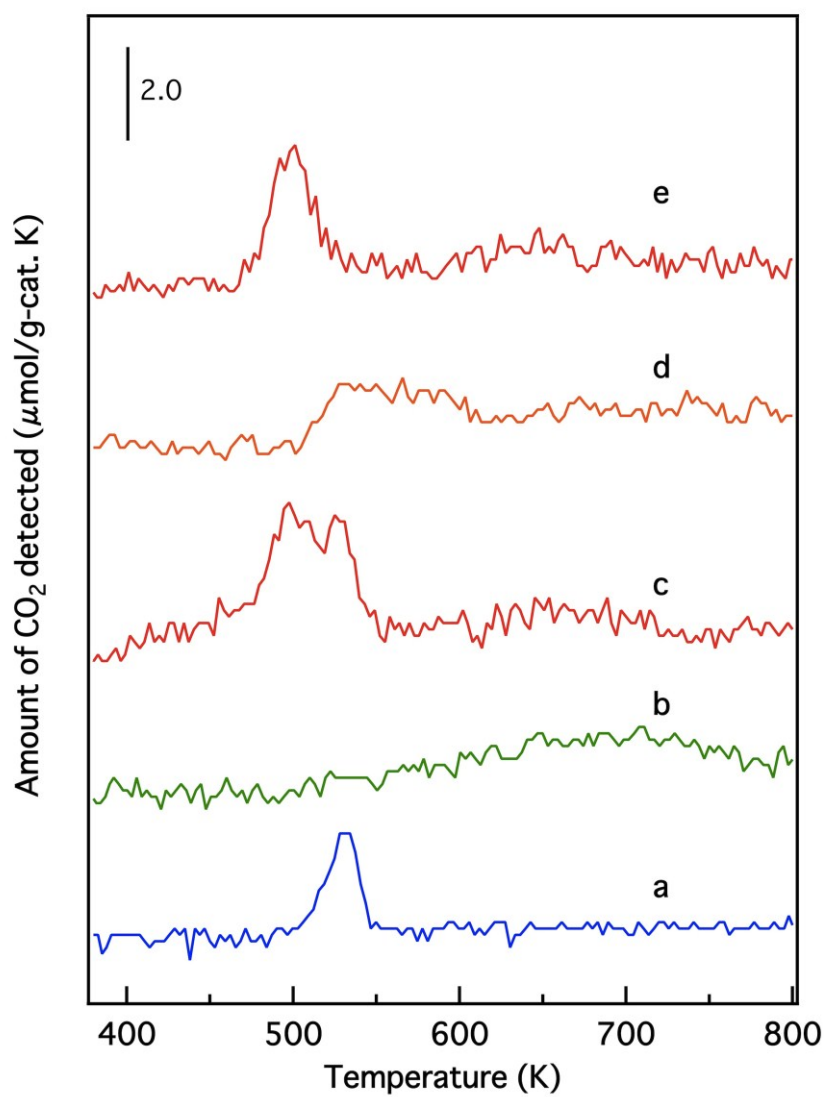


Fig. 3.11 CO-TPR profiles of the aged catalysts: (a) Rh/ZrO₂, (b) Rh/Zr-La-O, (c) Rh/Zr-Ce-O, (d) Rh/Zr-Pr-O, and (e) Rh/Zr-Nd-O.

3.3.5 Effect of La addition in the Rh-based catalysts on the performance of the steam reforming reaction

The steam reforming reaction is an important process in the three-way catalysis to produce hydrogen as a reductant to enhance NO_x conversion.^{19–23} Rhodium is known to catalyze such process.²⁴ Figure 3.12 shows the C_3H_6 conversion in the steam reforming reaction, as catalyzed by the fresh catalysts. The conversion of C_3H_6 started at ~ 550 K and reached almost 100% at ~ 750 K, regardless of the catalysts employed. Hydrogen production was confirmed on a mass spectrometer by monitoring the signal at $m/z = 2$. The conversion of C_3H_6 for the rhodium catalysts, supported on the lanthanoid-containing ZrO_2 , was slightly higher than that for the rhodium catalyst, supported on ZrO_2 , thus indicating that the steam reforming reaction is promoted by the addition of a lanthanoid to ZrO_2 . Figure 3.13 shows the C_3H_6 conversion in the steam reforming reaction, as catalyzed by the aged catalysts. Among the aged catalysts, Rh/Zr–La–O exhibited the highest activity. For example, the Rh/Zr–La–O-catalyzed C_3H_6 conversion was 73% at 773 K whereas that obtained from the Rh/ ZrO_2 -catalyzed reaction was only 24%. The addition of La, in the aged catalysts, was highly beneficial in significantly promoting the steam reforming reaction.

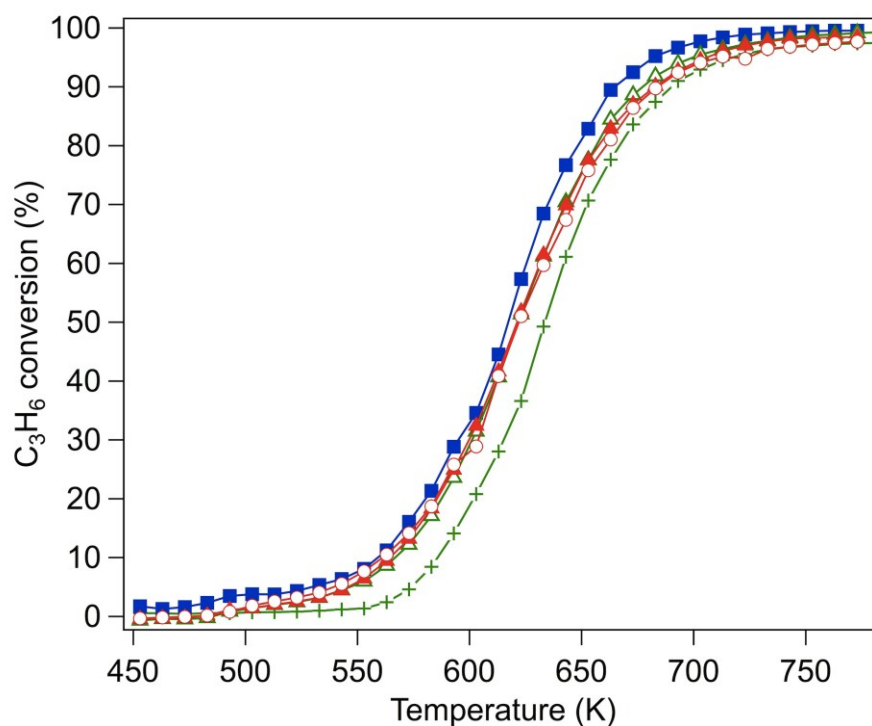


Fig. 3.12 C₃H₆ conversion in the steam reforming reaction over the fresh Rh catalysts: (+) Rh/ZrO₂, (■) Rh/Zr-La-O, (○) Rh/Zr-Ce-O, (△) Rh/Zr-Pr-O, and (▲) Rh/Zr-Nd-O.

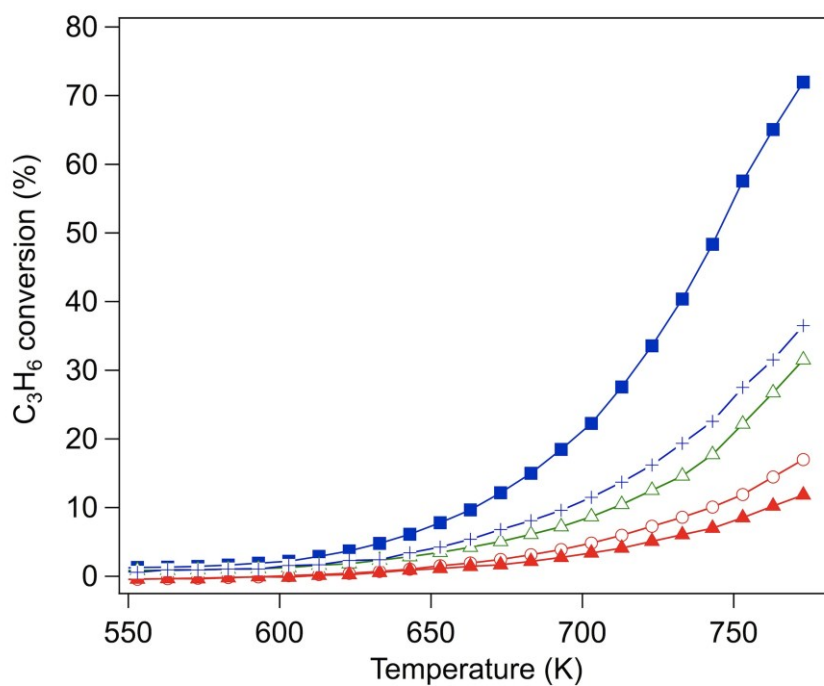


Fig. 3.13 C₃H₆ conversion in the steam reforming reaction over the aged Rh catalysts: (+) Rh/ZrO₂, (■) Rh/Zr-La-O, (○) Rh/Zr-Ce-O, (△) Rh/Zr-Pr-O, and (▲) Rh/Zr-Nd-O.

3.3.6 Effect of the steam reforming reaction on the oxidation state of rhodium

XPS measurements were conducted to understand the effect of the steam reforming reaction on the performance of the catalysts. XPS measurements were taken following each treatment. The catalysts were first treated in 5% oxygen at 773 K for 10 min and then cooled to room temperature under a N₂ flow; the steam reforming reaction was subsequently performed over the oxidized catalysts at increasing temperatures of up to 550 K, followed by cooling to room temperature under a N₂ flow. Figures 3.14 and 3.15 show the XPS spectra (Rh 3d_{5/2}) of the fresh and aged catalysts (Rh/ZrO₂, Rh/Zr–La–O, and Rh/Zr–Pr–O), respectively, following the above-mentioned treatments. XPS spectrum of Rh/ZrO₂, following the oxidation treatment, displayed a Rh 3d_{5/2} peak at 308.7 eV, corresponding to Rh³⁺ (Fig. 3.14a). Following the steam reforming reaction at up to 550 K, the Rh 3d_{5/2} peak shifted to 307.5 eV, which is a slightly higher binding energy value than the one associated with metallic Rh, indicating that rhodium is reduced by the steam reforming reaction; however, some rhodium species remain in the oxidized form (Fig. 3.14b). In the case of the Rh/Zr–La–O catalyst, some rhodium species are oxidized when subjected to the oxidation treatment (Fig. 3.14c). A Rh 3d_{5/2} peak at 307.2 eV, corresponding to metallic Rh was observed, after conducting the steam reforming reaction (Fig. 3.14d). In contrast, the Rh 3d_{5/2} peak, observed at 309 eV following the oxidation treatment of Rh/Zr–Pr–O (Fig. 3.14e) remained unchanged after the steam reforming reaction (Fig. 3.14f). This result shows that the reduction of the rhodium oxide on the Zr–Pr–O support does not take place during the steam reforming reaction.

To re-iterate, the steam reforming reaction over the fresh Rh/Zr–La–O reduces all the previously oxidized rhodium species to its metallic form. In contrast, only some of the rhodium species in the fresh Rh/ZrO₂ were reduced, and the rhodium species in the fresh Rh/Zr–Pr–O maintained their oxidized state following the steam reforming reaction. Similar results were obtained for the aged catalysts, as shown in Fig. 3.15. Likewise, the steam reforming reaction reduced the rhodium species in the aged Rh/Zr–La–O (Fig. 3.15d).

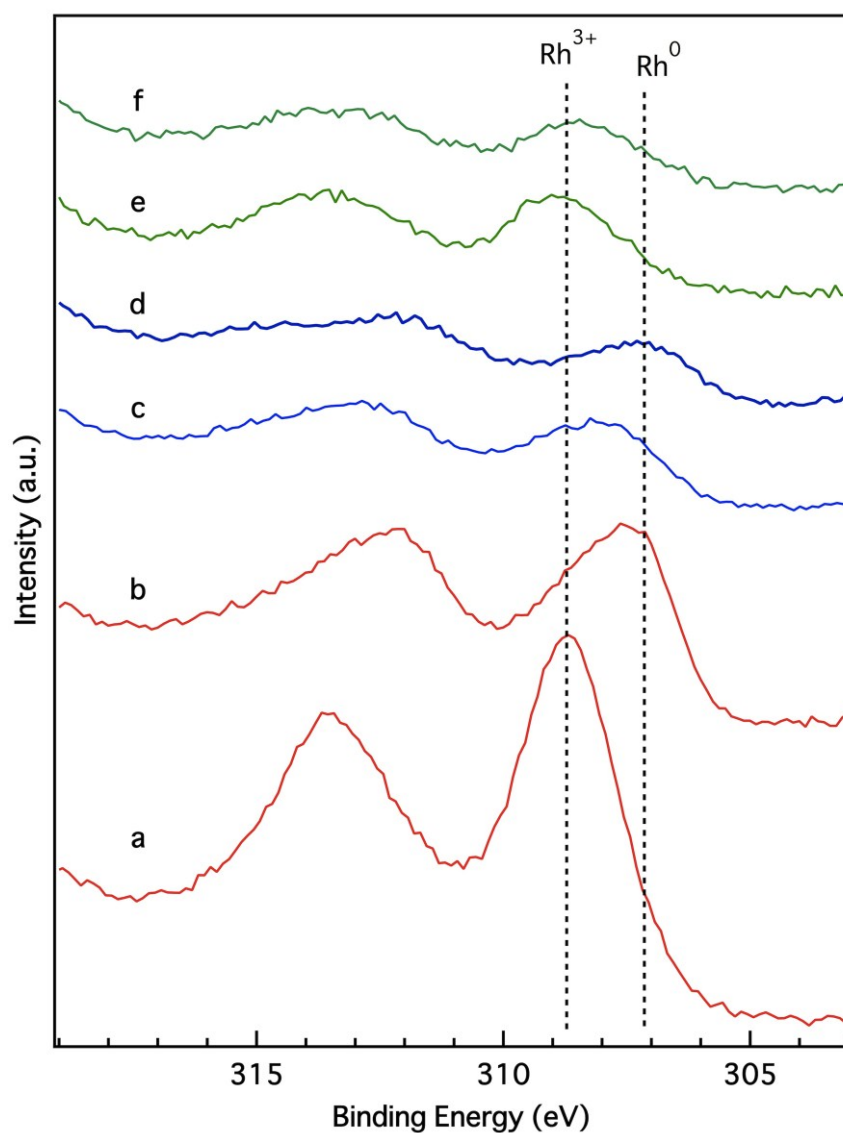


Fig. 3.14 XPS Rh 3d spectra of the fresh catalysts, subjected to different pre-treatments. (a) Rh/ZrO₂ after oxygen pre-treatment at 773 K, (b) Rh/ZrO₂ after oxygen pre-treatment at 773 K followed by the steam reforming reaction at up to 550 K, (c) Rh/Zr–La–O after oxygen pre-treatment at 773 K, (d) Rh/Zr–La–O treated in the same way as (b), (e) Rh/Zr–Pr–O after oxygen pre-treatment at 773 K, and (f) Rh/Zr–Pr–O treated in the same way as (b).

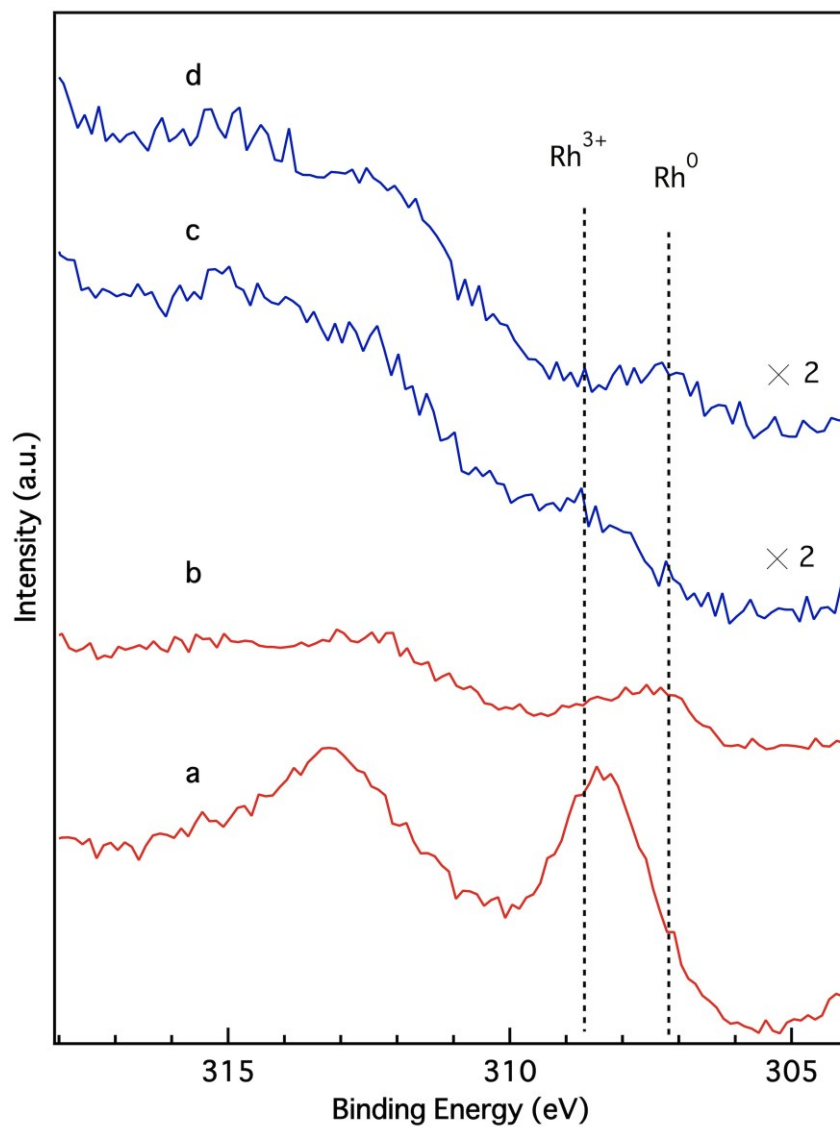


Fig. 3.15 XPS Rh 3d spectra of the aged catalysts, subjected to different pre-treatments. (a) Rh/ZrO₂ after oxygen pre-treatment at 773 K, (b) Rh/ZrO₂ after oxygen pre-treatment at 773 K followed by the steam reforming reaction at up to 550 K, (c) Rh/Zr-La-O after oxygen pre-treatment at 773 K, and (d) Rh/Zr-La-O treated in the same way as (b).

3.3.7 Effect of the steam reforming reaction on the three-way catalytic activity

The influence of the steam reforming reaction on the activity of the three-way catalysis is investigated by the following three comparison experiments. The first study examines the three-way catalytic activity of the aged catalysts in the absence of any pre-treatments. The second study involves the aged catalysts that were pre-treated under a 5% O₂ flow at 773 K for 5 min. The third study investigates the catalytic activity of the aged catalysts that were oxidized under a 5% O₂ flow at 773 K for 5 min followed by the steam reforming reaction at 773 K for 5 min. The aged catalysts studied are Rh/ZrO₂, Rh/Zr–La–O, and Rh/Zr–Pr–O. The resulting propene conversion profiles, obtained during the three-way catalysis process from 423 K to 773 K, are presented in Fig. 3.16. Oxidation pre-treatment of Rh/ZrO₂ showed a reduced activity in the region of 550–630 K (Fig. 3.16A Curve b) when compared with that of the non-treated Rh/ZrO₂ (Fig. 3.16A Curve a). However, the loss in the activity of the oxidized catalyst was entirely recovered by subjecting the oxidized catalyst to the steam reforming reaction (Fig. 3.16A Curve c). Oxidation pre-treatment of Rh/Zr–Pr–O also led to a decreased activity, however, the loss in activity was only partially recovered by the steam reforming reaction (Fig. 3.16B). Oxidation pre-treatment on Rh/Zr–La–O induced the same effect. However, not only was the loss in activity completely recovered by the steam reforming reaction, but the latter process also enhanced the activity of the catalyst when compared with that of the non-treated catalyst (Fig. 3.16C). These results were consistent with the XPS results (Figs. 3.14 and 3.15). XPS analysis confirmed the presence of reduced rhodium species in both Rh/ZrO₂ and Rh/Zr–La–O after the steam reforming reaction. Both catalysts showed a significant recovery in activity by the steam reforming reaction after the oxidation pre-treatment. Conversely, rhodium in Rh/Zr–Pr–O was not reduced by the steam reforming reaction, as shown in the XPS spectra in Fig. 3.14, hence the limited recovery in activity, as observed in Fig. 3.16B.

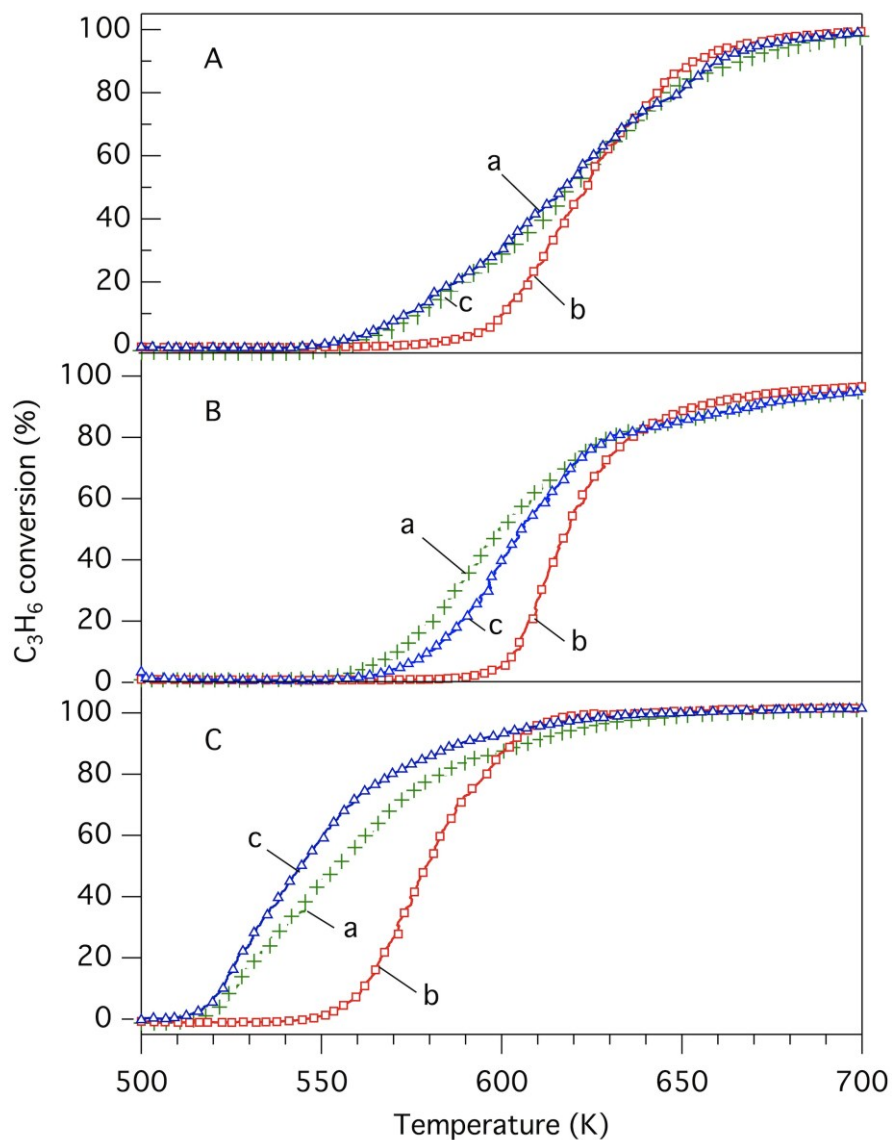


Fig. 3.16 The effect of the steam reforming reaction for the three-way catalytic C_3H_6 conversion by the aged catalysts: (A) Rh/ZrO₂, (B) Rh/Zr-Pr-O, and (C) Rh/Zr-La-O. For each catalyst, three types of pre-treatment were conducted: (a) no pre-treatment, (b) pre-treated with 5% oxygen at 773 K for 5 min, and (c) pre-treated with 5% oxygen at 773 K for 5 min followed by the steam reforming reaction at 773 K for 5 min.

3.3.8 Influence of La concentration on the catalytic activity

To investigate the influence of La concentration on the rhodium property, a series of Rh/Zr-La-O catalysts having La concentration within the range of 2.0 wt% to 20.0 wt% as oxides were tested. The hydrocarbon (C_3H_6), CO and NO_x light-off temperatures as a function of La content are shown in Fig. 3.17 and Fig. 3.18 for the fresh and aged catalysts, respectively. For the fresh catalysts, the three-way catalytic activity was improved as the La content increased, as was indicated by the decrease of light-off temperature (Fig. 3.17). After the aging treatment, the light-off temperature became higher indicating the deterioration of the catalyst. Although the addition of La to the support oxide enhanced the activity of the catalyst compared to that of Rh/ZrO₂, the high La concentration did not give better activity (Fig. 3.18); The highest catalytic performance was achieved at 6.0 wt% of La in Zr-La-O mixed oxide.

3.3.9 Influence of La concentration on the crystal structure

Structural alternations caused by the La addition were studied using XRD, as shown in Figs. 3.19 and 3.20 for the fresh and the aged catalysts, respectively. For fresh catalysts, La addition stabilized tetragonal and cubic zirconia structure. At high La content over 10 wt%, the cubic ZrO₂ structure is dominant. After the aging treatment at 1273 K, cubic ZrO₂ structure was not maintained for all La-containing ZrO₂ oxides. For example, monoclinic ZrO₂ phase was mainly observed for the samples which containing La less than 10 wt%. For the samples with more than 10 wt% of La, La₂Zr₂O₇ was clearly detected after the aging treatment. This has a pyrochlore structure that contains La and Zr with 1:1 ratio. The presence of three phases in the Zr-La-O as a function of La content in the aged catalysts was identified by using diffraction patterns as shown in Fig. 3.21. The diffraction intensity of monoclinic ZrO₂ decreased monotonically as La content increased. On the contrary, the intensity of the tetragonal ZrO₂ increased with La addition, reached a maximum at the La content of 6 wt%, and then decreased with further increase of La content. La₂Zr₂O₇ was observed only at more than 10 wt% of La concentration.

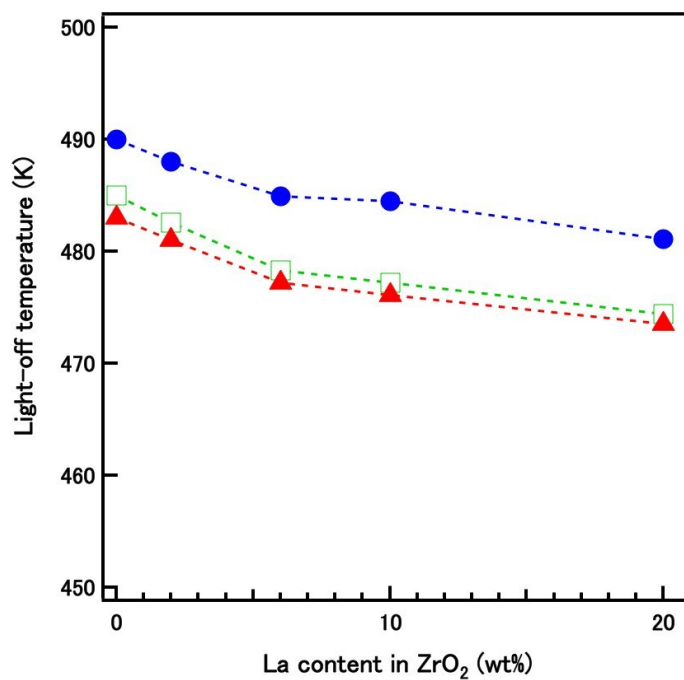


Fig. 3.17 Effect of La content on the light-off performance of C₃H₆ (●), CO (□) and NO_x (▲) for the fresh Rh/Zr-La-O.

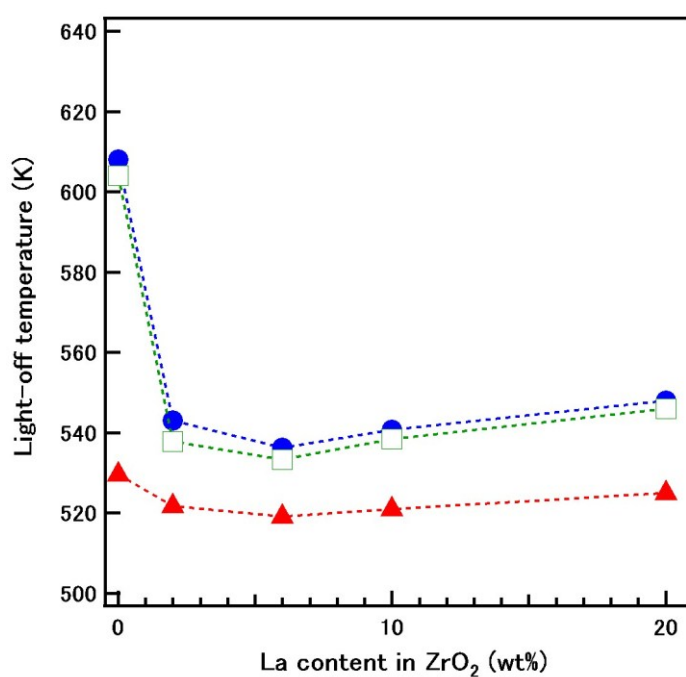


Fig. 3.18 Effect of La content on the light-off performance of C₃H₆ (●), CO (□) and NO_x (▲) for the aged Rh/Zr-La-O. Aging was conducted at 1273 K in a 2 % O₂, 10 % H₂O, N₂ atmosphere for 24 h.

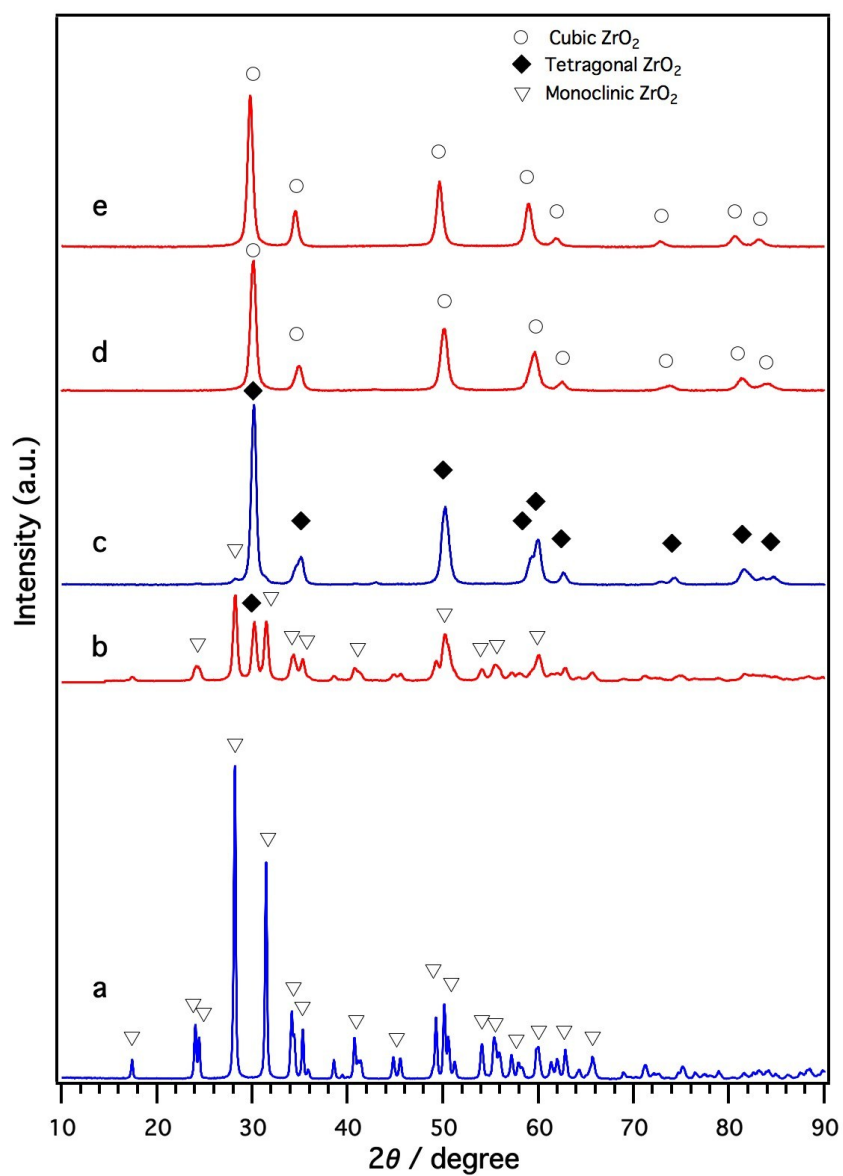


Fig. 3.19 XRD patterns of the fresh catalysts: (a) Rh/ ZrO_2 , (b) Rh/Zr-La-O, La=2.0 wt% (c) Rh/Zr-La-O, La=6.0 wt%, (d) Rh/Zr-La-O, La=10.0 wt% and (e) Rh/Zr-La-O, La=20.0 wt%.

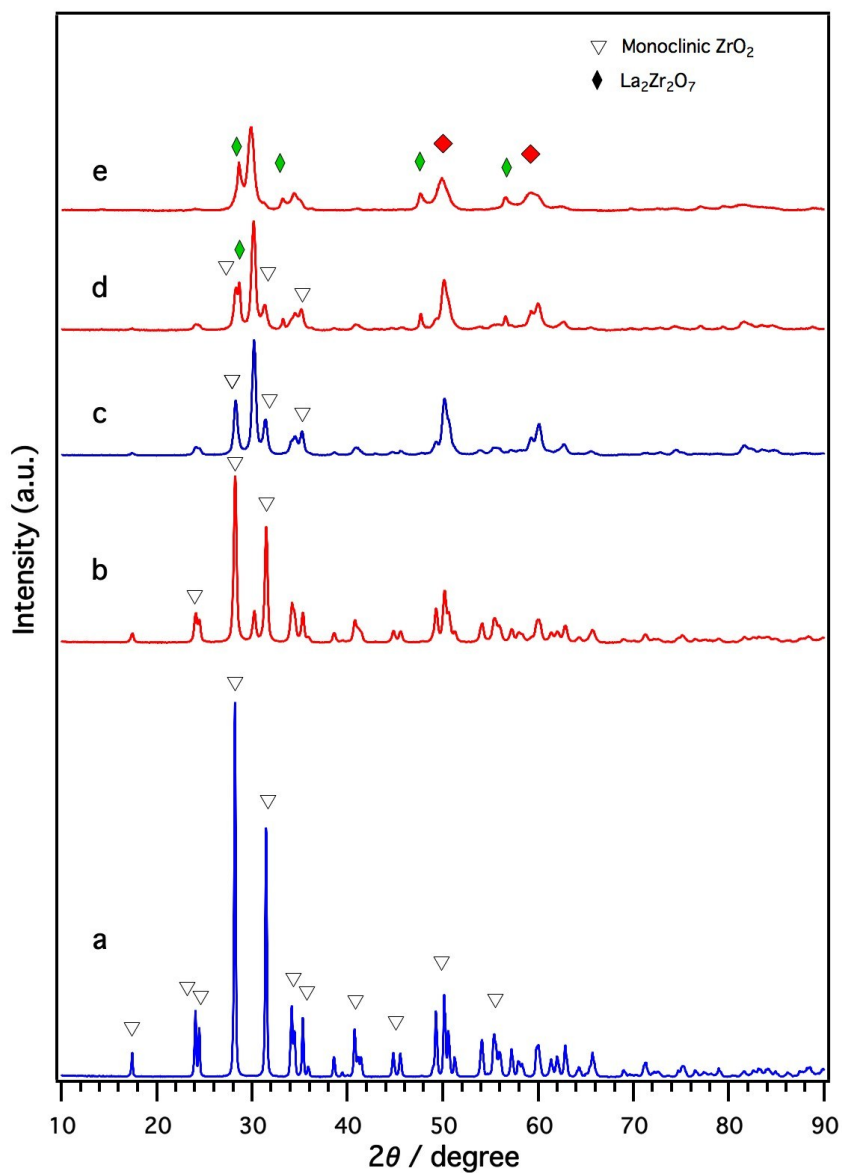


Fig. 3.20 XRD patterns of the aged catalysts: (a) Rh/ZrO₂, (b) Rh/Zr-La-O, La=2.0 wt% (c) Rh/Zr-La-O, La=6.0 wt%, (d) Rh/Zr-La-O, La=10.0 wt% and (e) Rh/Zr-La-O, La=20.0 wt%. Aging was conducted at 1273 K in a 2 % O₂, 10 % H₂O, N₂ atmosphere for 24 h.

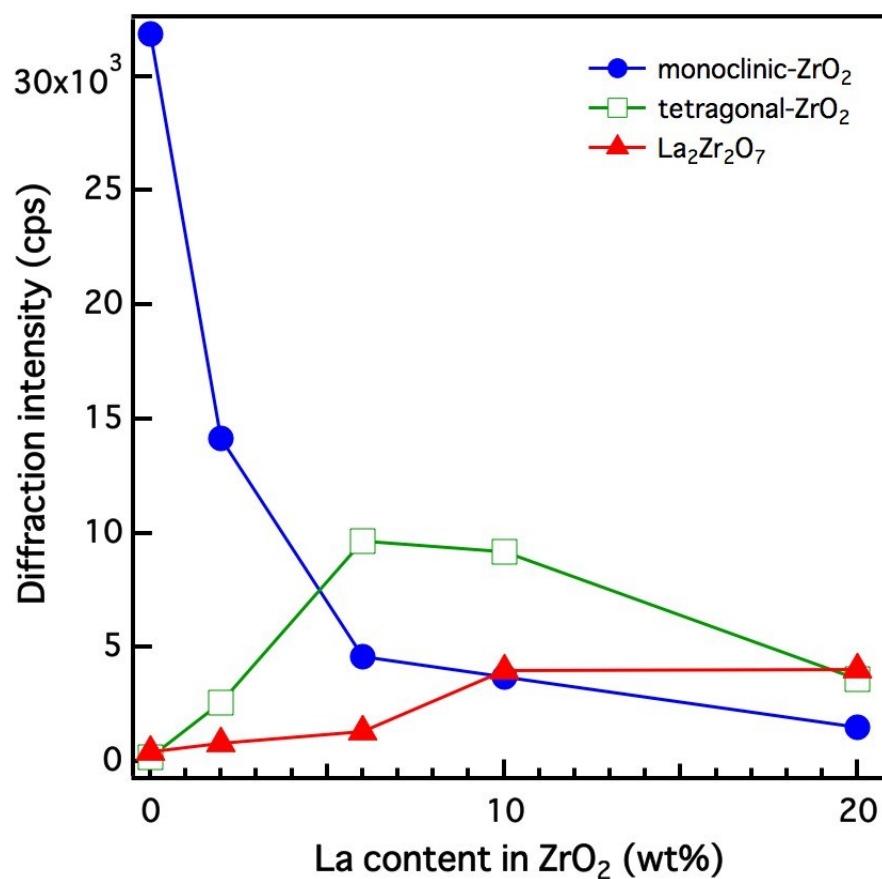


Fig. 3.21 Diffraction intensity of ZrO₂ phases as a function of La content in the aged catalysts. Aging was conducted at 1273 K in a 2 % O₂, 10 % H₂O, N₂ atmosphere for 24 h. Diffraction intensities were measured from the diffractions of $2\theta = 28.2^\circ$ for monoclinic-ZrO₂, $2\theta = 30.1^\circ$ for tetragonal-ZrO₂ and $2\theta = 28.6^\circ$ for La₂Zr₂O₇.

3.3.10 Influence of La concentration on the reducibility of rhodium

Temperature programmed reduction profiles of the fresh catalysts with an increasing of La amounts are shown in Fig. 3.22. For all fresh catalysts, rhodium supported La-containing catalysts exhibited a broad reduction profile starting at around 480 K, while a sharp peak was observed at 450 K for the fresh Rh/ZrO₂. The broad reduction profile started at slightly higher temperature for catalysts with higher La content in the supports; reduction started at 480 K for Rh/Zr–La(6)–O, 520 K for Rh/Zr–La(10)–O and 530 K for Rh/Zr–La(20)–O, respectively (the figures in the parentheses are La contents). The amount of CO₂ generated during the TPR process for each catalyst did not change with the increase of La amount.

Fig. 3.23 shows the CO-TPR profiles of the aged catalysts. A sharp peak was observed at 520 K for both Rh/ZrO₂ and Rh/Zr–La(6)–O, as shown in Fig. 3.23a and 3.23b, respectively. However, the La content was higher than 6 wt%, broad reduction profiles were observed. It should be noted that the reduction profiles had two peaks centered at 530 K and 680 K. These results indicated that La did affect the rhodium reducibility.

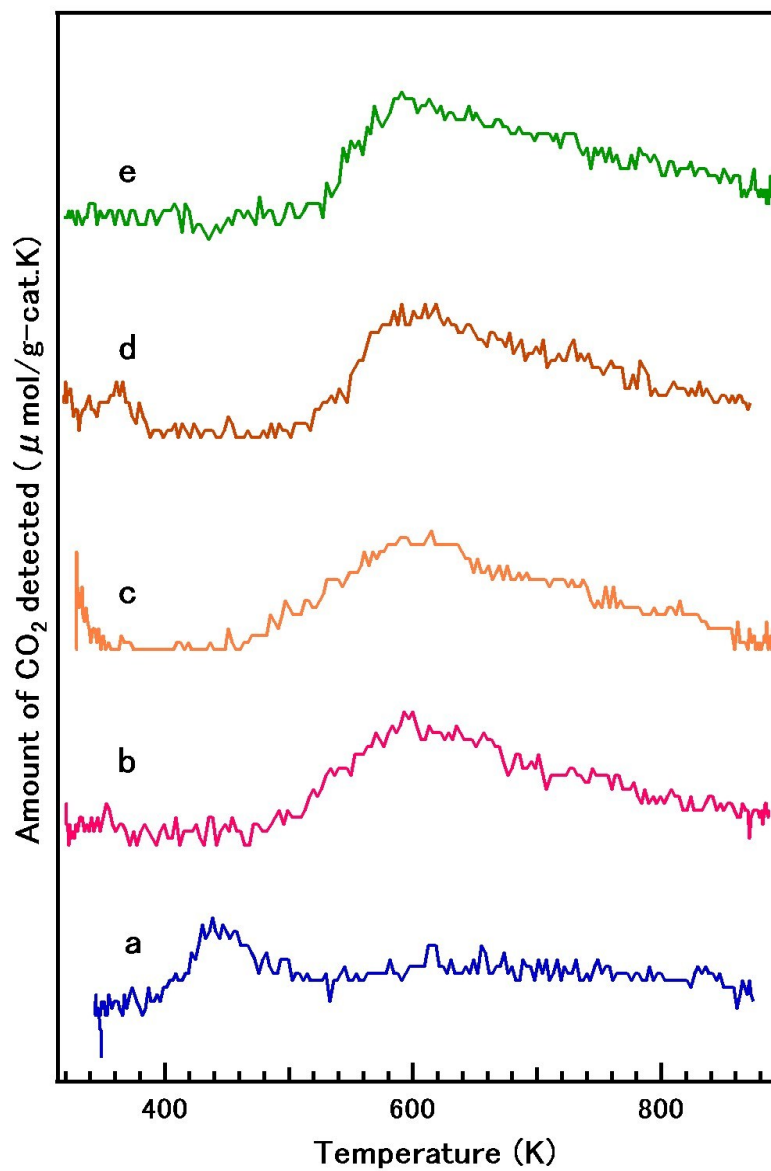


Fig. 3.22 CO-TPR profiles of the fresh catalysts: (a) Rh/ZrO₂, (b) Rh/Zr-La-O, La=2.0 wt% (c) Rh/Zr-La-O, La=6.0 wt%, (d) Rh/Zr-La-O, La=10.0 wt% and (e) Rh/Zr-La-O, La=20.0 wt%.

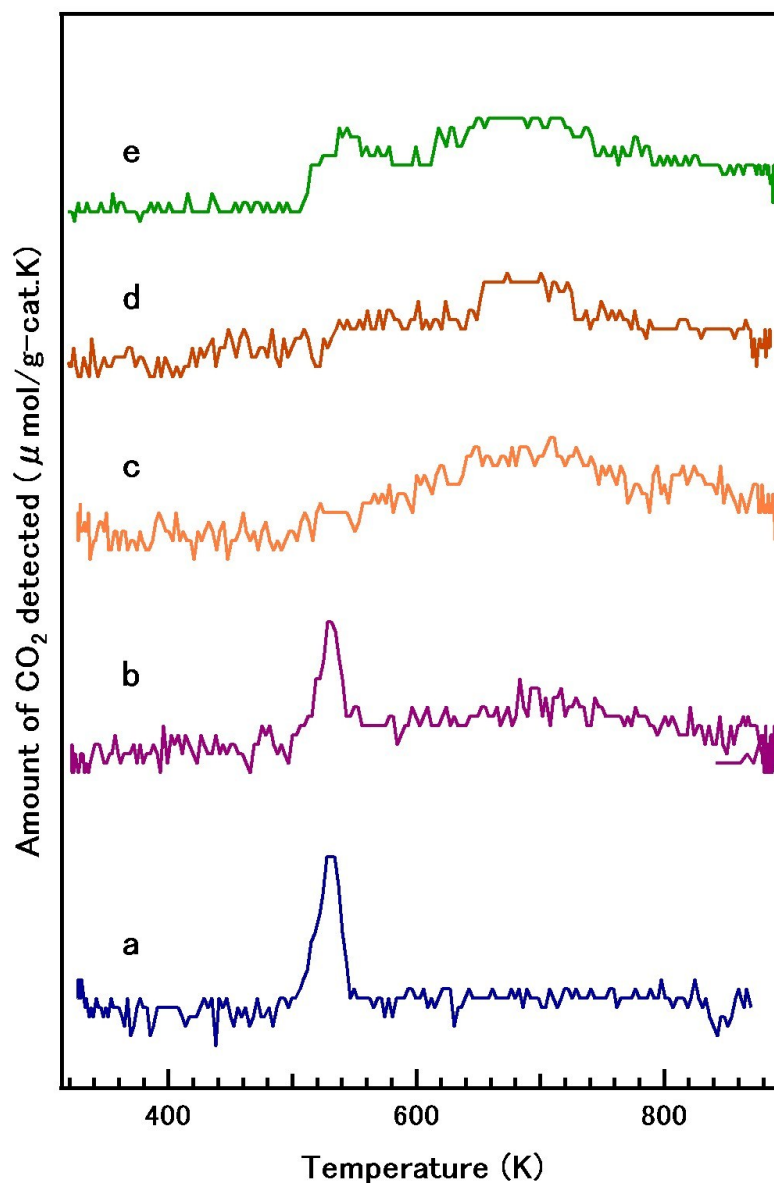


Fig. 3.23 CO-TPR profiles of the aged catalysts: (a) Rh/ZrO₂, (b) Rh/Zr-La-O, La=2.0 wt% (c) Rh/Zr-La-O, La=6.0 wt%, (d) Rh/Zr-La-O, La=10.0 wt% and (e) Rh/Zr-La-O, La=20.0 wt%.

3.3.11 Influence of aging time on the sintering of rhodium particles

To investigate the sintering process of rhodium particles and phase alteration of Zr–La–O support, we aged the Rh/Zr–La(6)–O catalyst at 1273 K for different aging time (1 h, 2 h, 6 h, 12 h, and 24 h). XRD patterns after these aging treatments are shown in Fig. 3.24. After aging at 1273 K for 1 h, monoclinic-ZrO₂ and tetragonal-ZrO₂ were observed. Since the tetragonal ZrO₂ was the main structure of the fresh Rh/Zr–La–O catalyst, aging at 1273 K altered a part of the support phase from tetragonal ZrO₂ to monoclinic ZrO₂. At this aging time (1273 K for 1 h), there were no diffractions of rhodium and that of La₂Zr₂O₇. After the aging for 24 h, however, the diffraction of rhodium at $2\theta = 41.07^\circ$ was detected (Fig. 3.24b, pattern 5). Similarly, the diffraction peaks of La₂Zr₂O₇ were observed after aging for 12 h and for 24 h (Fig. 3.24a, patterns 4 and 5). These results indicate that La₂Zr₂O₇ was gradually formed on the support and sintering of rhodium particles could be accelerated during the period from 12 to 24 h of the aging treatment. Phase stability and the local structure of La could have an impact for the rhodium sintering processes.

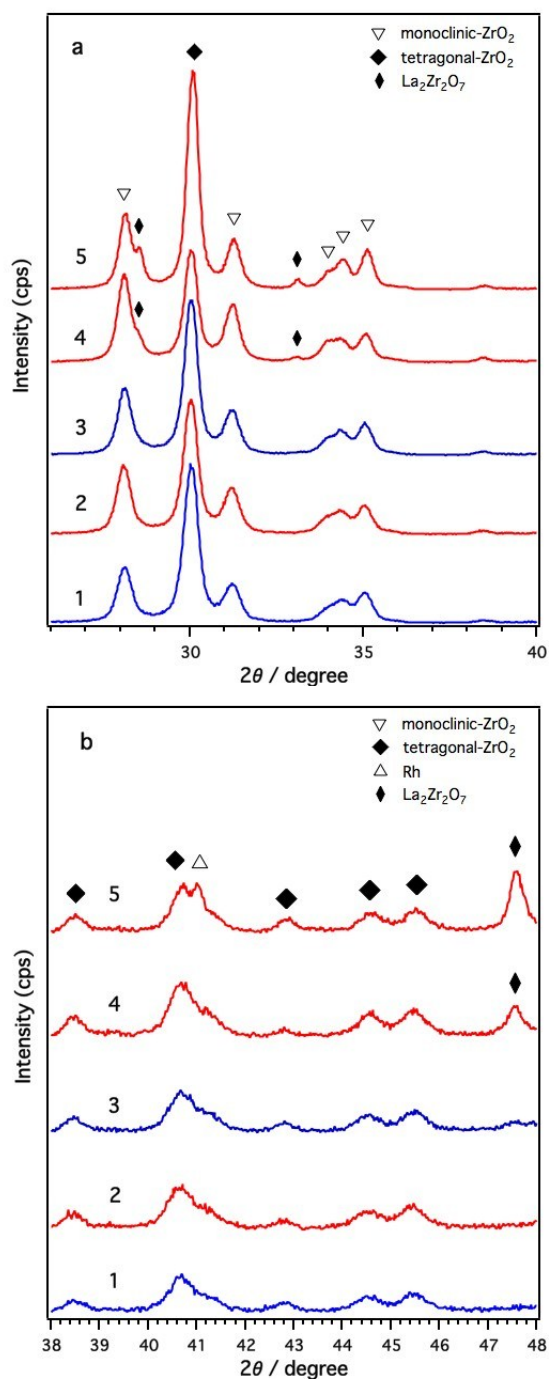


Fig. 3.24 XRD patterns of Rh/Zr-La-O with 6 wt% of La aged at 1273 K for 1) 1 h, 2) 2 h, 3) 6 h, 4) 12 h and 5) 24 h. Top panel (a) represents the region of $2\theta = 26^\circ$ to 40° , bottom panel (b) represents the region of $2\theta = 38^\circ$ to 48° in the same diffraction patterns.

3.4 Discussion

We have described in Chapter 2 that the Rh/Zr–La–O three-way catalyst is highly active under oxygen-fluctuating reaction conditions as opposed to Rh catalysts supported on ZrO₂ or lanthanoid-added ZrO₂.¹⁶ In this chapter, we investigated the catalytic performance of the catalysts before and after an aging treatment. In particular, we focused on the oxidation states of Rh in the Rh-based catalysts and on the tolerance behavior of the catalysts against oxidation pre-treatments.

The oxidation treatment of the fresh catalysts elicited differences between the catalysts in terms of the oxidation states of Rh. The latter were elucidated by XPS and the O/Rh molar ratios, as derived from the CO-TPR profiles (Table 3.3). Rh oxidized species (*i.e.*, Rh³⁺) were detected by XPS following oxidation treatment of Rh/ZrO₂. However, a relatively low O/Rh molar ratio of 0.14 was measured, demonstrating that only the surface of the Rh particles was oxidized to Rh³⁺. Strong Rh³⁺ XPS signals and considerably high O/Rh ratios from *ca.* 1.1 to 1.6 were obtained for Rh/Zr–Ce–O, Rh/Zr–Pr–O, and Rh/Zr–Nd–O. In contrast, Rh/Zr–La–O featured XPS peaks centered between the binding energies corresponding to Rh⁰ and Rh³⁺ and a relatively low O/Rh ratio of 0.7. In summary, the rhodium species, supported on the different lanthanoid-containing ZrO₂ supports, except for the Zr–La–O support, were oxidized to the high valence states, following the oxidation treatment. Thus, demonstrating that the Rh particles, supported on Zr–La–O, have a high tolerance to the oxidation treatment. The performance of the three-way catalyst correlated with these characteristic differences, as shown in Figs. 3.1 and 3.2. Both the fresh and aged Rh/Zr–La–O showed the highest performance especially after the oxidation treatment.

The high tolerance of fresh Rh/Zr–La–O against oxidation is possibly because of favorable chemical and/or electronic interactions between the highly dispersed Rh particles (diameter: 2 nm; dispersion >50%, as determined by CO chemisorption) and the La-modified ZrO₂ support. The aged catalysts featured larger Rh particles, as determined by TEM and CO chemisorption. Rh/Zr–La–O had plate-like Rh particles of *ca.* 100 nm in size and Rh/Zr–Pr–O had thick Rh particles of *ca.* 100–200 nm in size, based on TEM. Accordingly, the Rh dispersion in the aged catalysts, as assessed by CO chemisorption, drastically decreased to *ca.* 3–6%. Thus, it is

unlikely that the oxide support influences the catalytic performance through strong interactions between the Rh particles and the support.

XPS analysis of the catalysts, however, showed significant differences in the oxidation states of the Rh particles after the oxidation treatment. Rh, supported on lanthanoid-modified ZrO_2 , featured intermediate oxidation states except for Rh/Zr–Nd–O and Rh/ZrO₂ that exhibited Rh³⁺ signals (Fig. 3.9B). The Rh-based catalysts, following the three-way catalytic reaction, also possessed Rh species with different oxidation states, as determined by XPS. Rh/Zr–La–O, Rh/Zr–Ce–O, and Rh/Zr–Pr–O showed Rh⁰ signals whereas Rh/ZrO₂ and Rh/Zr–Nd–O exhibited Rh³⁺ signals (Fig. 3.9A).

The catalytic performances of the aged catalysts differed considerably especially after the oxidation treatment (Figs. 3.3b and 3.4b). Rh/Zr–La–O exhibited the best catalytic activity among all the catalysts. Additionally, the aged Rh/Zr–La–O exhibited the highest activity for the steam reforming reaction of C₃H₆. This reaction generates molecular hydrogen that reduces the previously oxidized Rh (Fig. 3.15), thereby regenerating the catalyst that was originally deactivated by the oxidation treatment (Fig. 3.16). The recovery effect by the steam reforming reaction was the largest for Rh/Zr–La–O (Fig. 3.16). The very broad CO-TPR profile, as featured by Rh/Zr–La–O only (Fig. 3.11b), suggests that the plate-like Rh particles in the aged Rh/Zr–La–O possess different reduction properties to those exhibited by the rhodium species in the other catalysts. However, this was not directly related to the superior performance of the catalyst. It is very likely that the molecular hydrogen, produced by the steam reforming reaction, reduces the oxidized Rh species to regenerate the catalytic activity of the catalyst. These results highlight the important role of the catalyst support for the self-regeneration of the catalyst under an oxidative atmosphere.

The highest three-way catalytic activity was achieved at 6 wt% of La addition. At this La content, tetragonal ZrO_2 phase was predominant (Fig. 3.19). On the contrary, for La content over the 6 wt%, $\text{La}_2\text{Zr}_2\text{O}_7$ appeared. From these results, La addition around 6 wt% could be a criterion for stabilizing ZrO_2 structure after 1273 K aging. CO-TPR results for aged catalysts suggested that the La amount affect the reducibility of rhodium, and La addition over the 6 wt% caused broad reduction profiles (Fig. 3.23). It was pointed out that oxygen vacancies in a lanthanoid-modified zirconia were detected by using neutron-scattering technique with a Rietveld analysis.^{30,31} They concluded that oxygen-vacancies induced by atomic displacements were formed in the structures of $\text{La}_{0.1}\text{Zr}_{0.9}\text{O}_{1.95}$ and $\text{Nd}_{0.1}\text{Zr}_{0.9}\text{O}_{1.95}$. They also pointed out that these oxygen vacancy sites might play an important role to produce surface OH groups that are

active for the water-gas shift reaction. These oxygen-defects in the supports could also relate to the observed low oxidation state of rhodium particles under oxidative conditions.

3.5 Conclusions

The high activity of fresh and aged Rh/Zr-La-O for three-way catalytic processes under an oxidative atmosphere is herein reported. Rhodium particles, supported on Zr-La-O, maintained their low oxidation state during the three-way catalytic reaction and even after the oxidation treatment unlike the rhodium particles, supported on ZrO₂ and other lanthanoid-containing ZrO₂. After aging at 1273 K, Rh/Zr-La-O exhibited superior performance for the steam reforming reaction. The steam reforming reaction enhanced the catalytic activity of Rh/Zr-La-O even though the catalyst was initially deactivated by an oxidation treatment. XPS results also confirmed the reduction of the rhodium species under the steam reforming reaction. The low valence state of rhodium, supported on Zr-La-O, was maintained by the steam reforming reaction, which produces molecular hydrogen that acts as a reductant. This effect was more pronounced in the aged Rh/Zr-La-O. These results highlight the importance of the catalyst support in designing three-way catalysts with high tolerance to oxidative reaction conditions.

References

1. R. Burch, J. P. Breen and F. C. Meunier, *Appl. Catal., B*, 2002, **39**, 283-303.
2. H. S. Gandhi, G. W. Graham and R. W. McCabe, *J. Catal.*, 2003, **216**, 433-442.
3. S. I. Matsumoto, *Catal. Today*, 2004, **90**, 183-190.
4. H. Muraki and G. Zhang, *Catal. Today*, 2000, **63**, 337-345.
5. M. V. Twigg, *Appl. Catal., B*, 2007, **70**, 2-15.
6. R. W. McCabe, R. K. Usmen, K. Ober and H. S. Gandhi, *J. Catal.*, 1995, **151**, 385-393.
7. K. C. Taylor, *Catal. Rev.;Sci. Eng.*, 1993, **35**, 457-481.
8. K. Dohmae, T. Nonaka and Y. Seno, *Surf. and Interface Anal.*, 2005, **37**, 115-119.
9. R. W. McCabe, R. K. Usmen, K. Ober and H. S. Gandhi, *J. Catal.*, 1995, **151**, 385-393.
10. R. Burch, P. K. Loader and N. A. Cruise, *Appl. Catal., A*, 1996, **147**, 375-394.
11. R. K. Usmen, R. W. McCabe, L. P. Haack, G. W. Graham, J. Hepburn and W. L. H. Watkins, *J. Catal.*, 1992, **134**, 702-712.
12. H. C. Yao, S. Japar and M. Shelef, *J. Catal.*, 1977, **50**, 407-418.
13. J. G. Nunan, H. J. Robota, M. J. Cohn and S. A. Bradley, *J. Catal.*, 1992, **133**, 309-324.
14. A. Trovarelli, *Catal. Rev.;Sci. Eng.*, 1996, **38**, 439-520.
15. T. Bunluesin, R. J. Gorte and G. W. Graham, *Appl. Catal., B*, 1998, **15**, 107-114.
16. H. Kawabata, Y. Koda, H. Sumida, M. Shigetsu, A. Takami and K. Inumaru, *Chem. Commun.*, 2013, **49**, 4015-4017.
17. T. Tanabe, A. Morikawa, M. Hatanaka, N. Takahashi, Y. Nagai, A. Sato, O. Kuno, H. Suzuki and H. Shinjoh, *Catal. Today*, 2012, **184**, 219-226.
18. U. Lindner and H. Papp, *Fresenius J. Anal. Chem.*, 1991, **341**, 387-394.
19. R. Burch and P. K. Loader, *Appl. Catal., A*, 1996, **143**, 317-335.
20. D. A. Constantinou and A. M. Efstathiou, *Appl. Catal., B*, 2010, **96**, 276-289.
21. T. Montini, L. De Rogatis, V. Gombac, P. Fornasiero and M. Graziani, *Appl. Catal., B*, 2007, **71**, 125-134.
22. K. Polychronopoulou, C. N. Costa and A. M. Efstathiou, *Appl. Catal., A*, 2004, **272**, 37-52.

23. K. Polychronopoulou, J. L. G. Fierro and A. M. Efstathiou, *J. Catal.*, 2004, **228**, 417-432.
24. B. I. Whittington, C. J. Jiang and D. L. Trimm, *Catal. Today*, 1995, **26**, 41-45.
25. J. Barbier-Jr and D. Duprez, *Appl. Catal., B*, 1994, **4**, 105-140.
26. C. Howitt, V. Pitchon and G. Maire, *J. Catal.*, 1995, **154**, 47-55.
27. D. J. C. Yates, L. L. Murrell and E. B. Prestridge, *J. Catal.*, 1979, **57**, 41-63.
28. J. C. Vis, H. F. J. Vantblik, T. Huizinga, J. Vangrondelle and R. Prins, *J. Catal.*, 1985, **95**, 333-345.
29. M. Machida, K. Murakami, S. Hinokuma, K. Uemura, K. Ikeue, M. Matsuda, M. R. Chai, Y. Nakahara and T. Sato, *Chem. Mater.*, 2009, **21**, 1796-1798.
30. C. K. Loong, J. W. Richardson, M. Ozawa and M. Kimura, *J. Alloy. Comp.*, 1994, 207, 174-177.
31. C. K. Loong, J. W. Richardson and M. Ozawa, *J. Catal.*, 1995, 157, 636-644.

Chapter 4

Highly active three-way catalysis of rhodium particles on a Y-stabilized La-containing ZrO₂ support

Chapter 4: Highly active three-way catalysis of rhodium particles on a Y-stabilized La-containing ZrO₂ support

4.1 Introduction

Three-way catalysis for automotive exhaust purification is an important process that has been extensively studied for several decades.¹⁻¹¹ Since emission regulations are constantly becoming more stringent worldwide,^{12, 13} there has been consistent focus on improving three-way catalytic activity and durability. The conditions to which a catalyst is subjected in automotive exhaust are severe: the temperatures and gas phase compositions quickly change over wide ranges. The most influential condition impeding catalytic activity is atmospheric changes in oxidant and reductant concentrations. Recently, a new type of engine operation was commercialized to minimize fuel consumption; the engine automatically switches off when the car stops for a short time. This new operation causes highly transient and fluctuating conditions, including high oxygen concentrations that deactivate three-way catalysts. Tolerance against oxidative conditions is crucial for designing a highly efficient three-way catalyst for practical applications.²

Rhodium is a key catalytic component in three-way catalysts for the effective conversion of CO, hydrocarbons and NO_x to H₂O, CO₂ and N₂.^{10, 14} However, rhodium has a number of drawbacks under oxidative conditions.^{3, 4} In the case of alumina supports, rhodium readily reacts with the support to form different phases at high temperatures. Rhodium is known to form oxides with various oxidation states, structures and morphologies (rafts or plate-like structures) on alumina supports.^{15, 16} Changes in size, shape and phase induced by rhodium interactions with alumina supports significantly affect the activity of the catalysts.^{17, 18} Bond formation between Rh and the support is possible for suppressing the sintering behaviour of rhodium.¹⁹ Zirconia has weaker interactions with rhodium than alumina does, and zirconia-modified alumina was reported to be useful for controlling the activity of rhodium.²⁰

Previously, we have demonstrated the high catalytic activity of rhodium supported on La-containing ZrO₂ (Rh/Zr–La–O) for the elimination of NO_x, CO and hydrocarbons, through a three-way catalytic process, from a synthetic automotive exhaust gas.^{21, 22} The catalyst showed better performance than other catalysts, especially after oxidative pre-treatment, though the

catalyst did not contain oxygen-storage components such as CeO_2 . The Rh/Zr–La–O catalyst showed high activity in the steam reforming reaction, even after an aging treatment that mimicked a mileage of 80 000 km for real vehicles. Exposure to steam reforming reaction conditions reduced the oxidized Rh on the Zr–La–O support, refreshing the deactivated catalyst. The state of rhodium was not only affected by interactions between the metal particles and the support, but also by the steam reforming reaction occurring over the catalyst. After the aging treatment, the Rh/Zr–La–O catalyst exhibited rhodium sintering and phase separation of the support, indicating that further work is required to develop more efficient catalysts.

In this chapter, we prepared a novel, highly active three-way catalyst, Rh supported on yttrium- and lanthanum-added zirconia (Rh/Zr–Y–La–O). We also investigated the effect of yttrium addition to ZrO_2 -based supports in detail. Yttrium is a typical stabilizing element for zirconia.²³ The redox properties and dispersion of rhodium, and the crystal structure of the support were significantly affected by the addition of Y. The importance of the steam reforming reaction was also demonstrated for the yttrium-added catalyst Rh/Zr–Y–La–O. These investigations aimed to identify the reason for the excellent three-way catalytic activity of Rh/Zr–Y–La–O.

4.2 Experimental

4.2.1 Catalyst preparation

The yttrium-stabilized ZrO_2 was prepared using an ammonia-assisted co-precipitation method where zirconium nitrate $\text{ZrO}(\text{NO}_3)_2 \cdot 6\text{H}_2\text{O}$ (60.8 g, > 98 %, Nacalai Tesque) and yttrium nitrate $\text{Y}(\text{NO}_3)_3 \cdot 6\text{H}_2\text{O}$ (8.7 g) were dissolved in 200 g of water and an aqueous NH_4OH solution (1 %, Wako Pure Chemical Industries, Ltd., Osaka, Japan) was added to raise the pH (≥ 12). The precipitate was filtered, dried at 423 K for 2 h in air, and then calcined at 773 K for 2 h in air to produce the $\text{ZrO}_2\text{--Y}_2\text{O}_3$ mixed oxide. The $\text{ZrO}_2\text{--La}_2\text{O}_3$ and Y-stabilized $\text{ZrO}_2\text{--La}_2\text{O}_3$ mixed oxides were also prepared using the ammonia-assisted co-precipitation method from $\text{Y}(\text{NO}_3)_3 \cdot 6\text{H}_2\text{O}$ and $\text{La}(\text{NO}_3)_3 \cdot 6\text{H}_2\text{O}$ (Rare Metallic Co., Ltd., Tokyo, Japan). For the preparation of Y-stabilized $\text{ZrO}_2\text{--La}_2\text{O}_3$, lanthanum nitrate, yttrium nitrate and zirconium nitrate were dissolved in water before adding an aqueous NH_4OH solution. The concentrations of Y and La were 10 and 5 wt % as oxides, respectively. The Y, La and Y–La mixed oxides were designated as Zr–Y–O, Zr–La–O and Zr–Y–La–O, respectively. The ZrO_2 support (Brunauer–Emmett–Teller (BET), surface area: $52.3 \text{ m}^2 \text{ g}^{-1}$) was purchased from Kishida Chemical Co., Ltd. (Osaka, Japan). Rhodium (0.33 wt % as rhodium metal) was loaded onto the oxide support by impregnation, using an aqueous solution of $\text{Rh}(\text{NO}_3)_3 \cdot \text{H}_2\text{O}$ (Dai-ichi Kigenso Kogyo, Osaka, Japan). The obtained Rh-loaded oxide supports were dried at 393 K for 12 h in air and subsequently calcined in air at 773 K. For evaluating the three-way catalytic reaction, the Rh-loaded ZrO_2 mixed oxide catalysts were deposited on a cordierite honeycomb. To do this, the Rh-loaded powder catalysts were mixed with distilled water and colloidal zirconia (ZSL-10D, Dai-ichi Kigenso Kogyo, Osaka, Japan) was used for binding the catalyst powder to the cordierite honeycomb. The slurry-coated cordierite honeycomb was dried at 473 K for 2 h in air, then calcined at 773 K for 2 h in air. The amount of catalyst coated on the cordierite honeycomb was 100 g dm^{-3} . The resulting products were termed “fresh” catalysts.

4.2.2 Three-way catalytic reaction

The activity of the Rh-based catalysts was evaluated using a fixed-bed continuous flow reactor. The reaction gas was a mixture of 500 ppm C₃H₆, 1000 ppm NO, 0.7 % CO, 0.2 % H₂, 0.6 % O₂, 13.6 % CO₂ and 10 % H₂O. Nitrogen was used as a diluent. The gas composition mimicked the actual exhaust gas emitted at ≈ 3000 rpm engine operation. The flow rate of the reaction gas was 26 dm³ min⁻¹, corresponding to an hourly gas space velocity of 60000 h⁻¹. Prior to catalytic performance measurements, the catalysts were pre-treated under a flow of the gas mixture at 773 K for 10 min and then cooled to 373 K under a flow of nitrogen. The three-way catalytic activity was evaluated over a range of temperatures from 373–773 K (at a heating rate of 30 K min⁻¹). The products were monitored using a flame ionization detector for hydrocarbons, infrared absorption for CO and chemical luminescence for NO using a Horiba MEXA-9100 system (Kyoto, Japan).

4.2.3 Aging procedure

Accelerated durability tests, or aging treatments, were conducted by treating the fresh catalysts at 1273 K for 24 h in a 2 % O₂ and 10 % H₂O atmosphere (diluent: N₂). This aging treatment simulated empirically a 80 000 km of mileage for real vehicles.

4.2.4 Steam-reforming reaction

The reaction gas was a mixture of 660 ppm C₃H₆ and 2 % H₂O (molar ratio of H₂O/C=10). Nitrogen was used as a diluent. The flow rate of the steam-reforming reaction gas was 26 dm³ min⁻¹ that corresponds to an hourly gas space velocity of 60000 h⁻¹. The activity of the steam-reforming reaction was measured using a fixed-bed continuous flow reactor the same as three-way catalytic activity measurements. Prior to the activity evaluations, the catalyst was pre-treated under three-way catalytic reaction gas at 773 K for 10 min and then cooled to 373 K under a flow of nitrogen.

4.2.5 Characterization

For each of the characterization techniques described in sections 4.2.5.1–4.2.5.5, catalysts were used in powder form without the cordierite honeycomb.

4.2.5.1 X-ray diffraction (XRD)

Powder XRD patterns were measured using a RINT-2000 (Rigaku Corporation, Tokyo, Japan) with monochromated Cu K α radiation ($\lambda = 1.54056 \text{ \AA}$). Crystalline phases were identified using PDF files. The mean Rh crystal size was determined from the Rh (111) diffraction peak at $2\theta = 40.1^\circ$ using Scherrer's equation.

4.2.5.2 Transmission electron microscopy (TEM)

TEM images were taken with a JEM-3000F microscope (JEOL Ltd., Tokyo, Japan). To image the catalyst after the catalytic reaction, the samples were treated under the reaction gas at 773 K for 10 min followed by cooling to room temperature under a nitrogen flow prior to specimen preparation. The approximate range of Rh particle sizes were evaluated from TEM images by counting about 10 to 20 particles from each sample.

4.2.5.3 Temperature-programmed reduction using CO (CO-TPR)

CO-TPR was carried out using CO (0.6 %) / He as the reductant gas ($100 \text{ cm}^3 \text{ min}^{-1}$) at a heating rate of 30 K min^{-1} . Prior to the TPR measurements, samples were pre-treated under a flow of 5 % O₂ at 773 K for 10 min and then cooled to 323 K under a flow of He. The O/Rh ratios were calculated from the amount of CO₂ formed during TPR. The supports without rhodium were also measured and the amount of evolved carbon dioxide was subtracted from the data of the rhodium-containing catalysts to estimate the rhodium oxidation state using the following equation 1.



4.2.5.4 *In situ* Fourier transform infrared (FT-IR) spectra

FT-IR spectra were recorded using a BioRad FTS-155 equipped with a diffuse reflectance *in situ* cell (ST Japan Inc., Tokyo, Japan). To clarify the state of rhodium after oxidation, spectra of adsorbed NO were measured. The sample was first pre-treated in 5 % O₂ in He at 773 K for 10 min and then cooled to 373 K under a flow of He. First, background spectra were taken at increasing temperatures from 373–773 K, with steps of 100 K in a flow of He. Then, the sample was cooled to 373 K under a flow of He and then the flow gas was switched to NO (1000 ppm) / He for each measurement. Spectra were recorded with a resolution of 4 cm⁻¹ at each increasing temperature from 373–773 K, with 100 K steps after exposure for 5 min to the gas flow containing the probed molecules for each measurement.

4.2.5.5 Other characterization techniques

Rhodium dispersion was measured using the CO pulse chemisorption method at 300 K. The catalysts were pre-treated as follows: the catalysts were first heated (heating rate of 30 K min⁻¹) in a flow of O₂ to 573 K and the temperature was held for 10 min. The catalyst temperature was then increased to 673 K in a H₂ flow and the temperature was maintained for 10 min, followed by cooling to 300 K in a He flow. Pulses of known amounts of CO were injected into the flowing gas and the CO concentrations at the outlet of the reactor were monitored using a thermal conductivity detector. The dispersion was calculated from the CO uptake, assuming that CO adsorbed to the surface of the Rh particles with a 1:1 stoichiometry for CO:surface Rh.³⁰ The rhodium particle size was estimated using the dispersion value from Equation 2,³¹

$$L = f \times M / (\rho \times N_A \times \pi \times r^2 \times D) \quad (2)$$

where L is the particle size (nm), f is the shape factor (spherical = 6), M is the atomic weight (103), ρ is the density (12.4 g cm⁻³), N_A is Avogadro's number (6.02×10^{23} mol⁻¹), r is the atomic radius (1.34×10^{-10} m) and D is the dispersion. The specific surface areas of the catalysts were measured by the BET one-point method using a Shimadzu Micrometrics Flowsorb 2300, SHIMADZU Corporation, Kyoto, Japan).

4.3 Results

4.3.1 Crystal phases of supports

Structural alterations caused by the introduction of Y and La into ZrO_2 were studied using XRD, as shown in Fig. 4.1. For fresh Rh/ZrO_2 , only the monoclinic ZrO_2 phase was detected (Fig. 4.1a). The addition of either Y or La to ZrO_2 stabilized the high temperature ZrO_2 phases; the cubic ZrO_2 phase was formed for $\text{Rh}/\text{Zr}-\text{Y}-\text{O}$ (Fig. 4.1c), and the tetragonal ZrO_2 phase was formed for $\text{Rh}/\text{Zr}-\text{La}-\text{O}$ (Fig. 4.1e). When both Y and La were added to ZrO_2 , the structure became cubic ZrO_2 . Regardless of the presence of La, addition of Y into zirconia caused the formation of the cubic phase (Fig. 4.1c and g). No diffraction peak of Rh was detectable for the fresh catalysts.

After the aging treatment at 1273 K, the structure of Rh/ZrO_2 did not change from monoclinic ZrO_2 (Fig. 4.1b). For $\text{Rh}/\text{Zr}-\text{La}-\text{O}$ after the aging treatment, the tetragonal ZrO_2 transformed into three phases. One was tetragonal ZrO_2 as the major phase, and the others were monoclinic ZrO_2 and $\text{La}_2\text{Zr}_2\text{O}_7$ as minor phases (Fig. 4.1f). $\text{La}_2\text{Zr}_2\text{O}_7$ had a pyrochlore structure with 1:1 molar ratio of La and Zr. In contrast, as shown in Fig. 4.1d and h, the cubic ZrO_2 phase was maintained, even after the aging treatment, for $\text{Rh}/\text{Zr}-\text{Y}-\text{O}$ and $\text{Rh}/\text{Zr}-\text{Y}-\text{La}-\text{O}$. The introduction of Y to ZrO_2 resulted in the formation of the cubic ZrO_2 phase for both the fresh and aged catalyst. Rhodium diffraction peaks for the aged catalysts were very weak but Rh 111 peak was detectable for some aged catalysts (Fig. 4.2).

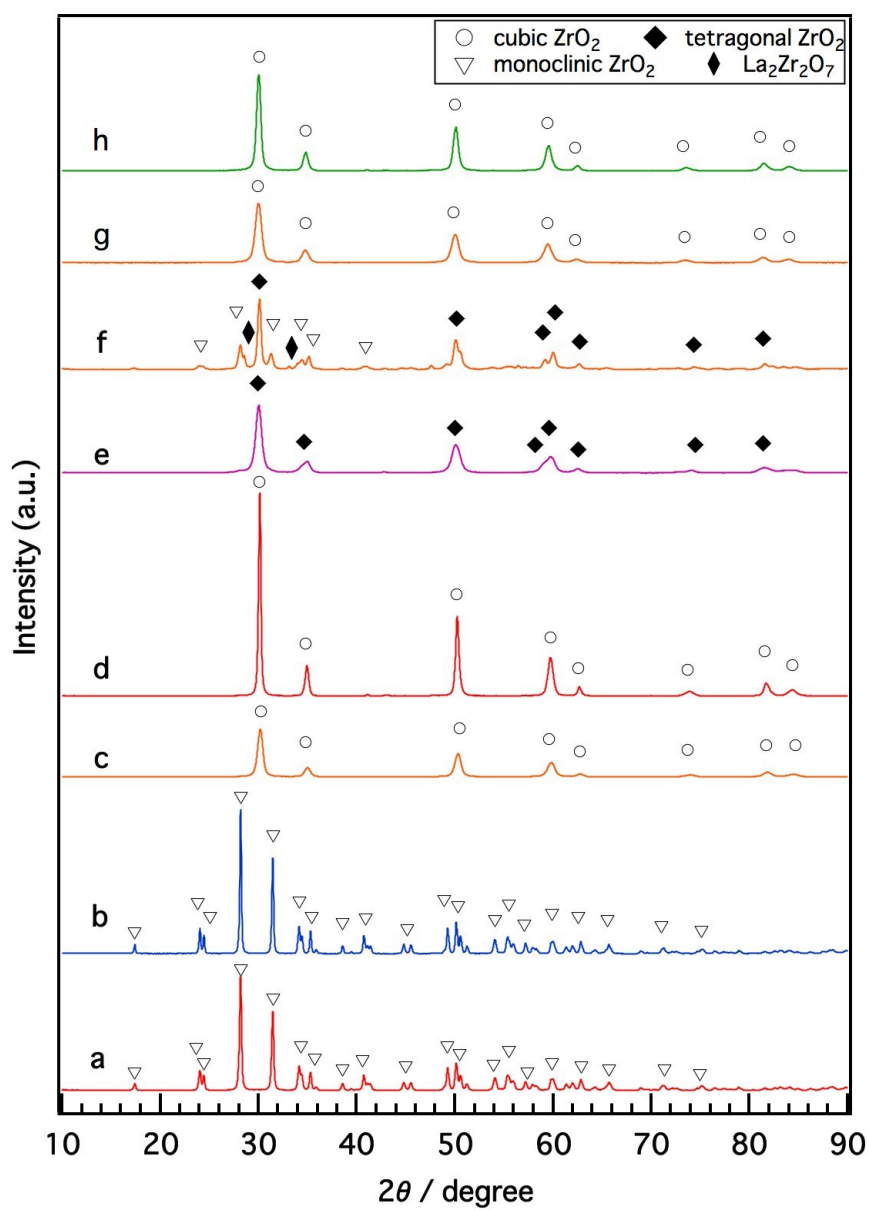


Fig. 4.1 XRD patterns of (a) fresh Rh/ ZrO_2 , (b) aged Rh/ ZrO_2 , (c) fresh Rh/Zr–Y–O, (d) aged Rh/Zr–Y–O, (e) fresh Rh/Zr–La–O, (f) aged Rh/Zr–La–O, (g) fresh Rh/Zr–Y–La–O and (h) aged Rh/Zr–Y–La–O. Aging was conducted at 1273 K in a 2 % O_2 , 10 % H_2O , N_2 atmosphere for 24 h.

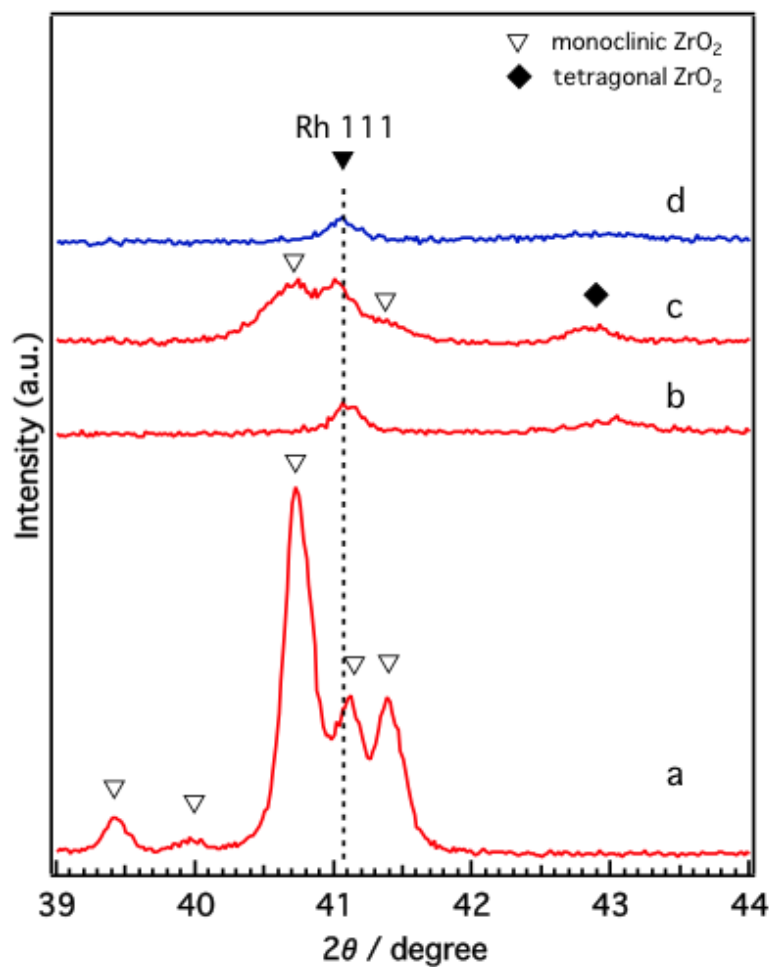


Fig. 4.2 XRD patterns for the aged catalysts of Rh111 region at (a) Rh/ZrO₂, (b) Rh/Zr–Y–O, (c) Rh/Zr–La–O and (d) Rh/Zr–Y–La–O. Aging was conducted at 1273 K in a 2 % O₂, 10 % H₂O, N₂ atmosphere for 24 h.

4.3.2 Effects of oxidation treatment on the performance of the three-way rhodium-based catalysts

Because of recently developed engine operations, catalytic activity after exposure to oxidative conditions is an important criterion for applications in real vehicles. We have previously reported that Rh/Zr–La–O showed higher three-way catalytic activity compared with Rh/ZrO₂ and rhodium supported on other lanthanide (Ce, Pr or Nd)-added ZrO₂.^{21, 22} In this study, the catalytic activities were evaluated for Y-stabilized ZrO₂ and for Y-stabilized Zr–La–O using two different pre-treatments. The first was a treatment under the reaction gas (simulated automotive exhaust) and the second was under oxidative conditions. For the fresh catalysts, their activities after treatment under the reaction gas and after the oxidation pre-treatment are shown in Figs. 4.3 and 4.4, respectively. Figures 4.7 and 4.8 present the activities of the aged catalysts after the two different pre-treatments. In each figure, the top panel shows hydrocarbon conversion and the bottom panel shows NO_x conversion. Corresponding CO conversions are also provided as Figs. 4.5 and 4.6 for the fresh catalysts, and Figs. 4.9 and 4.10 for the aged catalysts.

First, the effects of Y addition on the activity of the fresh catalysts were studied. After the reaction gas pre-treatment, the activity of Rh/Zr–Y–O decreased compared with Rh/ZrO₂ for both hydrocarbon conversion (Fig. 4.3a) and NO_x conversion (Fig. 4.3b). For Y addition to the Rh/Zr–La–O, hydrocarbon and NO_x conversion were both enhanced, as shown in Fig. 4.3a and 4.3b, respectively. This indicates that Rh/Zr–Y–La–O had higher catalytic activity than the previously reported Rh/Zr–La–O catalyst.

The effects of Y addition on the activities of the fresh catalysts that underwent the oxidative pre-treatment were also investigated. Figure 4 presents the results of the activity tests. After the oxidative pre-treatment, Rh/Zr–Y–O showed almost the same hydrocarbon conversion activity as Rh/ZrO₂ (Fig. 4.4a) and the activity of Rh/Zr–Y–La–O was comparable to that of Rh/Zr–La–O. For NO_x conversion, Y addition slightly enhanced the activity for Rh/Zr–Y–La–O and Rh/Zr–Y–O compared with the catalyst without Y (Fig. 4.4b). Rh/Zr–Y–La–O had the best catalytic activity after the oxidative pre-treatment.

The NO conversion started at 500K, which was lower temperature compared to the C₃H₆ conversion (520 K). The conversion of CO started at almost the same temperature as NO conversion (Figs. 4.5 and 4.6). NO must have reacted with CO and/or H₂ in the reaction gas

before C_3H_6 started to convert.

The effects of Y addition on the activities of the aged catalysts were also studied, as shown in Fig. 4.7. After the reaction gas pre-treatment, Rh/Zr-Y-O had higher hydrocarbon and NO_x conversion than Rh/ZrO₂. Also, Rh/Zr-Y-La-O had higher hydrocarbon and NO_x conversion than Rh/Zr-La-O (Fig. 4.7a and b). Among the tested catalysts, Rh/Zr-Y-La-O had the highest activity for hydrocarbon and NO_x conversions. After the oxidative pre-treatment of the aged catalysts (Fig. 4.8), the activity of Rh/Zr-Y-La-O was comparable to, or slightly lower than, that of Rh/Zr-La-O. Rh/Zr-Y-O also had activities similar to Rh/Zr-Y-La-O. Rh/ZrO₂ had much lower activity than the other catalysts under these conditions.

We measured the inlet and outlet temperatures of the catalyst bed at the working state of three-way catalysis by using thermocouples. When the conversion of C_3H_6 and NO started in three-way catalytic reaction at around 520K, the outlet temperature showed higher values than the inlet temperature (Fig. 4.11), indicating the occurrence of exothermic reaction (e.g. hydrocarbon oxidation). When the temperature raised up to 673 K, however, the outlet temperature became lower than the inlet temperature. This phenomenon demonstrated that the endothermic reaction such as steam-reforming reaction was taking place during the three-way catalysis.

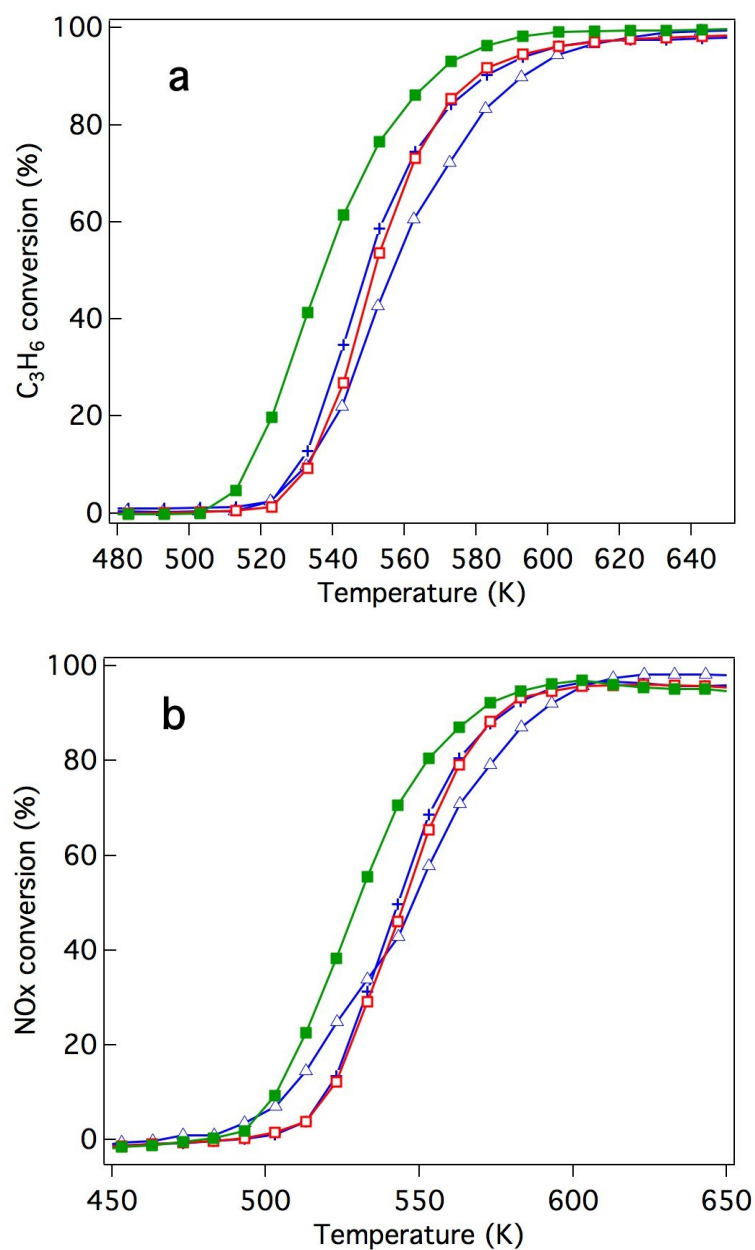


Fig. 4.3 Conversion of the fresh three-way catalysts that underwent the reaction gas pre-treatment for (a) C_3H_6 conversion and (b) NO_x conversion. The catalysts studied were (+) Rh/ZrO₂, (Δ) Rh/Zr-Y-O, (\square) Rh/Zr-La-O, and (\blacksquare) Rh/Zr-Y-La-O.

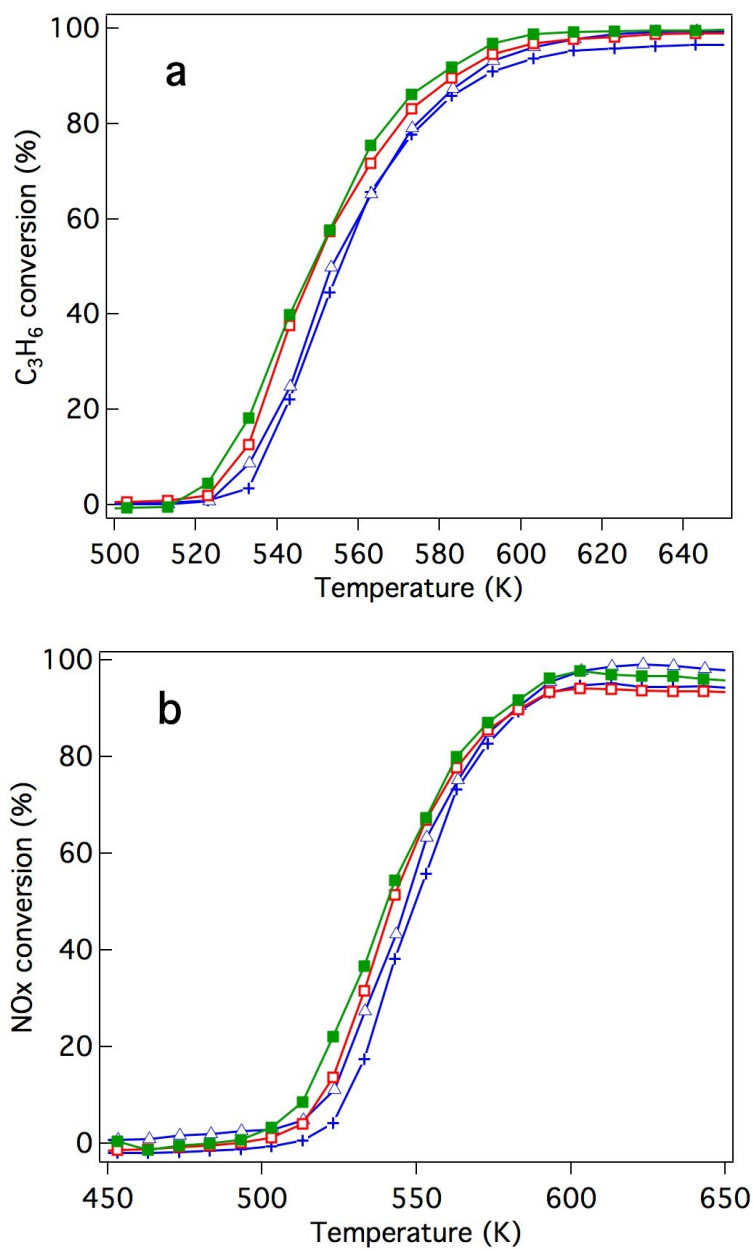


Fig. 4.4 Conversion of the fresh three-way catalysts that underwent the oxidation treatment for (a) C₃H₆ conversion and (b) NO conversion. The catalysts studied were (+) Rh/ZrO₂, (Δ) Rh/Zr-Y-O, (□) Rh/Zr-La-O, and (■) Rh/Zr-Y-La-O.

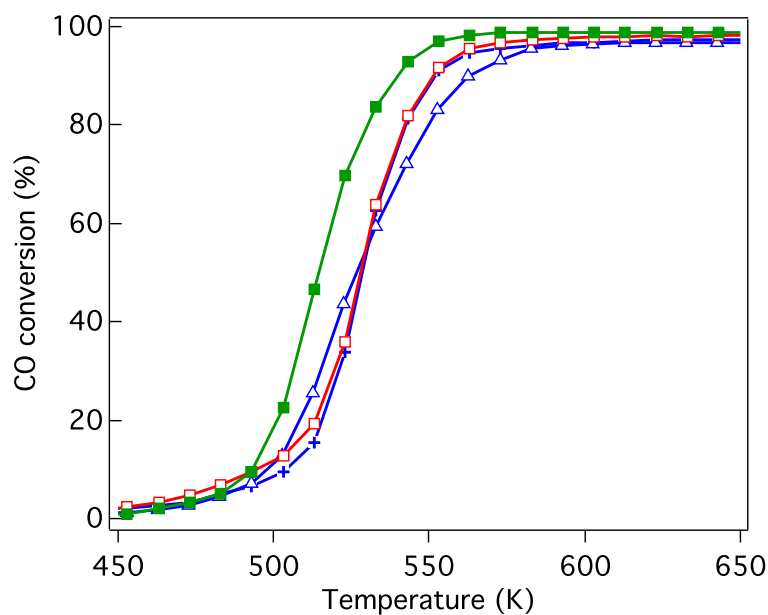


Fig. 4.5 CO conversion of the fresh three-way catalysts that underwent the reaction gas pre-treatment. The catalysts studied were (+) Rh/ZrO₂, (Δ) Rh/Zr-Y-O, (□) Rh/Zr-La-O, and (■) Rh/Zr-Y-La-O.

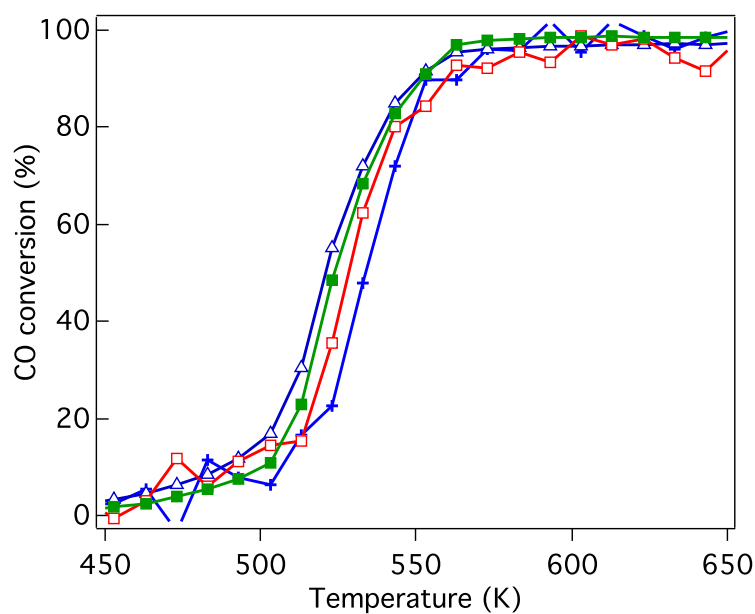


Fig. 4.6 CO conversion of the fresh three-way catalysts that underwent the oxidation treatment. The catalysts studied were (+) Rh/ZrO₂, (Δ) Rh/Zr-Y-O, (□) Rh/Zr-La-O, and (■) Rh/Zr-Y-La-O.

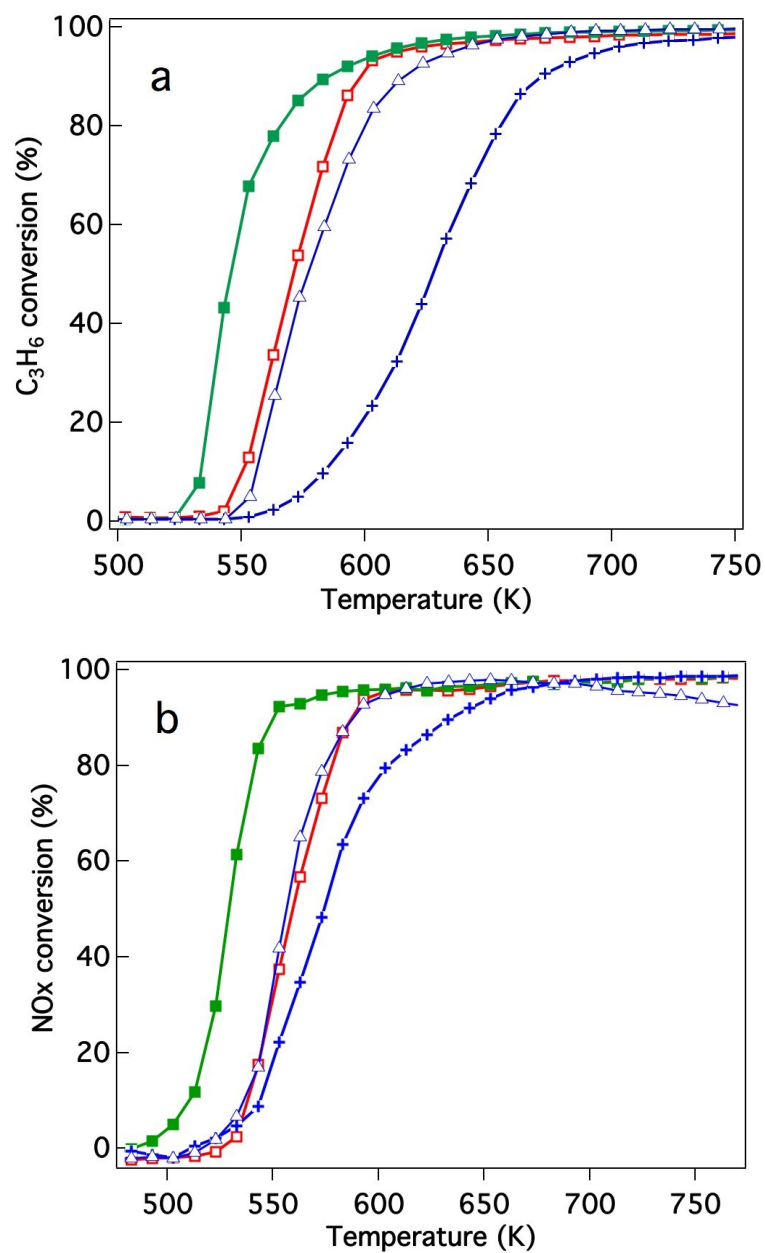


Fig. 4.7 Conversion by the aged three-way catalysts that underwent the reaction gas pre-treatment for (a) C₃H₆ conversion and (b) NO conversion. The catalysts studied were (+) Rh/ZrO₂, (Δ) Rh/Zr-Y-O, (□) Rh/Zr-La-O, and (■) Rh/Zr-Y-La-O.

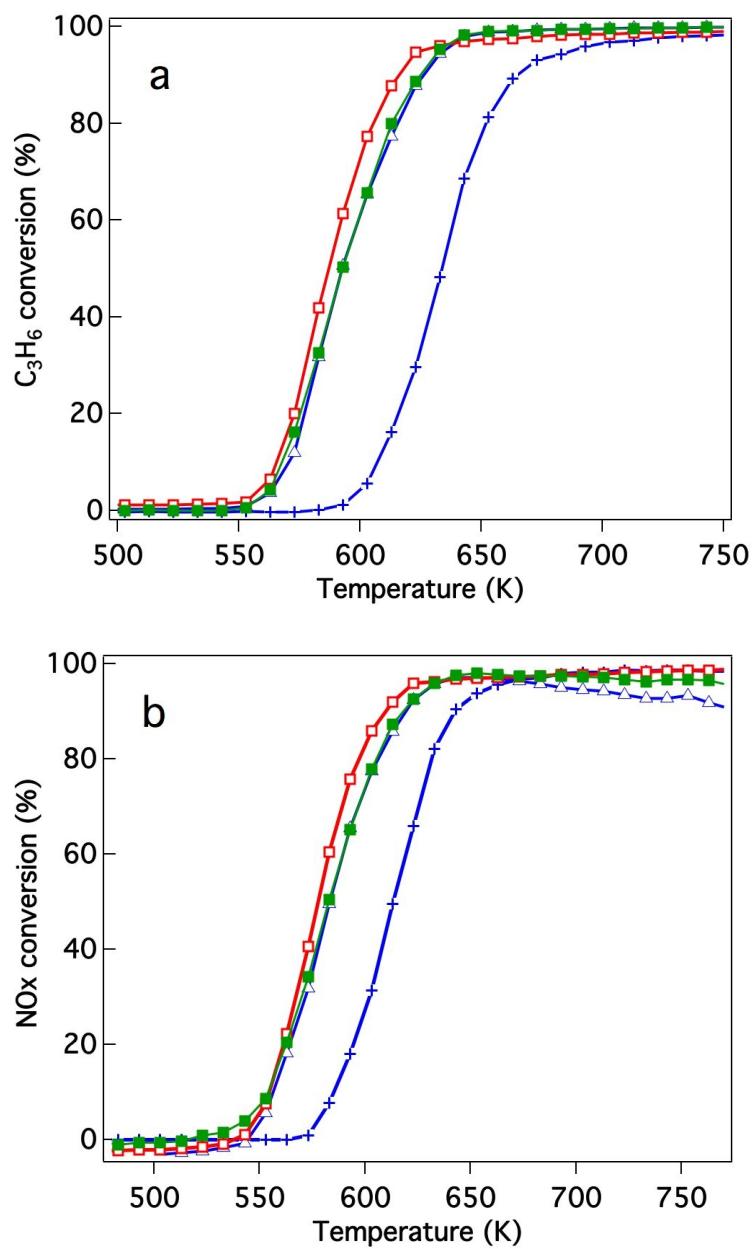


Fig. 4.8 Conversion by the aged three-way catalysts that underwent the oxidation treatment for (a) C₃H₆ conversion and (b) NO conversion. The catalysts studied were (+) Rh/ZrO₂, (Δ) Rh/Zr-Y-O, (□) Rh/Zr-La-O, and (■) Rh/Zr-Y-La-O.

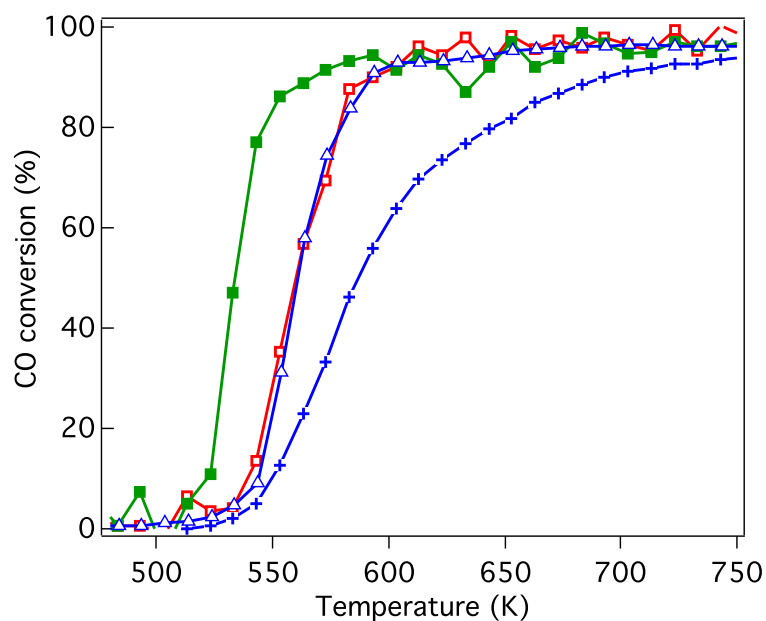


Fig. 4.9 CO conversion by the aged three-way catalysts that underwent the reaction gas pre-treatment. The catalysts studied were (+) Rh/ZrO₂, (Δ) Rh/Zr-Y-O, (\square) Rh/Zr-La-O, and (\blacksquare) Rh/Zr-Y-La-O.

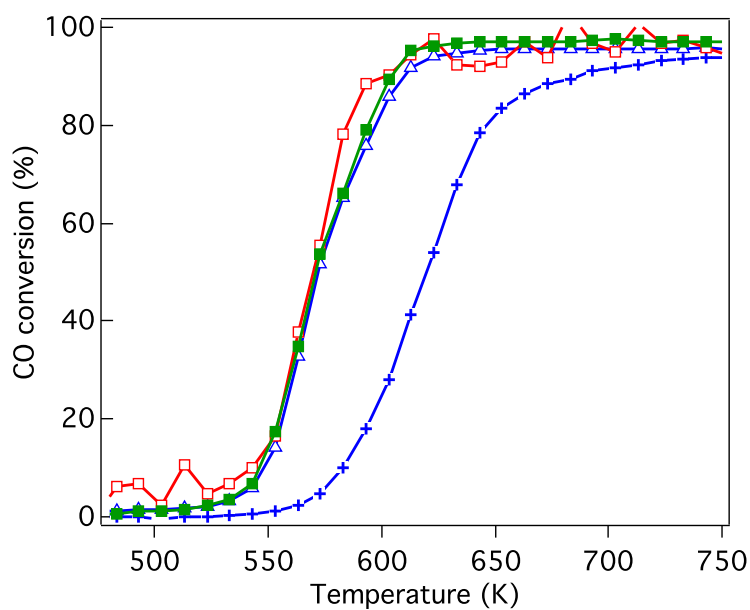


Fig. 4.10 CO conversion by the aged three-way catalysts that underwent the oxidation treatment. The catalysts studied were (+) Rh/ZrO₂, (Δ) Rh/Zr-Y-O, (\square) Rh/Zr-La-O, and (\blacksquare) Rh/Zr-Y-La-O.

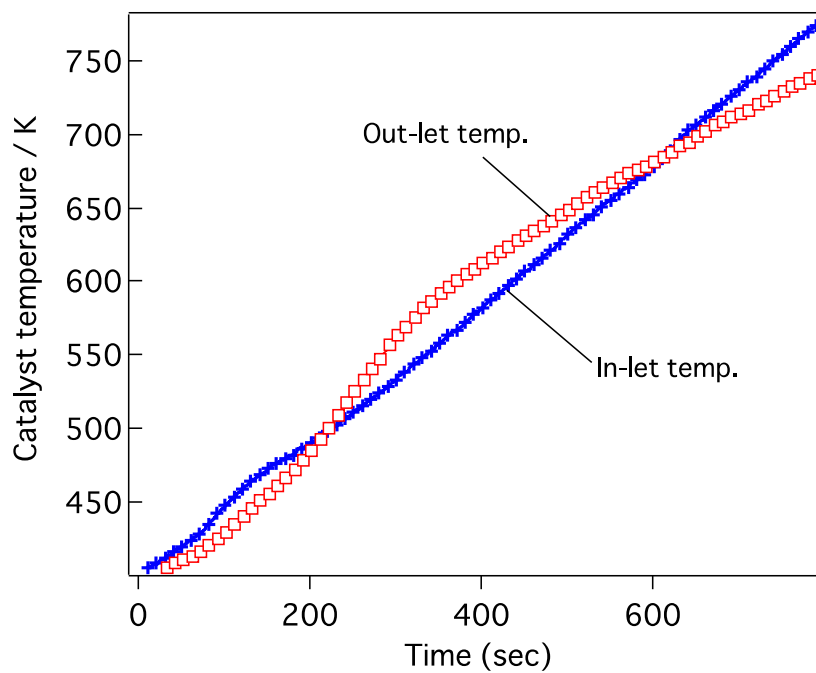


Fig. 4.11 Catalyst in-let and out-let temperature during the three-way catalytic activity measurement of aged Rh/Zr–Y–La–O. Aging was conducted at 1273 K and in 2 % O₂ and 10 % H₂O/N₂ for 24 h.

4.3.3 Rhodium particle sizes and dispersion on different supports

Figure 4.12 presents TEM images of the catalysts before and after the aging treatment. Figure 4.12a–d are images of fresh catalysts after the three-way catalytic run at 773 K for Rh/ZrO₂, Rh/Zr–Y–O, Rh/Zr–La–O and Rh/Zr–Y–La–O, respectively. Figure 4.12e–h are images of the aged catalysts presented in the same order as Fig. 4.12a–d. The particle size range of the support was 10–20 nm for Zr–Y–O (Fig. 4.12b), while for ZrO₂ the particle size range was 50–70 nm (Fig. 4.12a). Particle sizes for the Zr–La–O and Zr–Y–La–O supports both ranged from 10–20 nm (Fig. 4.12c and d). For the fresh catalysts, the support oxides formed smaller particles when La or Y was added. After the aging treatment, the particle size ranges for ZrO₂ and Zr–Y–O were 50–100 nm, indicating that the support particles of fresh catalysts sintered to form larger ones during the aging treatment (Fig. 4.12e and f). Conversely, the particle size ranges for Zr–La–O and Zr–Y–La–O were 10–20 nm, even after the aging treatment, implying that the La-containing supports do not readily sinter. The surface areas of these catalysts were in agreement with their particle sizes (Table 4.1). The BET surface areas of Rh/ZrO₂ and Rh/Zr–Y–O, in which support particle growth was observed, were 16.4 and 21.4 m²g⁻¹, respectively. Rh/Zr–La–O and Rh/Zr–Y–La–O, which had smaller particle sizes, had higher surface areas of 29.6 and 51.2 m²g⁻¹, respectively. The largest surface area was measured for Rh/Zr–Y–La–O, and the decrease in the surface area of this catalyst from the aging treatment was small (from 75.3 m²g⁻¹ to 51.2 m²g⁻¹) compared with the other catalysts.

The effect of Y addition on rhodium particle size is even more important. The rhodium particle size was approximately 1–2 nm for the fresh catalysts prepared in this study, as shown in Fig. 4.12a–d (the arrows indicate Rh particles). Table 4.1 lists the dispersion of Rh estimated by CO adsorption at 300 K for both the fresh and the aged catalysts. Rhodium dispersion in the fresh catalysts was greater than 50 % and Rh particle sizes estimated from the dispersion were approximately 2 nm, being consistent with the TEM observations. Rhodium particle sizes did not appear to be affected by the addition of Y. The presence of rhodium was confirmed from energy-dispersive x-ray (EDX) analysis for all the fresh and aged catalysts. For aged Rh/ZrO₂, spherical rhodium particles with diameters of approximately 10 nm were observed (Fig. 4.12e). Aged Rh/Zr–Y–O contained larger rhodium particles (diameter = 70 nm), as shown in Fig. 4.12f (EDX data are given as Fig. 4.13). For aged Rh/Zr–La–O, large rhodium particles (30–100 nm,

most likely thin, plate-like particles based on their pale contrasts) were observed (Fig. 4.12g, EDX data are given as Fig. 4.14). No nano-sized rhodium particles were detected in Rh/Zr–Y–O and Rh/Zr–La–O. In the TEM image of Rh/Zr–Y–La–O (Fig. 4.12h), a number of small rhodium particles (approximately 5 nm in size) were observed, while the particle size estimated by Scherrer's equation using the Rh 111 diffraction peak (Fig. 4.2) was approximately 80 nm, suggesting that larger particles were present in areas outside that covered in the TEM analysis. Although the Rh dispersion for all of the aged catalysts was quite low (below 10 %), aged Rh/Zr–Y–La–O exhibited the highest dispersion among the aged catalysts tested in this study. The rhodium particle sizes were calculated from the dispersion assuming that the particles were spherical. The values were 22.6, 27.7, 32.6 and 15.8 nm for Rh/ZrO₂, Rh/Zr–Y–O, Rh/Zr–La–O and Rh/Zr–Y–La–O, respectively. The smaller mean rhodium size for Rh/Zr–Y–La–O was consistent with the TEM observations.

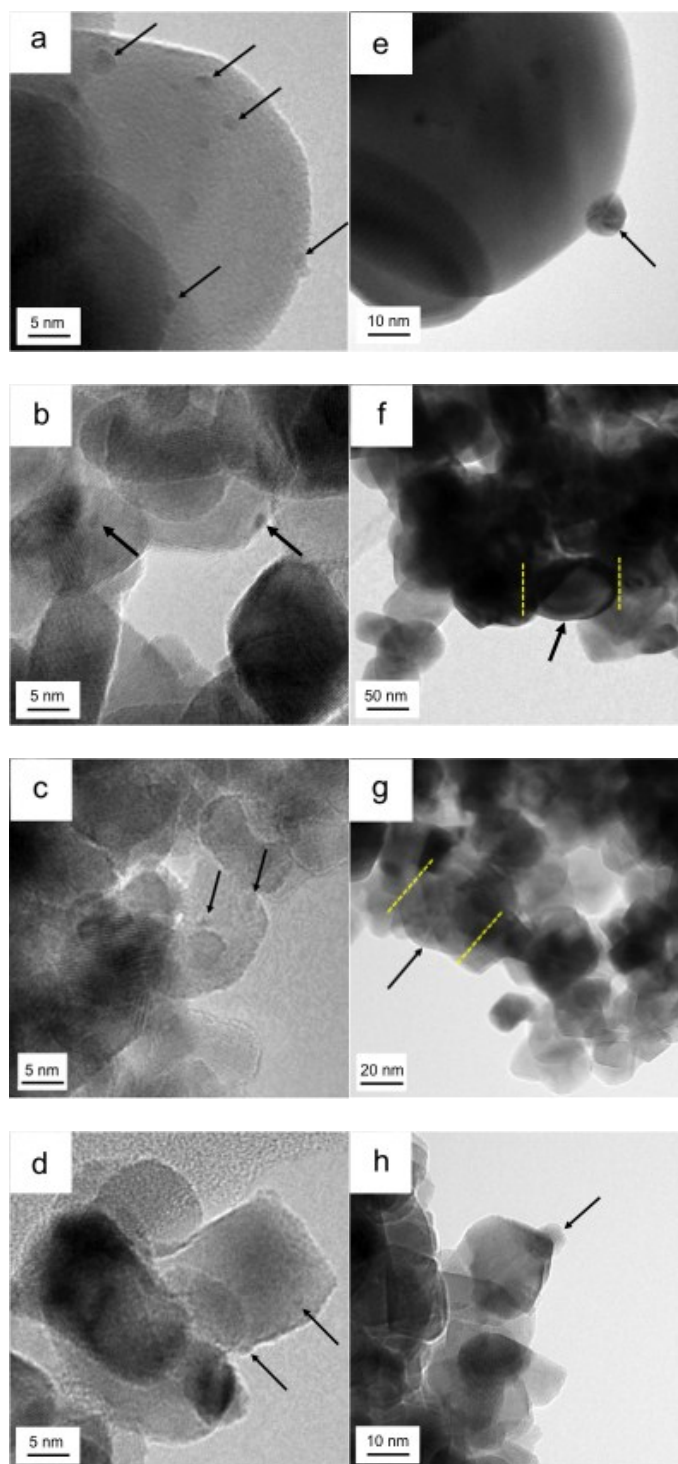


Fig. 4.12 TEM images of (a) fresh Rh/ZrO₂, (b) fresh Rh/Zr–Y–O, (c) fresh Rh/Zr–La–O, (d) fresh Rh/Zr–Y–La–O, (e) aged Rh/ZrO₂, (f) aged Rh/Zr–Y–O, (g) aged Rh/Zr–La–O, and (h) aged Rh/Zr–Y–La–O. Aging was conducted at 1273 K and in 2 % O₂ and 10 % H₂O/N₂ for 24 h.

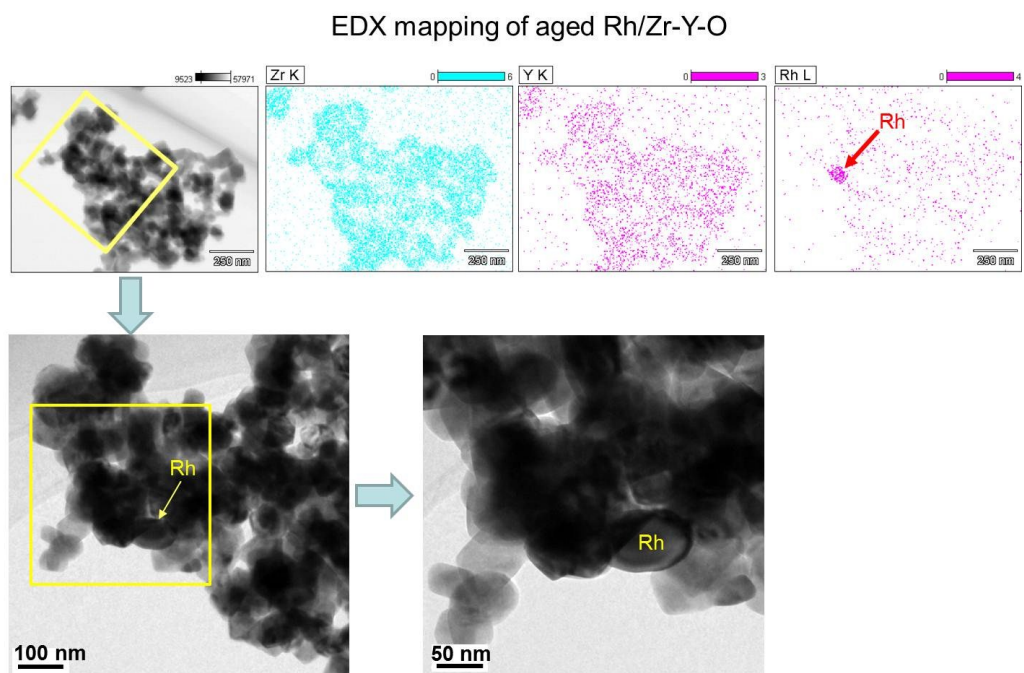
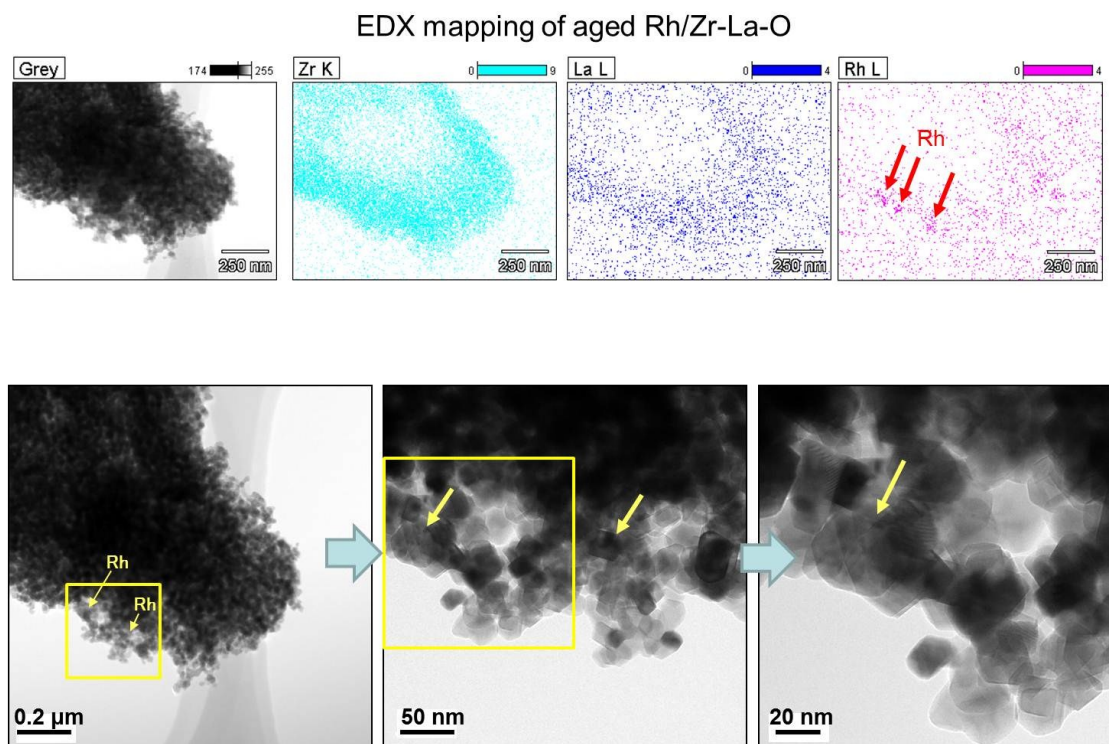


Fig. 4.13 EDX mapping of aged Rh/Zr-Y-O. Aging was conducted at 1273 K and in 2 % O₂ and 10 % H₂O/N₂ for 24 h.



EDX spectra of aged Rh/Zr-La-O

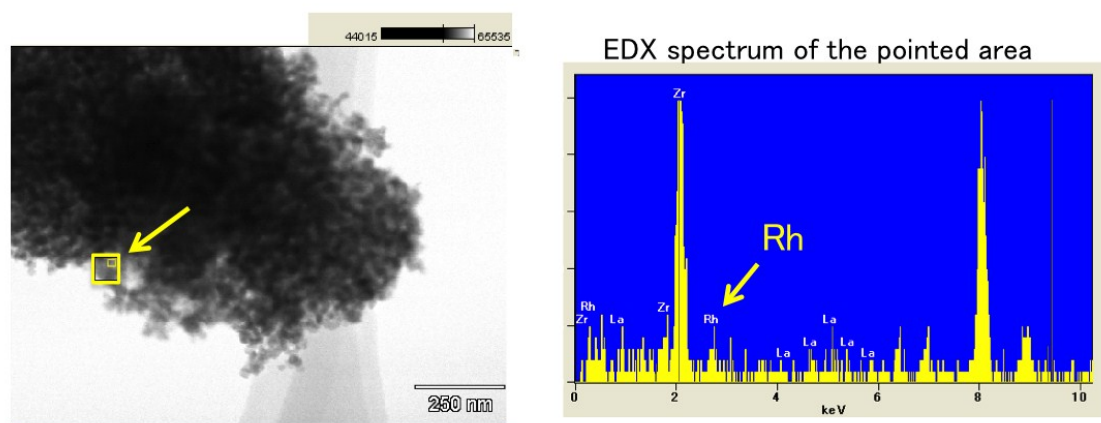


Fig. 4.14 EDX mapping and EDX spectrum of aged Rh/Zr-La-O. Aging was conducted at 1273 K and in 2 % O₂ and 10 % H₂O/N₂ for 24 h.

Table 4.1 Measured properties of the catalysts

Catalysts	BET surface area / $\text{m}^2 \text{g}^{-1}$		Rh dispersion ^a (%)	
	Fresh	Aged ^b	Fresh	Aged ^b
Rh/ZrO ₂	52.3	16.4	54.9	6.5
Rh/Zr–Y–O	57.3	21.4	68.3	5.3
Rh/Zr–La–O	85.8	29.6	87.4	4.5
Rh/Zr–Y–La–O	75.3	51.2	85.2	9.3

^a Determined by CO chemisorption.

^b Aged at 1273 K for 24 h in 2 % O₂ and 10 % H₂O/N₂ atmosphere.

4.3.4 Temperature-programmed reduction by CO (CO-TPR)

Temperature-programmed reduction profiles of the fresh catalysts are presented in Fig. 4.15. The O/Rh atomic ratios calculated from the TPR data are shown in Table 4.2. A higher O/Rh ratio (1.48) was measured for fresh Rh/Zr–Y–O compared with Rh/ZrO₂ (0.14). In our previous study, the oxidation state of rhodium on ZrO₂ analyzed by X-ray photoelectron spectroscopy (XPS) was trivalent after being oxidized by 5 % O₂. The difference between the low O/Rh ratio for Rh/ZrO₂ and the presence of trivalent rhodium from XPS results indicated that only the surface of rhodium particles were oxidized to Rh³⁺.²² Conversely, the O/Rh ratio was 1.48 for Rh/Zr–Y–O, indicating that all the rhodium particles were almost fully oxidized. Similarly, the amount of CO₂ generated during the TPR process increased by the addition of Y to Rh/Zr–La–O (Fig. 4.15c and d). A larger O/Rh ratio of 1.20 was measured for Rh/Zr–Y–La–O, while Rh/Zr–La–O had a lower O/Rh ratio of 0.70. The TPR profile also changed by Y addition to Rh/Zr–La–O. It should be noted that Rh/Zr–Y–La–O was more readily reduced at low temperature than Rh/Zr–La–O (Fig. 4.15c and d). These results indicate, for the fresh catalysts, that Y addition caused Rh to be more readily oxidized and the reducibility of Rh was also enhanced by the addition of Y to the La-containing catalyst. Figure 4.16 presents the CO-TPR profiles of the aged catalysts. A sharp peak was observed at 520 K for Rh/ZrO₂ and Rh/Zr–Y–O, as shown in Fig. 4.16a and b, respectively. Conversely, the aged Rh/Zr–La–O and Rh/Zr–Y–La–O catalysts exhibited a broad reduction profile starting at around 500 K (Fig. 4.16c and d). No significant effect of Y addition on the reduction profiles was detected for the aged catalysts.

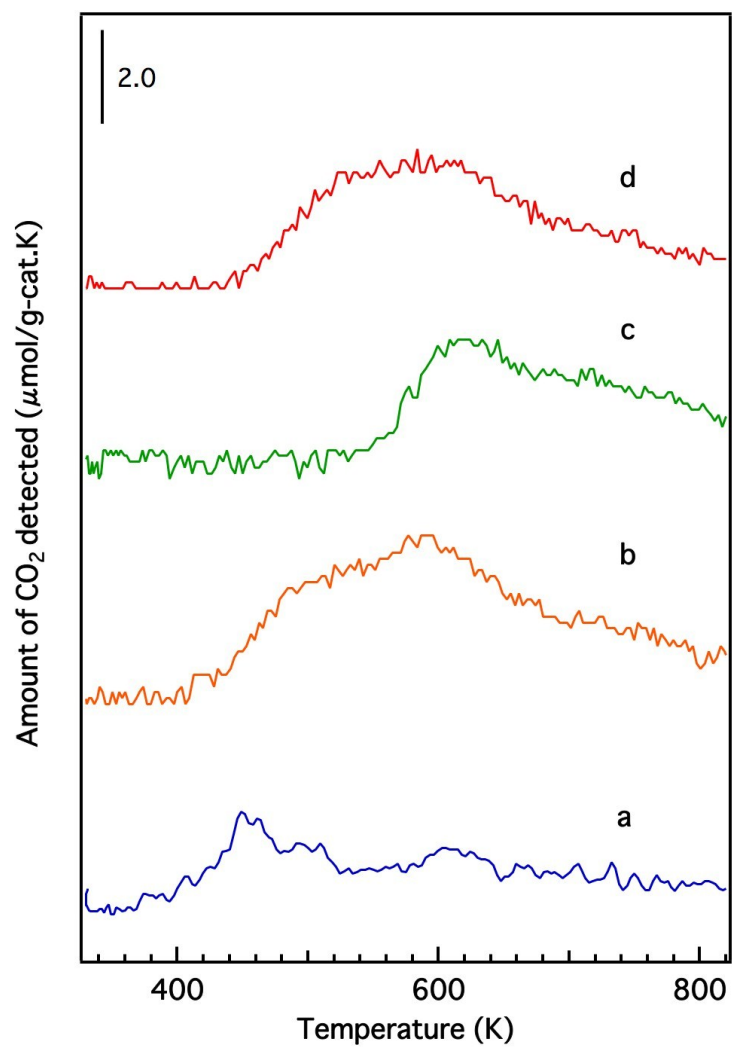


Fig. 4.15 CO-TPR profiles of the fresh catalysts: (a) Rh/ZrO₂, (b) Rh/Zr-Y-O, (c) Rh/Zr-La-O and (d) Rh/Zr-Y-La-O.

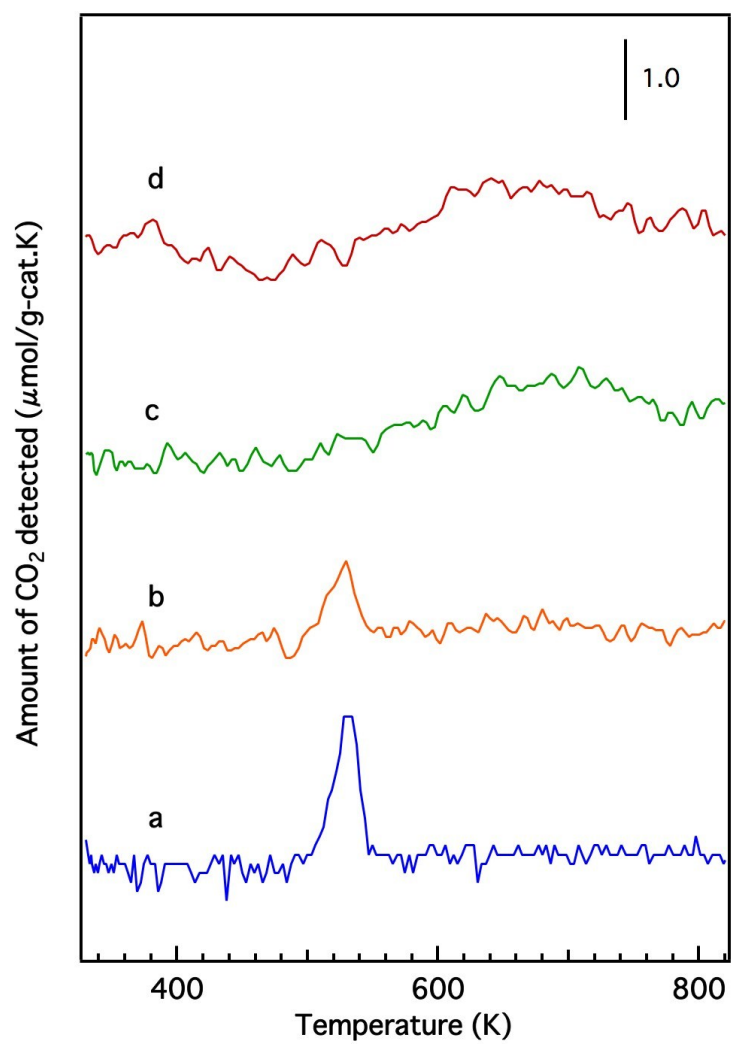


Fig. 4.16 CO-TPR profiles of the aged catalysts: (a) Rh/ZrO₂, (b) Rh/Zr–Y–O, (c) Rh/Zr–La–O and (d) Rh/Zr–Y–La–O.

Table 4.2 Amount of CO₂ (μmol g⁻¹) released during CO-TPR and O/Rh ratios

Catalysts	Amount of CO ₂ released / μmol g ⁻¹		O/Rh ratio ^a	
	Fresh	Aged ^b	Fresh	Aged ^b
Rh/ZrO ₂	45	59	0.14	0.20
Rh/Zr–Y–O	428	36	1.48	0.12
Rh/Zr–La–O	224	121	0.70	0.42
Rh/Zr–Y–La–O	344	155	1.20	0.54

^a Determined by CO-TPR.

^b Aged at 1273 K for 24 h in 2 % O₂ and 10 % H₂O/N₂ atmosphere.

4.3.5 Infrared spectra

Although XPS is a powerful tool to investigate the oxidation state of rhodium, the Y $3p_{3/2}$ signal at 311 eV overlaps with the Rh $3d_{5/2}$ signal at 307 eV. Therefore, in the case of Y-containing materials, information about rhodium was not accessible, especially when the loading of rhodium was as low as 0.33 wt %, as was the case in this study. For this reason, we employed NO molecules as probes for the Rh metallic state because it is widely accepted that NO readily forms $\text{Rh}^0\text{-NO}$ adsorbate on rhodium particles.^{24,25}

Figure 4.17 presents the IR absorption spectra of the Rh/Zr–La–O and Rh/Zr–Y–La–O catalysts after exposure to NO at various temperatures. Several bands associated with NO_x adsorbate were clearly detected for the La-containing catalysts. Bands at 1894, 1857, 1533, 1242 and 1185 cm^{-1} were observed for Rh/Zr–La–O (Fig. 4.17a). The band at 1857 cm^{-1} was assigned to $\text{Rh}^0\text{-NO}^{\delta+}$,²⁴ and the bands from 1533–1185 cm^{-1} were attributed to nitrate species.²⁶ The band at 1894 cm^{-1} was assigned to $\text{Rh}^1\text{-NO}^+$.²⁷ In the case of Rh/Zr–Y–La–O, the intensity of the $\text{Rh}^0\text{-NO}$ band at 1848 cm^{-1} was higher than for Rh/Zr–La–O at temperatures from 473–573 K (the magnified bands in Fig. 4.17). These results indicate that the amount of Rh^0 on the surface was higher for Rh/Zr–Y–La–O than for Rh/Zr–La–O.

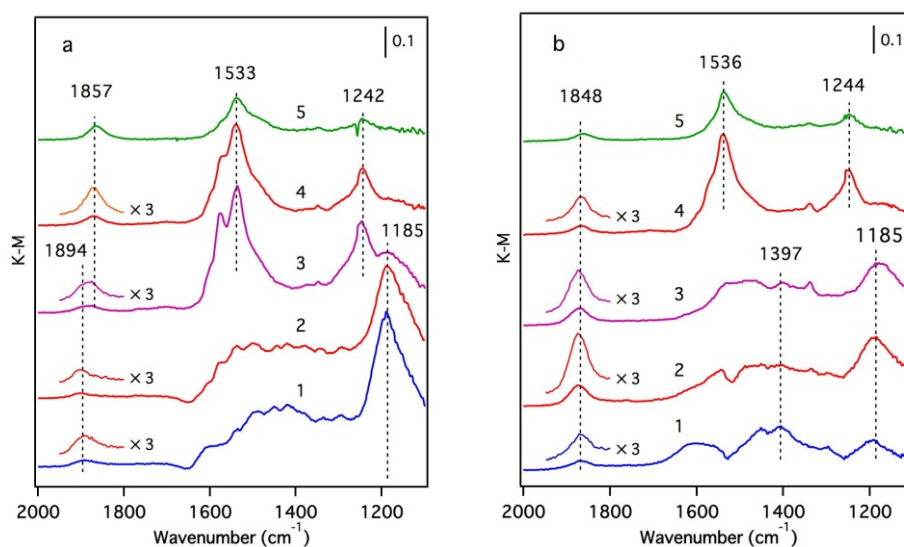


Fig. 4.17 IR spectra of NO adsorbed on fresh (a) Rh/Zr–La–O, (b) Rh/Zr–Y–La–O. Spectra were taken at (1) 373 K, (2) 473 K, (3) 573 K, (4) 673 K and (5) 773 K.

4.3.6 Steam reforming reaction activity and its effect on three-way catalysis

The steam reforming reaction is influential in three-way catalysis for enhancing NO_x conversion by producing hydrogen as a reductant. This reaction is known to proceed over Rh catalysts.^{28,29} Previously, we reported that exposure to the steam reforming reaction reduced the oxidized rhodium and recovered the activity of the catalyst.²² In this study, the effect of Y addition on this reaction was examined. Figure 4.18 presents C_3H_6 conversion in the steam reforming reaction over the fresh catalysts. The addition of Y to ZrO_2 resulted in a dramatic decrease in the activity of this reaction. Yttrium addition to La-containing ZrO_2 decreased the activity by a small amount, but the catalyst still maintained high activity. Figure 4.19 presents C_3H_6 conversion in the steam reforming reaction over the aged catalysts. Both Rh/Zr–La–O and Rh/Zr–Y–La–O exhibited superior activity compared with Rh/ZrO₂ and Rh/Zr–Y–O. It is evident that when Y was added to the support, the presence of La was highly effective in maintaining the catalyst's high steam reforming reaction activity for both fresh and aged catalysts.

The influence of the steam reforming reaction on the activity of the three-way catalysis was investigated for Rh/Zr–Y–O and Rh/Zr–Y–La–O to identify the impact of Y addition on the reaction. Figure 4.20a and b present the results for the aged Rh/Zr–Y–O and Rh/Zr–Y–La–O, respectively. First, the three-way catalytic activity of the aged catalysts was examined without any pre-treatment (curve 1 in each figure). The next experiments examined the three-way catalysis of the aged catalysts after pre-treatment under a 5 % O_2 flow at 773 K for 5 min (curves 2 in each figure). The final experiments investigated the three-way catalytic activity of the aged catalysts that were oxidized under a 5 % O_2 flow at 773 K for 5 min followed by the steam reforming reaction at 520 K for 5 min (curves 3 in each figure). The oxidative pre-treatment caused dramatic decreases in the three-way catalytic activities for the two tested catalysts. In the case of Rh/Zr–Y–O, which had low steam reforming activity, recovery of the three-way catalytic activity after the steam reforming reaction was limited (Fig. 4.20 a, curve 3). Conversely, Rh/Zr–Y–La–O showed a complete recovery (Fig. 4.20 b, curve 3) after the steam reforming reaction from the low activity after the oxidation treatment (Fig. 4.20 b, curve 2). Besides hydrogen and CO generated by the steam reforming reaction, C_3H_6 also recovered the three-way catalytic activity for Rh/Zr–La–O (results not shown). Recovery of the catalyst by the steam reforming reaction included the contribution of C_3H_6 as a reductant. These experiments

demonstrated that the regenerative effect of the steam reforming reaction worked well for Rh/Zr–Y–La–O, as was also observed for Rh/Zr–La–O in our previous study.²¹

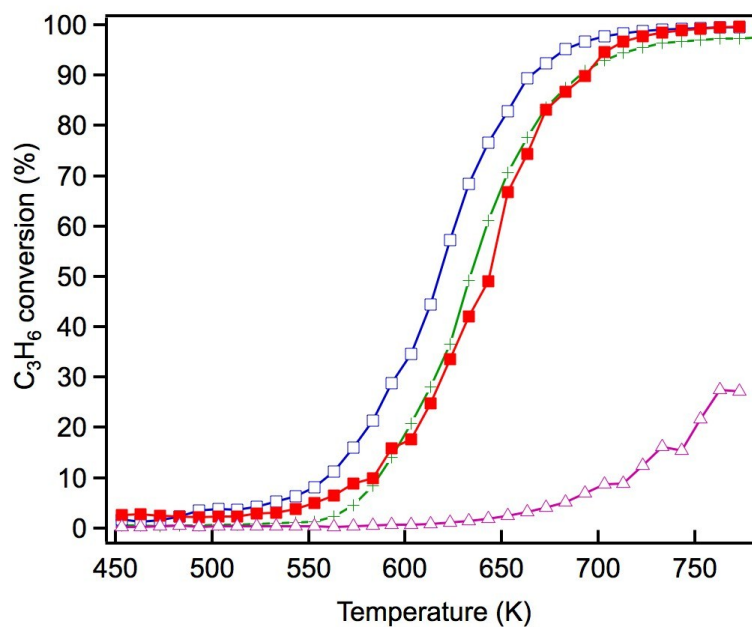


Fig. 4.18 C_3H_6 conversion in the steam reforming reaction over the fresh Rh catalysts: (+) Rh/ZrO₂, (Δ) Rh/Zr-Y-O, (\square) Rh/Zr-La-O and (\blacksquare) Rh/Zr-La-Y-O.

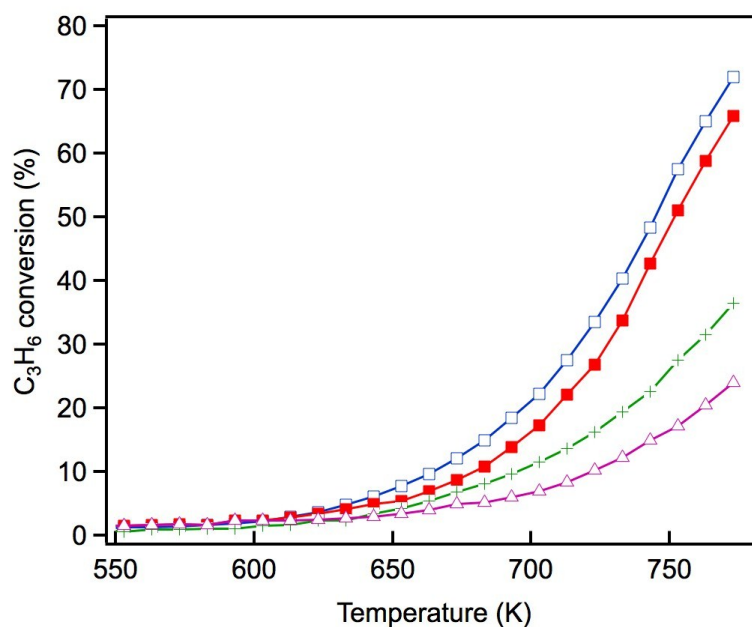


Fig. 4.19 C_3H_6 conversion in the steam reforming reaction over the aged Rh catalysts: (+) Rh/ZrO₂, (Δ) Rh/Zr-Y-O, (\square) Rh/Zr-La-O and (\blacksquare) Rh/Zr-La-Y-O.

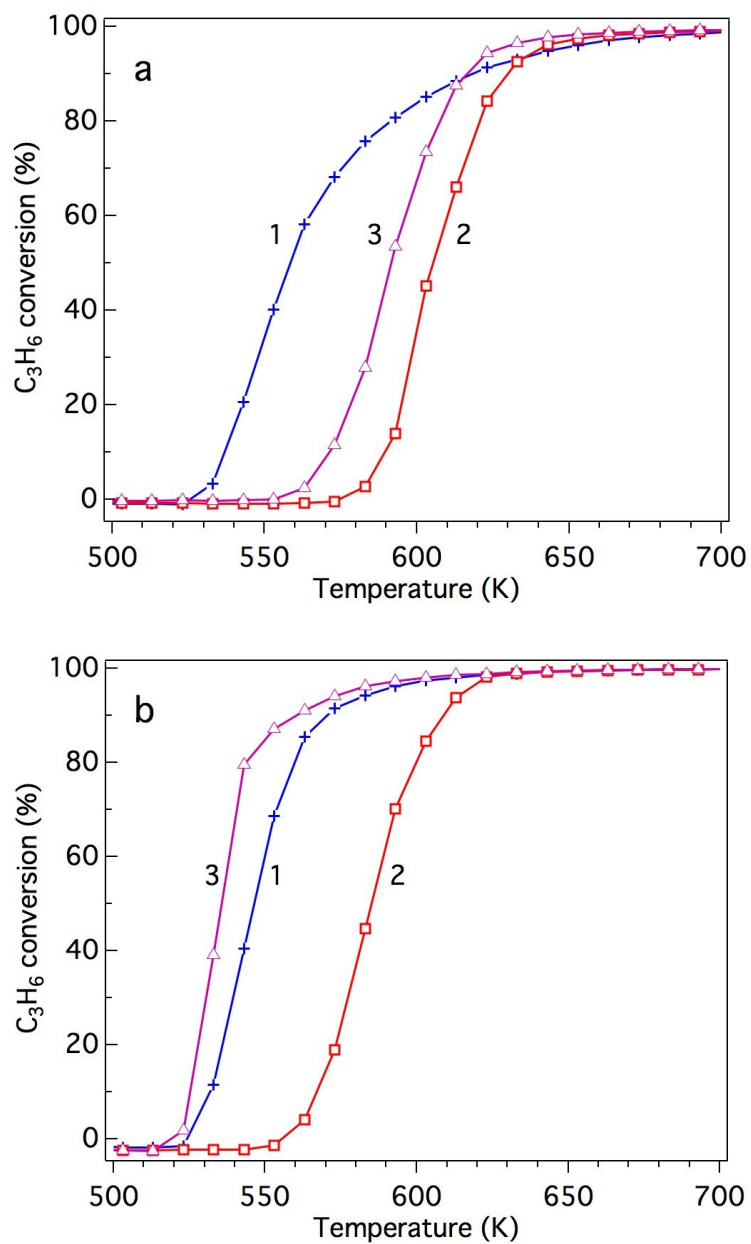


Fig. 4.20 Effect of the steam reforming reaction for the three-way catalytic C_3H_6 conversion by the (a) aged Rh/Zr-Y-O and (b) aged Rh/Zr-Y-La-O catalysts. Three types of pre-treatment were conducted: (1) no pre-treatment, (2) pre-treatment with 5 % oxygen at 773 K for 5 min, and (3) pre-treated with 5 % oxygen at 773 K for 5 min followed by the steam reforming reaction at 520 K for 5 min.

4.4 Discussion

We have previously reported that rhodium supported on Zr–La–O was highly active under fresh and the aged conditions.²² Rhodium supported on Zr–La–O maintained its low oxidation state during the three-way catalytic reaction and after the oxidative treatment. This performance was not achieved when other lanthanides (Ce, Pr, or Nd) were added to the zirconia supports. After the aging treatment, the Rh/Zr–La–O catalyst exhibited higher activity in the steam reforming reaction. It was confirmed that the catalytic activity was recovered because oxidized rhodium was reduced by the steam reforming reaction. The aging treatment transformed the structure of the Zr–La–O support from tetragonal to three phases: monoclinic-ZrO₂, tetragonal-ZrO₂ and pyrochlore (La₂Zr₂O₇). The treatment also altered the rhodium particle size from a few nanometers to 30–100 nm. In this chapter, Y was added to the ZrO₂-based supports to stabilize the structure and its effect was investigated based on the state of Rh, activity for the steam reforming reaction and the three-way catalytic performance. As a result, it was found that Rh/Zr–Y–La–O showed excellent three-way catalytic performance that was better than a previously reported Rh/Zr–La–O catalyst.^{21, 22}

For the fresh Rh/ZrO₂ and Rh/Zr–Y–O catalysts, Y addition to ZrO₂ enhanced the oxidation of Rh, as demonstrated by the results of O/Rh ratio derived from CO-TPR. The O/Rh ratio increased from 0.14 for Rh/ZrO₂ to 1.48 for Rh/Zr–Y–O (Table 2). The O/Rh ratio of 1.48 for Rh/Zr–Y–O was almost the stoichiometric value corresponding to the formation of fully oxidized Rh₂O₃ particles. Also, the introduction of Y induced a dramatic decrease in the steam reforming activity of the fresh catalysts (Fig. 4.18). As a result, the three-way catalytic activity of Rh/Zr–Y–O was low. The oxidation states of Rh for the two aged catalysts were similar to each other; the O/Rh ratios for Rh/ZrO₂ and Rh/Zr–Y–O were 0.20 and 0.12, respectively. The sharp TPR peaks (Fig. 4.16 a and b) suggest that only the surfaces of rhodium particles were oxidized to Rh₂O₃ in each aged sample. The steam reforming activities were very low for the aged catalysts. In particular, Rh/Zr–Y–O had the lowest activity (Fig. 4.19). The limited regeneration was demonstrated for the aged Rh/Zr–Y–O catalyst, as shown in Fig. 4.20 a. The lower three-way catalytic activities of these two catalysts can be readily explained by their low regeneration. The reason why the aged Rh/Zr–Y–O showed three-way catalytic activity higher than the aged Rh/ZrO₂ is unclear.

The enhancement of rhodium oxidation by Y addition was also observed for fresh Rh/Zr–Y–La–O. Also, the introduction of Y to Zr–La–O improved the reducibility of rhodium

oxides (lower reduction temperature at CO-TPR). Enhancement of rhodium oxidation was indicated by the increased O/Rh ratio from 0.70 for Rh/Zr–La–O to 1.20 for Rh/Zr–Y–La–O (Table 4.2). In our previous report,²² the oxidation state of rhodium on Zr–La–O after oxidative pre-treatment averaged between Rh⁰ and Rh³⁺ (Fig. 2.2 in Chapter 2, p. 33). These results indicate that rhodium particles became more readily oxidized after Y addition. The CO-TPR profile of the fresh Rh/Zr–Y–La–O showed that rhodium on Zr–Y–La–O was more readily reduced than that on Zr–La–O. Specifically, the reduction profile of Rh/Zr–La–O began at approximately 540 K, but in the case of Rh/Zr–Y–La–O, the profile started from a much lower temperature (440 K, Fig. 4.15c and d). IR spectra of adsorbed NO also revealed that the band assigned to Rh⁰-NO⁺ was enhanced by Y addition, especially at around 473 K, the temperature at which the three-way catalytic reaction started (Fig. 4.17b). This is also an indication of the presence of rhodium (0) on the surface, highlighting that the rhodium on Zr–Y–La–O was reduced more readily than on Rh/Zr–La–O. Also, Rh/Zr–Y–La–O demonstrated a high steam reforming activity that was comparable to Rh/Zr–La–O (Fig. 4.18). Therefore, the regeneration of Rh was likely pronounced during the three-way catalysis over Rh/Zr–Y–La–O.

Y addition did not affect rhodium oxidation for the aged catalysts as indicated by the results of the CO-TPR profiles (Fig. 4.16). Aged catalysts contain larger Rh particles as was indicated by their low Rh dispersion. Thus, it is unlikely that the oxide support influences the oxidation of rhodium through interactions between the Rh particles and the support. The XRD results for Rh/Zr–Y–La–O after the aging treatment showed that Y addition prevented phase separation (Fig. 4.1h). Stabilization of the support was also reflected in the changes of BET surface areas before and after the aging treatment. Rh/Zr–La–O decreased its surface area to 29.6 m²g⁻¹, while Rh/Zr–Y–La–O had a surface area as high as 51.2 m²g⁻¹. The relatively high rhodium dispersion for the aged Rh/Zr–Y–La–O (Table 4.1) was likely from the high surface area of the support after the aging treatment. The small rhodium particles in the TEM images correlated well with the dispersion for aged Rh/Zr–Y–La–O (Fig. 4.12). The high steam reforming activity was maintained, even after Y addition (Fig. 4.19). It was also confirmed that the steam reforming reaction recovered the catalytic activity that was deactivated by the oxidative treatment (Fig. 4.20b).

Steam-reforming reaction is endothermic reaction.³² The fact that the outlet temperature was lower compared to the inlet temperature during three-way catalysis above 673 K demonstrated that the endothermic reaction was taking place during the three-way catalysis (Fig. 4.11). Rh/Zr–Y–La–O showed high steam-reforming activity (Fig. 4.19), and correspondingly the

recovery of the catalyst was confirmed (Fig. 4.20b). Based on these findings, it is reasonable to conclude that the recovery of the catalyst by the steam-reforming reaction was taking place under the actual three-way catalysis conditions. Therefore, the recovery function of Rh/Zr–Y–La–O can be regarded as “self-regeneration”. Overall, Rh/Zr–Y–La–O showed excellent performance, even after the aging treatment.

4.5 Conclusions

High activity for fresh and aged Rh/Zr–Y–La–O in three-way catalytic processes was identified in this chapter. The effects of Y addition to the supports were also investigated in detail. Yttrium addition to Rh/Zr–La–O increased the oxidation of rhodium compared with Rh/Zr–La–O, but the reducibility of rhodium was also enhanced, as indicated by CO-TPR. Rh/Zr–Y–La–O showed high steam reforming activity, comparable to Rh/Zr–La–O. Thus, the regeneration of Rh was likely pronounced for Rh/Zr–Y–La–O. In the case of Rh/Zr–Y–O, rhodium particles were fully oxidized after an oxidation treatment. Yttrium addition to ZrO₂ dramatically decreased the steam reforming activity. Rhodium particles on ZrO₂ and Zr–Y–O are readily oxidized during reaction, leading to low three-way catalytic activity.

After the aging treatment, Rh/Zr–Y–La–O showed higher rhodium dispersion than the other tested catalysts. This is likely because of the relatively high surface area of the support after the aging treatment and stabilization of ZrO₂ by the addition of Y. Excellent steam reforming activity was maintained for Rh/Zr–Y–La–O after the aging treatment. The high steam reforming activity regenerates deactivated oxidized Rh, providing the best three-way catalytic activity. These results demonstrate the importance of the catalyst support in designing three-way catalysts. Our findings highlight the potential to design and develop effective three-way catalysts with high tolerances to oxidative reaction conditions in recently developed vehicles and engines.

References

1. H. Shinjoh, M. Hatanaka, Y. Nagai, T. Tanabe, N. Takahashi, T. Yoshida and Y. Miyake, *Top. Catal.*, 2009, 52, 1967.
2. J. R. Theis and R. W. McCabe, *Catal. Today*, 2012, 184, 262.
3. R. Burch, P. K. Loader and N. A. Cruise, *Appl. Catal. A*, 1996, 147, 375.
4. K. Dohmae, Y. Nagai, T. Tanabe, A. Suzuki, Y. Inada and M. Nomura, *Surf. Inter. Anal.*, 2008, 40, 1751.
5. C. P. Hwang, C. T. Yeh and Q. M. Zhu, *Catal. Today*, 1999, 51, 93.
6. M. Zimowska, J. B. Wagner, J. Dziedzic, J. Camra, B. Borzeczka-Prokop and M. Najbar, *Chem. Phys. Lett.*, 2006, 417, 137.
7. R. W. McCabe, R. K. Usmen, K. Ober and H. S. Gandhi, *J. Catal.*, 1995, 151, 385.
8. M. Uenishi, H. Tanaka, M. Taniguchi, I. Tan, Y. Nishihata, J. i. Mizuki and T. Kobayashi, *Catal. Commun.*, 2008, 9, 311.
9. S. I. Matsumoto, *Catal. Today*, 2004, 90, 183.
10. H. Muraki and G. Zhang, *Catal. Today*, 2000, 63, 337.
11. H. S. Gandhi, G. W. Graham and R. W. McCabe, *J. Catal.*, 2003, 216, 433.
12. M. Shelef and R. W. McCabe, *Catal. Today*, 2000, 62, 35.
13. G. C. Koltsakis and A. M. Stamatelos, *Prog. Ener. Comb. Sci.* 1997, 23, 1.
14. M. Shelef and G. W. Graham, *Catal. Rev. Sci. Eng.*, 1994, 36, 433.
15. Z. WengSieh, R. Gronsky and A. T. Bell, *J. Catal.*, 1997, 170, 62.
16. D. J. C. Yates and E. B. Prestridge, *J. Catal.*, 1987, 106, 549.
17. M. A. Newton, *Chem. Soc. Rev.*, 2008, 37, 2644.
18. M. A. Newton, B. Jyoti, A. J. Dent, S. G. Fiddy and J. Evans, *Chem. Commun.*, 2004, 2382.
19. T. Tanabe, A. Morikawa, M. Hatanaka, N. Takahashi, Y. Nagai, A. Sato, O. Kuno, H. Suzuki and H. Shinjoh, *Catal. Today*, 2012, 184, 219.
20. R. Burch and P. K. Loader, *Appl. Catal. A*, 1996, 143, 317.
21. H. Kawabata, Y. Koda, H. Sumida, M. Shigetsu, A. Takami and K. Inumaru, *Chem. Commun.*, 2013, 49, 4015.
22. H. Kawabata, Y. Koda, H. Sumida, M. Shigetsu, A. Takami and K. Inumaru, *Catal. Sci. Technol.*, 2014, 4, 697.

23. H. G. Scott, *J. Mater. Sci*, 1975, 10, 1527.
24. C. Dujardin, A. S. Mamede, E. Payen, B. Sombret, J. P. Huvenne and P. Granger, *Top. Catal.*, 2004, 30-1, 347.
25. T. Chafik, A. M. Efstathiou and X. E. Verykios, *J. Phys. Chem. B*, 1997, 101, 7968.
26. M. Haneda, K. Shinoda, A. Nagane, O. Houshito, H. Takagi, Y. Nakahara, K. Hiroe, T. Fujitani and H. Hamada, *J. Catal.*, 2008, 259, 223.
27. E. Rogemond, N. Essayem, R. Frety, V. Perrichon, M. Primet, M. Chevrier, C. Gauthier and F. Mathis, *J. Catal.*, 1999, 186, 414.
28. J. Barbier-Jr and D. Duprez, *Appl. Catal. B*, 1994, 4, 105.
29. J. P. Breen, R. Burch and H. M. Coleman, *Appl. Catal. B*, 2002, 39, 65.
30. J. A. Anderson, M. Fernandez Garcia (Eds.), *Supported Metals in Catalysis*, ICP, London, 2005, p. 140.
31. "Shokubai-kouza", vol. 5, Catalyst design, ISBN: 4061914057, Kodan-sha, 1985, p.141.
32. M. E. Domine, E. E. Iojoiu, T. Davidian, N. Guilhaume and C. Mirodatos, *Catal. Today*, 2008, 133, 565.

Chapter 5

Summary and General Conclusions

Chapter 5: Summary and General Conclusions

5.1 Summary of each Chapter

The first subject of this thesis is to develop highly active three-way catalyst for the new engine operation by adopting zirconia based catalysts. The second subject is to introduce the basis of designing active three-way catalysis of rhodium including the knowledge of the support effect. Here are the summarized results obtained in each chapter.

5.1.1 Summary of Chapter 2

In Chapter 2, we studied the catalytic activities and properties of rhodium supported lanthanoid (La, Pr)-containing zirconia mixed oxides, and showed that the advantages and scope of rhodium catalysts supported on non-oxygen storage function. It was demonstrated that rhodium on a La-containing ZrO_2 support can be stabilized at a relatively lower valence state. This phenomenon brought about the high catalytic performance of Rh/Zr-La-O under fluctuating oxygen conditions even though the catalyst has no oxygen storage function. Rhodium particles maintained a low oxidation state on the $\text{ZrO}_2\text{-La}_2\text{O}_3$ mixed oxide even after treatment with 5% O_2 at 773 K, highlighting the significant effect of the La addition.

5.1.2 Summary of Chapter 3

We investigated the influence of aging treatment on the catalytic activity of the catalyst reported in Chapter 2. In chapter 3, we described the findings that Rh/Zr-La-O was active for three-way catalysis from fresh though 1273 K aged conditions even after treatment under the oxidative atmosphere. Rhodium supported on lanthanoid- (La, Ce, Pr, or Nd) containing ZrO_2 was investigated as a three-way catalyst following an aging treatment (oxidation at 1273 K) that

simulates 80 000 km mileage in real vehicles. The properties of rhodium were assessed by transmission electron microscopy, CO chemisorption, and temperature-programmed reduction using CO. The oxidation states of rhodium before and after the aging treatment were evaluated by X-ray photoelectron spectroscopy. Rhodium supported on lanthanum-containing ZrO_2 (Rh/Zr–La–O) was highly active for the removal of NO_x and hydrocarbons from a synthetic auto exhaust. The support determined the oxidation state of rhodium after the aging treatment: rhodium supported on Zr–La–O maintained its low oxidation state during the three-way catalytic reaction and after the aging treatment, whereas rhodium supported on ZrO_2 and other lanthanoid-containing ZrO_2 was converted to the higher oxidation states. The Rh/Zr–La–O catalyst, following the aging treatment, exhibited superior activity for the steam reforming reaction. The hydrogen, produced from the steam reforming reaction, reduced the previously oxidized Rh in Rh/Zr–La–O, thereby regenerating the catalyst that was previously deactivated by an oxidation treatment. Self-regeneration of the Rh/Zr–La–O catalyst by the steam reforming reaction was more efficient when compared with that of the other lanthanoid-containing ZrO_2 catalysts. These results highlight the potential of the present strategy for developing active three-way catalysts with high tolerance to oxidative conditions.

5.1.3 Summary of Chapter 4

A novel, highly active three-way catalyst, rhodium supported on Y- and La-added zirconia (Rh/Zr–Y–La–O) was found in this chapter. Rh/Zr–Y–La–O showed superior performance compared with a previously reported Rh on La-added ZrO_2 (Rh/Zr–La–O) catalyst. The effects of Y addition to ZrO_2 -based supports were investigated in detail. CO temperature programmed reduction and *in situ* Fourier transform infrared spectra of adsorbed NO species indicated that Y addition to La-containing ZrO_2 enhanced the reducibility of rhodium supported on the catalyst and more metallic Rh was exposed on the surface after oxidation for Rh/Zr–Y–La–O than for Rh/Zr–La–O. Before and after an aging treatment at 1273 K that simulated 80 000 km travelled by vehicles, Rh/Zr–Y–La–O showed high steam reforming activity. After the aging treatment, Rh/Zr–Y–La–O was deactivated using an oxidation treatment, but its three-way catalysis activity was completely regenerated after a short (5 min) exposure to steam reforming reaction conditions, demonstrating self-regeneration capability. After the aging treatment,

Rh/Zr–Y–La–O showed higher rhodium dispersion than other catalysts. This was attributed to the high surface area of the support after aging and the stabilization of ZrO₂ from the addition of Y. These findings highlight the role of catalyst supports in designing effective three-way catalysts with high tolerance to the oxidative conditions in new vehicles and engines.

5.2 General Conclusions

From the summary of each chapter, we can highlight the importance of metal-support interactions for the rhodium property.

1. Rhodium supported on La-containing ZrO_2 support achieved high activity in three-way catalysis under fluctuating oxygen conditions even though the catalyst has no oxygen storage function.
2. It is concluded that Rh/Zr-La-O has a function to maintain its rhodium oxidation state in a low valence state not only by the interaction of the support but also by the surface reaction (steam-reforming reaction) that produce hydrogen as a reductant. This phenomenon brought about the high catalytic performance of Rh/Zr-La-O under fluctuating oxygen conditions and the oxidative reaction conditions even though the catalyst has no oxygen storage function.
3. High activity for fresh and aged Rh/Zr-Y-La-O in three-way catalytic processes was also identified with superior performance compared with Rh on La-added ZrO_2 (Rh/Zr-La-O) catalyst. Stabilization of ZrO_2 by the addition of Y maintained both rhodium dispersion and excellent steam reforming activity after the aging treatment. Thus, the regeneration of Rh was likely pronounced for Rh/Zr-Y-La-O, providing the best three-way catalytic activity.

These findings became a probable new strategy for highly active three-way catalysts by controlling the oxidation state of the nano-sized metal particles while taking advantage of the metal-support interaction. Our conclusions highlight the potential to design and develop effective three-way catalysts with high tolerances to oxidative reaction conditions in recently developed vehicles and engines.

List of Publications

Original papers and oral presentations corresponding to this thesis are listed below:

Chapter 2.

1. Paper

Active three-way catalysis of rhodium particles with low oxidation state maintained under oxidative atmosphere on La-containing ZrO₂ support

Hisaya Kawabata, Yuki Koda, Hirosuke Sumida, Masahiko Shigetsu, Akihide Takami and Kei Inumaru

Chem. Commun., 2013, **49** (38), 4015 – 4017

2. Presentation

Effect of La incorporation for the three-way catalysis of rhodium supported on ZrO₂

Hisaya Kawabata, Yuki Koda, Hirosuke Sumida, Masahiko Shigetsu, Akihide Takami and Kei Inumaru

110th, *Catalysis Society of Japan Meeting*, At Kyusyu University, 2012. 9. 25

Chapter 3.

1. Paper

Self-regeneration of three-way catalyst rhodium supported on La-containing ZrO₂ in an oxidative atmosphere

Hisaya Kawabata, Yuki Koda, Hirosuke Sumida, Masahiko Shigetsu, Akihide Takami and Kei Inumaru

Catal. Sci. Technol., 2014, **4** (3), 697 – 707

2. Presentation

Support effect of ZrO₂-La₂O₃ mixed oxide for three-way catalysis of rhodium particles

Hisaya Kawabata, Yuki Koda, Hirosuke Sumida, Masahiko Shigetsu, Akihide Takami and Kei Inumaru

112th, *Catalysis Society of Japan Meeting*, At Akita University, 2013. 9. 18

Chapter 4.

1. Paper

Highly active three-way catalysis of rhodium particles on a Y-stabilized La-containing ZrO₂ support: Effect of Y on the enhanced reducibility of rhodium and self-regeneration

Hisaya Kawabata, Yuki Koda, Hirosuke Sumida, Masahiko Shigetsu, Akihide Takami and Kei Inumaru

Catal. Sci. Technol., 2015, **5** (1), 584 – 594

Acknowledgements

This thesis is based on research papers that have been published during 2011- 2015 from Department of Applied Chemistry, Graduate School of Engineering, Hiroshima University under the management of Professor Kei Inumaru. I would like to express my sincere appreciation for kind suggestions and careful reviewing of the manuscripts. This thesis would not have been completed without the years of this encouragement. I am deeply grateful to Professor Tsuneji Sano, Associate Professor Masahiro Sadakane and Professor Tsuru Toshinori for reviewing and discussing on the dissertation. I would like to thank all the members in Laboratory of Inorganic Material Chemistry managed by Professor Kei Inumaru for productive discussions. I would like to thank Dr. Akihide Takami and Mr. Masahiko Shigetsu of Mazda Motor Corporation for helpful suggestions, allowing me to preparing this thesis. I would like to also thank Dr. Hirosuke Sumida, Ms. Yuki Koda for recording XPS spectra and TEM analysis, and valuable discussions. I wish to thank all the members in the three-way catalyst team of the Technical Research Center of Mazda Motor Corporation, especially Dr. Hiroshi Yamada, Mr. Yasuyuki Matsumura for their useful suggestions.

Finally, I cannot finish this acknowledgement without thanking my family.

Hisaya Kawabata

Hiroshima

January 2015